DISPERSION of *nano* MATRICES into CELLULOSE NETWORK

BY
MAHAMUDA SULTANA
STUDENT ID NO: F0412033218

A THESIS PAPER SUBMITTED AS A REQUIREMENT FOR THE PARTIAL FULFILMENT OF THE DEGREE OF MASTERS OF PHILOSOPHY (M. PHIL) IN CHEMISTRY

DEPARTMENT OF CHEMISTRY
FACULTY OF ENGINEERING
BANGLADESH UNIVERSITY OF ENGINEERING AND TECHNOLOGY (BUET)
DHAKA-100, BANGLADESH

AUGUEST 2016

BANGLADESH UNIVERSITY OF ENGINEERING AND TECHNOLOGY (BUET) DHAKA-100, BANGLADESH
DETARTMENT OF CHEMISTRY

THESIS APPROVAL

This thesis titled DISPERSION OF *nano*-MATRICES INTO CELLULOSE NETWORK submitted by Mahamuda Sultana, Roll No: F0412033218, Session: April 2012 has been accepted as satisfactory in partial fulfillment of the requirement for the degree of master of philosophy (M. Phil) in chemistry on 10 August , 2016.

Board of Examiners:

1. Dr. Md. Rafique Ullah
   Professor
   Department of Chemistry
   BUET, DHAKA-1000,
   Bangladesh
   ..... 10.08.2016
   Chairman (Supervisor)

2. Prof. Dr. Al-Nakib Chowdhury
   Vice-Chancellor
   Pabna University of Science & Technology (PUST), Pabna
   ..... 10.8.16
   Member (Co-Supervisor)

3. Head,
   Department of Chemistry
   BUET, DHAKA-1000,
   Bangladesh
   ..... 10.08.2016
   Member (Ex-Officio)

4. Dr. Md. Nazrul Islam
   Professor
   Department of Chemistry
   BUET, DHAKA-1000,
   Bangladesh
   10/08/2016
   .....
   Member

5. Dr. Omar Ahmed
   Professor
   Department of Chemistry
   University of Dhaka, Dhaka
   10-8-16
   Member (External)

DECLARATION

This thesis work has been done by the candidate herself and does not contain any material extracted from elsewhere or from a work published by anybody else. The work for this thesis has not been presented elsewhere by the author for any degree or diploma.

Mahamuda

Date: 22th August, 2016.

Mahamuda Sultana
M. Phil Student
Roll no: F0412033218
Session: April, 2012
Department of Chemistry
BUET, Dhaka-1000

Dedicated to my parents

Md. Mosharof Hossen
and
Monowara Hossen

ACKNOWLEDGEMENT

At the beginning, all praise to the almighty Allah, who has given me the strength and opportunity to complete this thesis work as an M. Phil student in the Department of Chemistry at Bangladesh University of Engineering and Technology (BUET), Dhaka, Bangladesh.

I would to express my sincere gratitude and respect to my supervisor Dr. Md. Rafique Ullah, Professor, Department of Chemistry, Bangladesh University of Engineering and Technology (BUET) for his supervision, advice patience and support during my research work. I am proud of having worked on this dissertation under his guidance.

I am also indebted to my co-supervisor Dr. Al-Nakib Chowdhury, Professor and Vice-Chancellor, Pabna University of Science and Technology, Pabna for his excellent cooperation and fruitful suggestion during my research work.

I highly indebted to Dr. Md. Shafiul Azam, Assistant Professor, Department of Chemistry, Bangladesh University of Engineering and Technology (BUET) for his guidance, suggestion, academic support and appreciation.

I would like to extend my gratitude to Dr. Md. Manwarul Islam, Professor, Department of Chemistry, Bangladesh University of Engineering and Technology (BUET) for his valuable advice.

I am also grateful to Dr. Md. Nazrul Islam, Professor, Department of Chemistry, Bangladesh University of Engineering and Technology (BUET) for his valuable suggestions on my technical report.

I would also like to express my gratitude to Dr. Md. Shakhawat Hossain Firoz, Associate Professor, Department of Chemistry, Bangladesh University of Engineering and Technology (BUET), Dr. Abu Bin Imran, Assistant Professor, Department of Chemistry, Bangladesh University of Engineering and Technology (BUET) for their valuable advice and support.

I feel myself very much fortunate to express my gratitude and thanks to my all respected teachers in our department for their continuous inspiration. I would like to thank all my lab mates especially Md. Jukaul Islam, Saidur Rahman and Ratan Kumar Paul for their co-operation in the laboratory. I also thank all stuffs of the chemistry department in BUET for their kind support.

Mahamuda Sultana
Author
August 2016

Contents

Chapter 1: Introduction

Chapter 2: Experimental

Chapter 3: Results and Discussion

Abstract

The *nano* particles of Nickel Oxides and Manganese Oxides was prepared chemically by precipitation and forced hydrolysis method respectively. NiO particles are synthesized by air calcination of $Ni(OH)_2.NiCO_3.xH_2O$; which is precipitated from aqueous solution containing $NiCl_2$ as the nickel source and NH_4HCO_3 act as the precipitation agent. Mn_3O_4 *nano* particles were prepared by forced hydrolysis of Mn(II) acatate. Aqueous solution of $Mn(OOCCH_3)_2.4H_2O$ was heated over at 80^0c for 2 hours. The resulting brown dispersed product is washed for several times. After that dried in air to obtain Mn_3O_4 nano particles.

The *nano* particles loaded MCC was fabricated by simply filtering the (MCC) suspension containing *nano* NiO and *nano* Mn_3O_4 through a sheet of filter paper. The *nano* particles are attracted to the MCC fibers by electrostatic interaction. Certain amount of MCC is taken in a beaker containing double distilled water. At a fixed condition, a small amount of *nano* NiO and Mn_3O_4 is added to the suspension. Through keeping the same reaction condition the suspension is filtered and dried to obtain final product.

The *nano* metal oxides and the *nano* metal oxides dispersed in MCC metrics were characterized by a wide range of experimental techniques Viz, IR spectroscopy, X-ray diffraction, Scanning electron microscope and EDX.

IR spectral analysis analysis of the samples yielded useful information on the identification of the compounds. From the spectra the band characteristics of NiO, Mn_3O_4, MCC, NiO/MCC, Mn_3O_4/MCC confirmed the presence of the components in each substrate.

X-ray scattering patterns of the *nano* metal oxides and MCC indicating the crystalline nature. The *nano*-size of metal oxides (NiO and Mn_3O_4) are ensured through calculating the crystallite size (using XRD method). Surface morphology obtained by SEM provides many interesting results. The surface of *nano* Mn_3O_4 and *nano* NiO are granular and consist of particles ranging from nm to μm level. Surface of *nano* NiO/MCC and *nano* Mn_3O_4/MCC shows that *nano* metal oxide distribution over the substrate is not homogeneous.

EDX analysis ensures that the composition of Mn and O is Mn_3O_4 and Ni and O in NiO.

For the removal of dyes for solution nano NiO/MCC and MCC is used as adsorbents. The adsorption capacity q_t at any time of MB on *nano* NiO/MCC is slightly higher than cellulose.The Adsorption kinetic study exhibits that the adsorption of MB on MCC and MCC/ *nano* NiO composites are better fit to pseudo second order kinetic model than the pseudo first order kinetic model by giving greater r^2 value. To better understand the interactions between MB and the adsorbents, the equilibrium experimental data were analyzed using Freundlich and Langmuir isotherm models. From the fitting parameters, regression coefficients (R2) suggest that the Langmuir model fits the adsorption better, which implies that both MCC and *nano* NiO/MCC likely possess homogeneous adsorption surface and the adsorption of MB on these two adsorbents is likely monolayer.

The measurement of the antibacterial activity of individual drug pure Mn_3O_4 nanoparticles and MCC /*nano* Mn_3O_4composite was done by Mueller-Hinton agar disk diffusion method. A total seven bacterial stains including selected gram positive and gram negative bacteria were selected to assess susceptibility pattern.

It can be seen that both *nano* Mn_3O_4 and *nano* Mn_3O_4/MCC suggesting a antibacterial activity against the bacteria samples tested. This results implies that Mn_3O_4 nanoparticles and *nano* Mn_3O_4/MCC composite kill some bacteria and interact with them strongly.

Chapter 1

INTRODUCTION

In the recent years, we are globally battling with the worldwide crisis of raw materials since it is a non-renewable source. It is inevitable that the global conservation of natural resources of raw materials and fossil fuel supplies will be largely depleted in a matter of decades. Fortunately, we have abundant renewable sources from the nature itself to replace the fossil fuels effectively.

Despite the sudden surge in technological advancement in the last century, we are also facing various difficulties along with the positive aspects. As our achievements in different sectors reaches peaks every day, the demand for its supply of natural resources also increases. i.e., food, fuel, energy and materials that is highly dependent of diminishing fossil fuel resources. The prosperity in technological advancement abled us to live longer, thus consume world resources for further period of time.

New problem arises every century and we dig deeper to fight against it every time. Cellulose is a common organic polymer and is considered as an important raw material. In addition to its abundancy worldwide, it displays an interesting physical properties such as a low density together with high mechanical characteristics. However, due to its high Tg close to its decomposition temperature, cellulose cannot be melted and processed as a thermoplastic [1]. Cellulose has been in the center of attention due to its possible use in production of biofuels [2]. Cellulose is extensively used as a raw material in the paper industry in the production of paper and cupboard products [3]. Cellulose also show its versatility in numerous application [4,5]. Moreover, it can be chemically modified to yield cellulose derivatives [6,7]. These are widely used in various industrial sectors in addition to being used as a source for commodity goods [8-10].

Nanotechnology is the study of manipulating matter on an atomic and molecular scale. Generally, a nanotechnology deal with structures arise between 1 to 100 nanometer in at least one dimension and involves developing materials or devices within that size. Quantum mechanical effects are very important at these scale [11].

Nanotechnology is very diverse, ranging from extension of conventional device physics to completely new approaches based upon molecular self-

assembly, from developing new materials with dimension on the nanoscale to investigating whether we can directly control matter on the atomic scale.

1.1 *nano* Materials:

1.1.1 Basic Concepts

Nanomaterials are materials that have structural components smaller than 1 micrometer in at least one dimension. While the atomic and molecular building blocks (∼0.2 nm) of matter are considered nanomaterials, examples such as bulk crystals with lattice spacing of nanometers but macroscopic dimensions overall, are commonly excluded.

Nanomaterials are made of many different chemicals and compounds. Once formed, these materials are extremely small which give the *nano* product unique properties. All materials in *nano* scale size have quite a large surface area to volume ratio. This single characteristic paves way for new quantum mechanical effects. Due to these effects the size of the particle reduces, which causes a change in the electronic properties of the solid. When the size of the material becomes micro, there will not be any interference of the quantum effect. But the effect will start its play as soon as the material becomes *nano*-sized. There will also be changes in the physical as well as catalytic activities of the material.

Thus, it is understood that there is a drastic change in properties, when the material changes from macro-scale to *nano*-scale. These changes can be very unique and can be used for a variety of applications. The change in characteristics that occur when a material changes its scale from micro to *nano.*

1. Copper – Opaque to transparent
2. Platinum – Inert to catalytic
3. Aluminum – Stable to combustible
4. Gold – Solid to liquid
5. Silicon – Insulator to conductor

1.1.2 Nano particles:

Nanoparticles are particles with at least one dimension smaller than 1 micron and potentially as small as atomic and molecular length scales (~0.2 nm). Nanoparticles can have amorphous or crystalline form and their surfaces can act as carriers for liquid droplets or gases. To some degree, *nano*-particulate matter should be considered a distinct state of matter, in addition to the solid, liquid, gaseous, and plasma states, due to its distinct properties (large surface area and quantum size effects). Examples of materials in crystalline nanoparticle form are fullerenes and carbon nanotubes, while traditional crystalline solid forms are graphite and diamond. Many authors limit the size of nanomaterials to 50 nm or 100 nm, the choice of this upper limit being justified by the fact that some physical properties of nanoparticles approach those of bulk when their size reaches these values. However, this size threshold varies with material type and cannot be the basis for such a classification. A legitimate definition extends this upper size limit to 1 micron, the sub-micron range being classified as *nano.*

Nanomaterials are made of many different chemicals and compounds. Once formed, these materials are extremely small which give the *nano* product unique properties. There are four main classes of materials that are used to make *nano* sized products including metal, carbon, composites, and dendrimers. These products have a variety of applications and are used in the automotive industry, biomedical industry, in films, and much more.

Nano scale material is unique because of its size, ranging from one nanometer to several hundreds of nanometers. Electrical, optical, and chemical properties are very different at *nano* scale than at a larger scale. One reason that properties are so different are that more than half of the materials atoms are on the surface. Large scale items have much less percentage of atoms at the surface.

Metal based nanomaterials are those such as *nano* gold, quantum dots and *nano* silver. Quantum dots come in several sizes with a maximum size of several hundred nanometers. The dot contains semiconductor crystals that are packed together so thousands of atoms are all in a very small area. Other metal based chemicals used at this small scale include types of metal oxides.

Carbon based *nano*materials are those that are mostly made of carbon. The carbon is shaped into hollow tubes, ellipsoids or spheres. Ellipsoidal and spherical carbon nanomaterials are called fullerenes. Hollow tube shaped materials are called nanotubes.

According to their physical state Nanoparticles are generally classified based on their dimensionality, morphology, composition, uniformity, and agglomeration. An important additional distinction should be made between nanostructured thin films or other fixed nanometer-scale objects (such as the circuits within computer microprocessors) and free nanoparticles. The motion of free nanoparticles is not constrained, and they can easily be released into the environment leading to human exposure that may pose a serious health risk. In contrast are the many objects containing nanostructured elements that are firmly attached to a larger object, where the fixed nanoparticles should pose no health risk when properly handled. An example of this important distinction is the material asbestos, which is perfectly safe in its primary state (basically a type of solid rock), but is a significant health hazard when mined or worked in such a way as to produce the carcinogenic nanometer-scale fibrous particles that become airborne (aerosol) and are therefore readily absorbed in the lungs. It is also very important to recognize that not all nanoparticles are toxic; toxicity depends on at least chemical composition and shape in addition to simply size and particle ageing. In fact, many types of nanoparticles seem to be non-toxic, others can be rendered non-toxic, while others appear to have beneficial health effects. An important lesson we are in the process of learning from nanoscience is that simple classifications of physical behavior (and therefore toxicity) are overly limiting and that we must study toxicology of each material and each morphology, in addition to particle ageing, to obtain accurate information to inform policy and regulatory processes.

1.1.3 Application of *nano* Materials:

Nanomaterials (*nano*-crystalline materials) are materials possessing grain sizes on the order of a billionth of a meter. They manifest extremely fascinating and useful properties, which can be exploited for a variety of structural and non-structural applications Since nanomaterials possess unique, beneficial chemical, physical, and mechanical properties, they can be used for a wide variety of applications. These applications include, but are not limited to,

1.1.3.1 Nanomaterial Applications using Nanocomposites

A nanocomposite is a matrix to which nanoparticles have been added to improve a particular property of the material. The properties of nanocomposites have caused researchers and companies to consider using this material in several fields. Applications being developed for nanocomposites include a nanotube-polymer nanocomposite to form a scaffold which speeds up replacement of broken bones, making a graphene-epoxy nanocomposite with very high strength-to-weight ratios, a nanocomposite made from cellulous and nanotubes used to make a flexible battery.

The following survey of nanocomposite applications introduces you to many of the uses being explored, including:

[1] **Producing batteries with greater power output.** Researchers have developed a method to make anodes for lithium ion batteries from a composite formed with silicon *nano*-spheres and carbon nanoparticles. The anodes made of the silicon-carbon nanocomposite make closer contact with the lithium electrolyte, which allows faster charging or discharging of power.

[2] **Speeding up the healing process for broken bones.** Researchers have shown that growth of replacement bone is speeded up when a nanotube-polymer nanocomposite is placed as a kind of scaffold which guides growth of replacement bone. The researchers are conducting studies to better understand how this nanocomposite increases bone growth.

[3] **Producing structural components with a high strength-to-weight ratio**. For example an epoxy containing carbon nanotubes can be used to produce nanotube-polymer composite windmill blades. This results in a strong but lightweight blade, which makes longer windmill blades practical. These longer blades increase the amount of electricity generated by each windmill.

[4] **Using graphene to make composites with even higher strength-to-weight ratios**. Researchers have found that adding graphene to epoxy composites may result in stronger/stiffer components than epoxy composites using a similar weight of carbon nanotubes. Graphene

appears to bond better to the polymers in the epoxy, allowing a more effective coupling of the graphene into the structure of the composite. This property could result in the manufacture of components with higher strength-to-weight ratios for such uses as windmill blades or aircraft components.

1.1.3.2 Nanomaterial Applications using Nanoparticles

Applications being developed for nanoparticles include deliver chemotherapy drugs directly to cancer tumors, resetting the immune system to prevent autoimmune diseases, delivering drugs to damaged regions of arteries to fight cardiovascular disease, create photo-catalysts that produce hydrogen from water, reduce the cost of producing fuel cells and solar cells, clean up oil spills, water pollution and air pollution.

1.1.3.2.1 Nanoparticle Applications in Medicine

The surface change of protein filled nanoparticles has been shown to affect the ability of the nanoparticle to stimulate immune responses. Researchers are thinking that these nanoparticles may be used in inhalable vaccines.

Researchers at Rice University have demonstrated that cerium oxide nanoparticles act as an antioxidant to remove oxygen free radicals that are present in a patient's bloodstream following a traumatic injury. The nanoparticles absorb the oxygen free radicals and then release the oxygen in a less dangerous state, freeing up the nanoparticle to absorb more free radicals.

Researchers are developing ways to use carbon nanoparticles called *nano*-diamonds in medical applications. For example *nano*-diamonds with protein molecules attached can be used to increase bone growth around dental or joint implants.

Researchers are testing the use of chemotherapy drugs attached to *nano*-diamonds to treat brain tumors. Other researchers are testing the use of chemotherapy drugs attached to *nano*-diamonds to treat leukemia

1.1.3.2.2 Nanoparticle Applications in Manufacturing and Materials

A synthetic skin, that may be used in prosthetics, has been demonstrated with both self-healing capability and the ability to sense pressure. The material is a composite of nickel nanoparticles and a polymer. If the material is held together after a cut it seals together in about 30 minutes giving it a self-healing ability. Also the electrical resistance of the material changes with pressure, giving it a sense ability like touch.

Silicate *nano* particles can be used to provide a barrier to gasses (for example oxygen), or moisture in a plastic film used for packaging. This could slow down the process of spoiling or drying out in food. Zinc oxide nanoparticles can be dispersed in industrial coatings to protect wood, plastic, and textiles from exposure to UV rays. Silicon dioxide crystalline nanoparticles can be used to fill gaps between carbon fibers, thereby strengthening tennis racquets. Silver nanoparticles in fabric are used to kill bacteria, making clothing odor-resistant.

1.1.3.2.3 Nanoparticle Applications and the Environment

Researchers are using photocatalytic copper tungsten oxide nanoparticles to break down oil into biodegradable compounds. The nanoparticles are in a grid that provides high surface area for the reaction, is activated by sunlight and can work in water, making them useful for cleaning up oil spills. Researchers are using gold nanoparticles embedded in a porous manganese oxide as a room temperature catalyst to breakdown volatile organic pollutants in air. Iron nanoparticles are being used to clean up carbon tetrachloride pollution in ground water. Iron oxide nanoparticles are being used to clean arsenic from water wells.

1.1.3.2.4 Nanoparticle Applications in Energy and Electronics

Researchers have used nanoparticles called nano-tetrapods studded with nanoparticles of carbon to develop low cost electrodes for fuel cells. This electrode may be able to replace the expensive platinum needed for fuel cell catalysts.

Researchers at Georgia Tech, the University of Tokyo and Microsoft Research have developed a method to print prototype circuit boards using standard inkjet printers. Silver nanoparticle ink was used to form the conductive lines needed in circuit boards.

Combining gold nanoparticles with organic molecules creates a transistor known as a NOMFET (Nanoparticle Organic Memory Field-Effect Transistor). This transistor is unusual in that it can function in a way similar to synapses in the nervous system.

A catalyst using platinum-cobalt nanoparticles is being developed for fuel cells that produces twelve times more catalytic activity than pure platinum. In order to achieve this performance, researchers anneal nanoparticles to form them into a crystalline lattice, reducing the spacing between platinum atoms on the surface and increasing their reactivity.

Researchers have demonstrated that sunlight, concentrated on nanoparticles, can produce steam with high energy efficiency. The "solar steam device" is intended to be used in areas of developing countries without electricity for applications such as purifying water or disinfecting dental instruments.

A lead free solder reliable enough for space missions and other high stress environments using copper nanoparticles. Silicon nanoparticles coating anodes of lithium-ion batteries can increase battery power and reduce recharge time. Semiconductor nanoparticles are being applied in a low temperature printing process that enables the manufacture of low cost solar cells.

A layer of closely spaced palladium nanoparticles is being used in a hydrogen sensor. When hydrogen is absorbed, the palladium nanoparticles swell, causing shorts between nanoparticles. These shorts lower the resistance of the palladium layer.

1.1.3.2.5 Nanomaterial Applications using Carbon Nanotubes

Applications being developed for carbon nanotubes include adding antibodies to nanotubes to form bacteria sensors, making a composite with nanotubes that bend when electric voltage is applied bend the wings of morphing aircraft, adding boron or gold to nanotubes to trap oil spills, include smaller transistors, coating nanotubes with silicon to make anodes the can increase the capacity of Li-ion batteries by up to 10 times.

1.1.3.2.6 Nanomaterial Applications using Nanowires

Applications being developed for carbon nanotubes include using zinc oxide nanowires in a flexible solar cell, silver chloride nanowires to decompose organic molecules in polluted water, using nanowires made from iron and nickel to make dense computer memory - called "race track memory.

1.1.3.2.7 Nanomaterial Applications using Graphene

Applications being developed for graphene include using graphene sheets as electrodes in ultra-capacitors which will have as much storage capacity as batteries but will be able to recharge in minutes, attaching strands of DNA to graphene to form sensors for rapid disease diagnostics, replacing indium in flat screen TVs and making high strength composite materials.

1.2 Cellulose Materials

1.2.1 Basic Concepts

It is widely known that polysaccharides are produced by plants. These are a linear polymer with very long macromolecular chains of one repeating unit, cellobiose. Cellulose is crystalline, infusible and insoluble in all organic solvents [12]. Biodegradation of cellulose proceed by enzymatic oxidation, with peroxides secreted by fungi. Cellulose can also be degraded by bacteria. As for starch degradation products are non-toxic [13]. Cellulose is the most common biopolymer and the common organic compound on Earth and about 33 percent of all plant matter is cellulose. The total cellulose content in cotton is 90 percent and in wood it is 50 percent.

Cellulose esters represent a class of polymers that have the potential to participate in the carbon cycle via microbiologically catalyzed de-esterification and decomposition of the resulting cellulose and organic acids. Cellulose acetate is currently used in high volume applications ranging from fibers, to films, to injection moulding thermoplastics. It has the physical properties and relatively low material costs that have exerted to exclude other biodegradable polymers from being widely accepted in the marketplace.

1.2.2 Microcrystalline Cellulose

Cellulolysis is the process of breaking down cellulose into smaller polysaccharides called cellodextrins or completely into glucose units; this is a hydrolysis reaction. Because cellulose molecules bind strongly to each other, cellulolysis is relatively difficult compared to the breakdown of other polysaccharides. However, this process can be significantly intensified in a proper solvent, e.g. in an ionic liquid.

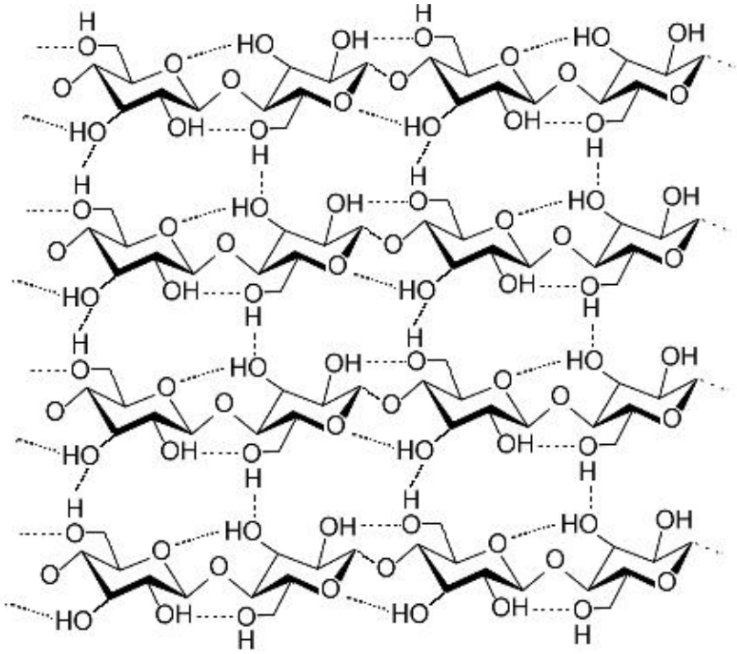

Figure 1.2.2: Structure for micro-crystalline cellulose

1.3 Cellulose /nano Metal Composite

The chemical modification of both components, metal NPs and cellulose matrices, appear a very promising field of research to develop new functional materials. The combination of diverse metal NPs in cellulosic matrices is an important but less exploited strategy to prepare multifunctional composites.

It is well known that the properties of nanocomposite materials depend not only on the properties of their individual components but also on morphological and interfacial characteristics arising from the combination of distinct materials [14]. Therefore, the use of polymers such as cellulose, starch, alginate, dextran, carrageenan, and chitosan among others, gain great relevance not only due to their

renewable nature and biodegradability, but also because a variety of formulations can be exploited depending on the envisaged functionality [15, 16].

This chapter has focus on the use of cellulose as the matrix in the production of nanocomposites. Cellulose has critical importance namely because is the most abundant and widespread biopolymer on Earth. Owing to its abundance and specific properties, it is important noted for the development of environmental friendly, biocompatible, and functional composites, quite apart from its traditional and massive use in papermaking and cotton textiles [17]. Additionally, different types of cellulose are available for the preparation of nanocomposites, namely vegetable cellulose (VC), bacterial cellulose (BC) and nano-fibrillated cellulose (NFC). Although sharing similar chemistry and molecular structure, the different kinds of cellulose show important differences in terms of morphology and mechanical behavior. For example, BC and NFC are composed of fibers with nano-sized dimensions as compared to VC, which might impart new properties, and in some cases improvements to the ensuing nanocomposite materials [18].

There are a variety of metal NPs that can be used as dispersed phases in bio-nano-composites with cellulose. In the last decades there has been great progress in the colloidal synthesis of inorganic NPs. Colloidal metal NPs have received great attention due to their unique optical, electronic, magnetic, antimicrobial properties. Their small size, large specific surface area and tunable physio-chemical properties that differ significantly from the bulk analogues led to intense research on their use in composite materials [19]. This section gives example of research on metal NPs used as fillers in cellulose nanocomposites. The applications of these materials are related with the type of NPs present though new properties arise due to the combined use of the metal NPs and cellulose.

1.3.1 Cellulose/Silver Composite

Nowadays a renewed interest in Ag antimicrobial materials has reappeared mainly due to the increase of multi-drug resistance of microbial strains to conventional antibiotics. The design of protective medical clothing or antibacterial packaging materials are examples of this current trend [25]. Ag NPs are well known by their strong cytotoxicity towards a broad range of microorganisms, such as bacteria and fungi [27].

Similarly, to other applications, well dispersed Ag NPs in the cellulose matrix are required otherwise the antimicrobial effect decreases. However, important parameters such as particle size distribution, metal content, cationic silver release and interaction with the surface of cellulose are also relevant parameters that influence the antimicrobial activity of these nanocomposites [23]. Due to the high water holding capacity and biocompatibility, BC wound dressing materials with improved antimicrobial activity have been prepared using Ag [57]. Other examples include the development of antibacterial food-packaging materials [25, 28], bactericidal paper for water treatment [21] and the study of laundering properties of nanocomposites [24, 29].

The cellulose fibers can be chemically functionalized creating reactive sites in order to control the in situ synthesis of Ag NPs. Few examples are known of composites of NFC and metal NPs [28]. Thus NFC functionalization with fluorescent Ag nanoclusters has been performed by dipping nano-cellulose films into a colloid of Ag protected with poly (methacrylic acid) (PMAA) [64]. The electrostatic assembly of commercial Ag NPs onto NFC mediated by polyelectrolyte linkers have been described as a possible route to scale up the preparation of Ag/NFC composites [20].

Nanostructured metals such Ag and Au are well known substrates for surface enhanced Raman scattering (SERS). Strong enhancement of the Raman signals is observed for certain molecules chemisorbed to the surface of these metals. Therefore, the combined use of these metal NPs and cellulose is of great interest to develop molecular detection and bio-sensing platforms [26]. In this context, the use of cellulose nanocomposites might bring several advantages such as the fabrication of handy and low cost substrates in the form of paper products. A study on the use of distinct cellulosic matrices containing Ag NPs has shown that the BC/Ag nanocomposites were more sensitive as compared to the vegetable analogues, namely in bio-detection of amino acids [26]. The use of filter paper with Ag NPs or Au NPs demonstrate the potential of these materials as SERS platforms to study diverse analytic such as p-hydroxybenzoic [22], single-walled carbon nanotubes [30] and binary mixtures of 9-aminoacridine-acridine and acridine-quinacrine separated by paper chromatography [31].

1.3.2 Cellulose/Gold composite

The noble metal gold has long been a cornerstone precious metal occupying a premier position in the world economy, representing wealth and high value. Traditionally it has been used in its yellow lustrous bulk metallic form for monetary and jewelry applications and over recent decades as an electrical conductor and chemically inert contact material in the electronics industry [32]. Au NPs are among the most studied particles in modern materials science namely due to the number of available methods to produce colloids with uniform particle sizes and well-defined morphologies. Stable Au NPs colloids have been prepared whose particles surfaces are efficiently stabilized by citrate anions in hydrosols or by alkanethiols when organic solvents are used [37].

Cellulose/Au nanocomposites have been used as catalysts in glucose oxidation [33]. It has been reported that good dispersion of Au NPs in cellulose allowed effective contact with reactants making these materials good catalysts for the reduction of 4-nitrophenol. [38] Furthermore, cellulose can be used in several solvents having potential applicability in a variety of reactions. Another interesting possibility is the transformation of renewable biomass resources into valuable chemicals. Selective conversion of cellulose or cellobiose into gluconic acid catalyzed by polyoxometalate- [39] or CNT-supported by Au NPs [40] has been demonstrated. Agglomeration of the Au NPs in the cellulose nanocomposites has been described as a major limitation decreasing the catalytic activity of the composite materials.

Cellulose based sensors have great interest in several applications including in fields as diverse as medical diagnosis, environmental control and food safety. It is important to develop materials that show good electron transfer capability, biocompatibility, stability and easy accessibility towards the analyte. Additionally, large surface area for immobilization of the analytes, rapid response, high sensitivity, good reproducibility and anti-interference are also required characteristics. As expected, it is a great challenge to develop a single material that include all these important characteristics [36].

Cellulose based sensors are inexpensive, disposable, and environmentally friendly. These materials transport liquids via capillary action with no need of external power [41]. BC/Au nanocomposites have been reported to exhibit good

sensitivity, low detection limit and fast response toward hydrogen peroxide making these materials suitable matrices for enzyme immobilization [34-36]. The practical application of these nanocomposites for glucose biosensors in human blood samples has been reported.

The values obtained showed good agreement with corresponding values obtained in hospital trials. The entrapment of Au NPs and enzymes in a paper coating material of sol–gel derived silica has been reported as a versatile material to be used as an entrapment medium and hydrophobic agent. This characteristic allowed more reproducible enzyme loading on rough and non-uniform paper surfaces [41].

Conductive or semi-conductive nanocomposites containing Au NPs are very attractive for electronic applications. Although uniform NPs dispersions are required for many applications, for some cases controlled aggregation issued as an advantage. Electrical conductive cellulose films containing Au NPs have been prepared by self-assembly showing electrically conducting above a gold loading of 20 wt.[37]. The mechanism of electronic conduction in Au NPs-cellulose films is strongly dependent on the resistivity of the film [42].

1.3.4 Cellulose/Copper Composite

Copper NPs were found to be good candidates as efficient catalysts in hydrogen production [49]. An important use for Cu NPs include the fabrication of low electrical resistance materials due to their remarkable conductive properties [50]. In addition, Cu NPs and their oxides show broad spectrum biocide effects and the antimicrobial activity has been reported in studies of growth inhibition of bacteria, fungus, and algae [47]. Antimicrobial nano-coatings of Cu NPs on cellulose have been fabricated via electrostatic assembly [47].

In this process, a chemical pre-treatment step was performed in order to impart surface charge on the cotton substrate that promoted binding of cupric ions, followed by chemical reduction to yield metal nanostructured coatings. The resulting composites showed high effectiveness killing to multi-drug resistant pathogen A. baumannii. Compared to the Ag analogous there was no particle leaching for the copper nanocomposites.

The use of microcrystalline cellulose as a porous natural material supporting copper ions has been demonstrated [43, 46]. Reducing agent and respective amount have critical importance to achieve Cu NPs (or the metal oxides) with controlled particle size. Conversion of CuO into Cu using cellulose as a reducing agent under alkaline hydrothermal conditions was described as a green process for the production of Cu at power low cost [44]. This process gives rise to the conversion of cellulose into value-added chemicals, such as lactic acid and acetic acid. The possibility of modifying the surface of cellulosic fibers and using chitosan has also been reported [45]. In this case, chitosan-attached cellulose fibers were used in the immobilization of Cu ions followed by a reduction step in the presence of borohydride to obtain Cu NPs. Unlike Au e Ag, non-coated Cu NPs oxidize extensively under ambient atmosphere. Although this detrimental effect is limited by incorporating the Cu NPs in bacterial cellulose, stable Cu/cellulose composites have been prepared by using Cu nanowires as inorganic fillers [48]. These nanocomposites are attractive for the emerging technologies based on electronic paper.

1.3.5 Cellulose/Platinum composite

Platinum is an useful material for numerous industrial catalytic applications and several reports have described the synthesis of Pt NPs using a variety of methods [51]. This metal is also considered the best electro-catalyst for the four-electron reduction of oxygen to water in acidic environments as it provides the lowest over potential and the highest stability [57]. The preparation of Pt/cellulose nanocomposites generally involves the reduction of ionic Pt by addition of a reducing agent ($NaBH_4$, HCHO,) in the presence of cellulose, which might act as a structural-directing agent [54].

Nanocomposites of Pt and amorphous carbon films were obtained by the catalyzed carbonization of cellulose fibers [55]. This type of NPs has been synthesized using $NaBH_4$ as reducing agent in hydrothermal conditions in the presence of nanoporous cellulose [54]. The Pt NPs were well dispersed and stabilized in the cellulose network thus avoiding particle aggregation. Cationic cellulose bearing ammonium ions at the surface has also been used to produce this type of nanocomposites [53]. In this method, the attachment of negatively charged Pt NPs onto cationic cellulose substrates was promoted via electrostatic interactions, which result into high surface coverage of the fibers.

Thermally stable proton-conducting membranes have been prepared by the in situ deposition of Pt NPs on BC membranes, via liquid phase chemical deoxidization method in the presence of the reducing agents $NaBH_4$ or HCHO [57]. The obtained black nanocomposite has been reported to display high electro-catalytic activity, with good prospects to be explored as membranes in fuel cell field [56]. However, in case of Pt/cellulose nanocomposites, the reducing groups of cellulose are less effective in the reduction of metal precursors. A supercritical CO2/ water system for reducing H_2PtCl_6 precursor to PtNPs using suspended crystalline cellulose nano-fibrils of cotton has been described [51]. In this methodology VC was employed in a direct reduction route to form cellulose/Pt nanocomposites using a renewable reducing agent. The same authors have reported the use of cellulose nanocrystals (large surface area per unit weight in relation to normal cellulose fibers) for the same purpose. In this alternative the reaction temperature can be lowered to achieve Pt NPs with an average diameter of approximately 2 nm and with narrow particle size distribution [52].

The incorporation of irregularly shaped Pt NPs dispersed in IL and cellulose acetate lead to a nanocomposite that exhibits synergistic effects in the activity and durability enhancement of the catalyst [58]. The authors have suggested that the presence of IL caused higher separation of the cellulose macromolecules which result in a higher flexible and lower viscous material. The ensuing nanocomposites displayed higher catalytic activity and stability when compared to the Pt NPs dispersed in the IL. Potential uses of cellulose/Pt nanocomposites in catalysis comprise the hydrogenation of cyclohexene [58] and hydrogen production [59].

1.3.6 Cellulose/Cobalt composite

Co NPs in cellulose matrices has been a topic of interest due to the potential application as magnetic nanocomposites. However, due to easy oxidation their use has been associated to the formation of metal alloys such as FeCo. The properties of magnetic Co NPs are determined in large extent by surface atoms. In addition, crystallinity, size distribution, particles shape and neighboring particles, affect the response of the material when submitted to a magnetic field. Therefore, the matrix in which the NPs are embedded, in this case cellulose, has strong influence on the magnetic properties of the NPs as well as the distance between them [60].

The structure and morphology of Co NPs synthesized in cellulose matrix and resulting magnetic properties have been reported [60]. The authors have used two distinct chemical routes to investigate the effect on the structural properties of the NPs. In the borohydride reduction amorphous Co–B or co-oxide composites were obtained in which a detrimental effect on the magnetic properties was observed as compared to bulk Co. In contrast, using a NaH_2PO_2 reduction method, well-ordered ferromagnetic cobalt nanocrystals were obtained in which the magnetic properties of the samples resemble those of bulk cobalt.

1.3.7 Cellulose Metal alloys

The properties of metallic systems can be significantly varied by blending the metal components into intermetallic compounds and alloys. The diversity of compositions, structures, and properties of metallic alloys not only can originate new properties but might also improve certain properties of the metal components due to synergistic effects [62]. The association of metal alloys (typically bimetallic) to cellulose yields interesting materials with well-defined, controllable properties and structures on the nanometer scale coupled with easier processing capability of the matrix. A tubular FeCo bimetallic nanostructure was obtained by using a cellulose/cobalt hexacyanoferrate (Fe–CN–Co) composite material as precursor [63]. The metal was then deposited onto a cellulose template via H2 gas-phase reduction that converted the precursor in FeCo bimetallic NPs. The FeCo NPs formed hollow tubular structures that mimic the original precursor composite morphology via a template-direct assisted method.

Lightweight porous magnetic aerogels made of nano-fibrils of VC and BC have been compressed into a stiff magnetic nano-paper [61]. The thick cellulose fibrils act as templates for the growth of discrete ferromagnetic cobalt ferrite NPs forming a dry, lightweight, porous and flexible magnetic aerogel with potential application in microfluidics devices and as electronic actuators. PdCu/BC nanocomposites showing high catalytic activity have been obtained, in which the PdCu NPs were homogeneously and densely precipitated at the surface [63]. Although the cost of these materials need to be considered, these composites are of potential interest in water remediation processes because the Pd Cu alloy is considered the best catalyst for the denitrification of polluted water.

1.4 Adsorption Phenomena

1.4.1 Adsorption

Adsorption is a surface phenomenon. It may be defined as a process in which the concentration of a chemical species is greater in the surface than in the bulk resulting from inelastic collision suffered by molecules on the surface. The species that is absorbed is called adsorbate and the material of the surface on which adsorption takes place is called adsorbent. Adsorption strictly refers to accumulation of adsorbates on the surface only due to residual field of force.

The adsorption surface is generally a solid or liquid. Surface of solid or liquids have certain properties and characteristic that makes them different from the bulk of matter. Although there is no chemical distinction between the molecules or atoms on the surface and the molecules or atoms in the bulk, energy considerations lead to quite dissimilar properties. When two immiscible and chemically non-reactive phases are brought into contact with each other, adsorption is a common observation, which means that the concentration of one phase is greater at the interface than the bulk. This occurs due to unsaturation of the surface atoms. Most studies of the adsorption from solution have been concerned with equilibrium conditions and predominantly with the adsorption isotherm. Generally, two types of adsorption have been distinguished: (a) Physical adsorption (Physisorption) and (b) Chemical adsorption (chemical adsorption). Physical adsorption results purely from physical forces like van der Waals forces and chemical adsorption is due to formation of chemical bonds.

There are three adsorption isotherms known as which are used most frequently.

1.4.2 Langmuir adsorption isotherm

Langmuir derived a relation between gas pressure and amount of gas adsorbed at a constant temperature. The Langmuir equation can be written as

$$X = \frac{X_m bp}{(1 + bp)}$$

$$\frac{1}{X} = \frac{1}{X_m bp} + \frac{1}{X_m}$$

Where X = amount adsorbed at a defined concentration, $X_m = k_1 + k_2$,
k_1 and k_2 are the rate constant for the adsorption and desorption, respectively, b = constant and p = pressure.

1.4.3 Freundlich adsorption isotherm

The variation of adsorption with concentration of the substance in solution is usually represented by Freundlich isotherm as follows:

$$y = kC^{\frac{1}{n}}$$

taking log in both side of the above equation, we get the following:

$$\log y = \log k + \frac{1}{n} \log c$$

Where, y = mass of substance per unit mass of adsorbent, C = equilibrium concentration of solid in solution, k and n are the empirical constants

1.4.4 Factor affecting adsorption

A. **Temperature**

The level of adsorption at any particular concentration decreases with the increase in temperature; that is the overall process is exothermic. At higher temperature the adsorbed molecules have greater vibrational energies and therefore, more likely to desorb from the surface.

B. **Nature of the solvent**

The solvent has an important effect, since it computes with the surface of the absorbent in attracting the solute. There are three different ways to describe the influence of solvent on absorption behavior of the solvent: (a) its interaction with the solute in solution (b) its interaction with the absorbed layer, and (c) its interaction with the solute in the absorbed layer. However, when the solvent is water, it is worthless to consider the solvent effect.

C. Particle and pore size

The adsorption efficiency increases as mean diameter of the particle decreases. Large surface area is available for adsorption with the small particles. Another reason is the reduced diffusive path length of the interior of small adsorbent particles and the adsorbate particles require less energy of jump from one active site to another, resulting in higher uptake by the adsorbent.

D. pH of the solution

The effect of pH is extremely important when the adsorbing species is capable of ionizing in response to prevailing pH. It is well known that substances absorb poorly when they are ionized. When the pH is such that an adsorb able to compound exists in ionic form, adjacent molecules of the adsorbed species on the absorbent surface will repel each other to a significant degree, because they carry the same electrical charges. Thus the adsorbing species cannot be packed together very densely on the surface. This is the common observation that non-ionized form of acidic and the basic compounds adsorb much better than their ionized counterparts. The acidic species thus adsorb better at low pH and basic species adsorb better at high pH.

1.4.5 Adsorption from solution

Adsorption from solution is much simpler than that of gas adsorption. A known mass of adsorbent is kept in touch with a known volume of solution at a given temperature until there is no further change in the concentration of the supernatant solution. This concentration can be determined by a variety of methods involving chemical or radiochemical analysis such as colorimetry, refraction index, etc. The experimental data are usually expressed in terms of an

apparent adsorption isotherm in which the amount of solute adsorbed at a given temperature per unit mass of adsorbents calculated from the decreases of solution concentration is plotted against the equilibrium concentration. By analogy with the gas adsorption, one might hope to calculate the monolayer capacity, the application of an equation of the individual isotherm has a pattern of a sharp knee followed by a clear plateau; the monolayer capacity is then given by the height of the plateau.

1.5 Antibacterial Activities:

Infectious diseases still represent an important cause of morbidity and mortality among humans especially in developing countries. Even though pharmaceutical industries have produced a number of new anti-microbial drugs in the last years, resistance to these drugs by microorganism has increased. Bactericidal nanomaterials, particularly metallic nano particles, opened a new avenue in medical science. Appropriate antimicrobial drug use has unquestionable benefit, but physicians and the public frequently use these agents inappropriately. Inappropriate use results from physicians providing antimicrobial drugs to treat viral infections, using inadequate criteria for diagnosis of infections that potentially have a bacterial etiology, unnecessarily prescribing expensive, broad-spectrum agents, and not following established recommendations for using chemo prophylaxis. The availability of antibiotics over the counter, despite regulations to the contrary, also fuel inappropriate usage of antimicrobial drugs in India. The easy availability of antimicrobial drugs leads to their incorporation into herbal or "folk" remedies, which also increases inappropriate use of these agents.

Widespread antibiotic usage exerts a selective pressure that acts as a driving force in the development of antibiotic resistance. The association between increased rates of antimicrobial use and resistance has been documented for nosocomial infections as well as for resistant community acquired infections. As resistance develops to "first-line" antibiotics, therapy with new, broader spectrum, more expensive antibiotics increases, but is followed by development of resistance to the new class of drugs.

The bactericidal effect of silver nanoparticles on the micro-organisms is very well known. In this study, antibacterial effect of Mn_3O_4 and cellulose/Mn_3O_4 has tasted.

1.5.1 Bacteria

Bacteria are single celled microbes. The cell structure is simpler than that of other organisms as there is no nucleus or membrane bound organelles. Instead their control center containing the genetic information is contained in a single loop of DNA. Some bacteria have an extra circle of genetic material called a

plasmid. The plasmid often contains genes that give the bacterium some advantage over other bacteria. For example, it may contain a gene that makes the bacterium resistant to a certain antibiotic.

Bacteria are found in every habitat on Earth: soil, rock, oceans and even arctic snow. Some live in or on other organisms including plants and animals including humans. There are approximately 10 times as many bacterial cells as human cells in the human body. A lot of these bacterial cells are found lining the digestive system. Some bacteria live in the soil or on dead plant matter where they play an important role in the cycling of nutrients. Some types cause food spoilage and crop damage but others are incredibly useful in the production of fermented foods such as yoghurt and soy sauce. Relatively few bacteria are parasites or pathogens that cause disease in animals and plants.

1.5.2 Types of Bacteria

There are two main groups, the bacteria and the cyanobacteria. Bacteria include all of the commonly known species such as Escherichia coli (E. coli bacteria), Salmonella bacteria, Staphylococci, Listeria and the Clostridia. Cyanobacteria form a separate type of bacteria that are able to photo synthesis– they can also be called blue-green algae.

Cyanobacteria still exist in large numbers today but their importance in the development of life on Earth is due to their existence here millions of years ago. Cyanobacteria were very successful and grew everywhere. Their ability to photo synthesis created all the oxygen that is in our atmosphere today. Most living organisms today depend on oxygen and without cyanobacteria, it is very unlikely that this life would have evolved.

There are seven main groups of bacteria, distinguished by their shape and the type of cell wall they possess. Four of the seven types make up the majority of all bacteria:

I. Gram positive cocci
II. Gram negative cocci
III. Gram positive bacilli
IV. Gram negative bacilli

Cocci are spherical cells, bacilli are rod-shaped. Bacteria of either shape that have thick cell walls are termed gram positive because of the way they take up the Gram stain. Those with thin cell walls are termed gram negative.

1.5.2.1 Gram Positive Bacteria

The gram positive cocci include the well-known species Staphylococcus and Streptococcus. Bacteria from both species fall into the category of friendly bacteria; they do no harm and perform useful functions in the human body and in the environment. Some species can also be pathogenic. Staphylococcus aureus can cause impetigo and scalded skin syndrome, food poisoning and toxic shock syndrome. Streptococcus pyogenes is the culprit usually responsible for tonsillitis and severe sore throats (‘strep throat’), but it can cause many other infections.

Gram positive bacilli include Corynebacterium diphtheriae, which causes diphtheria, Listeria monocytogenes, found in unpasteurized dairy products and responsible for dangerous infectious in pregnant women, and bacteria from the species Lactobacillus, friendly bacteria found in the gut.

This group also includes two of the most dangerous types of bacteria known to humans. One is the Bacillus species that causes anthrax, and the other is Clostridium. One Clostridium species causes tetanus, another leads to botulism, a deadly form of food poisoning.

1.5.2.2 Gram Negative Bacteria

There are two main types of gram negative cocci, both belonging to the genus Neisseria. Neisseria meningitidis causes a form of meningitis, Neisseria gonorrhoeae causes the sexually transmitted infection gonorrhae. The two species are more commonly called the meningococcus and the gonococcus.

Gram negative bacilli are a large and varied group that are subdivided into several further categories. The Enterobacteria include many species that cause food poisoning in humans – E. coli, Salmonella, Shigella, Proteus, and also the plague bacterium Yersinia pestis. The Vibrio group contain bacteria that are shaped more like commas than rods – and include the bug that is responsible for cholera.

Helicobacter pylori (H. pylori) is also a gram negative bacillus. This bacterium has been identified in the last 25 years as a major cause of stomach ulcers.

Other gram negative bacilli are Haemophila influenzae, which causes pneumonia, Bordetella pertussis, which causes whooping cough, and Brucella bacteria, which are associated with brucellosis in cattle.

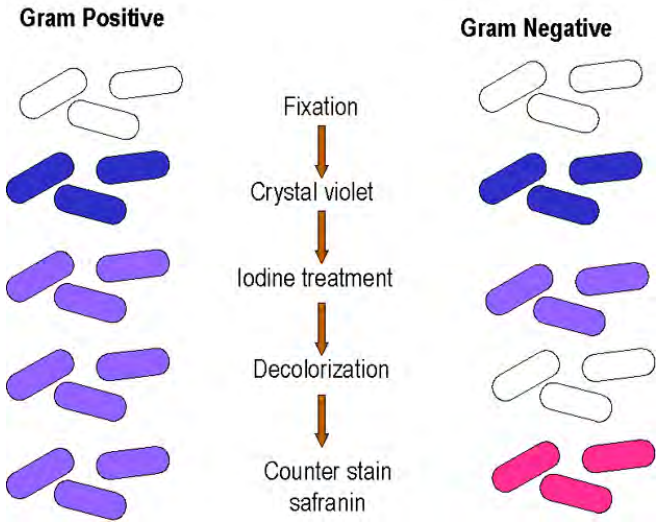

Figure 1.5.2: Difference between gram-positive and Gram-negative bacteria

1.5.3 Susceptibility Testing

Antibiotic sensitivity is the susceptibility of bacteria to antibiotics. Antibiotic susceptibility testing (AST) is usually carried out to determine which antibiotic will be most successful in treating a bacterial infection in vivo.

1.5.3.1 Factors Influencing Antimicrobial Susceptibility Testing:

A. pH

The pH of each batch of Müeller-Hinton agar should be checked when the medium is prepared. The exact method used will depend largely on the type of equipment available in the laboratory. The agar medium should have a pH between 7.2 and 7.4 at room temperature after gelling. If the pH is too low, certain drugs will appear to lose potency (e.g., aminoglycosides, quinolones, and macrolides), while other agents may appear to have excessive activity (e.g.,

tetracyclines). If the pH is too high, the opposite effects can be expected. The pH can be checked by one of the following means:

a) Macerate a sufficient amount of agar to submerge the tip of a pH electrode.

b) Allow a small amount of agar to solidify around the tip of a pH electrode in a beaker or cup.

c) Use a properly calibrated surface electrode.

B. Moisture

If, just before use, excess surface moisture is present, the plates should be placed in an incubator (35°C) or a laminar flow hood at room temperature with lids ajar until excess surface moisture is lost by evaporation (usually 10 to 30 minutes). The surface should be moist, but no droplets of moisture should be apparent on the surface of the medium or on the petri dish covers when the plates are inoculated.

C. Effects of Thymidine or Thymine

Media containing excessive amounts of thymidine or thymine can reverse the inhibitory effect of sulfonamides and trimethoprim, thus yielding smaller and less distinct zones, or even no zone at all, which may result in false-resistance reports. Müeller-Hinton agar that is as low in thymidine content as possible should be used. To evaluate a new lot of Müeller-Hinton agar, Enterococcus faecalis ATCC 29212, or alternatively, E. faecalis ATCC 33186, should be tested with trimethoprim/sulfamethoxazole disks. Satisfactory media will provide essentially clear, distinct zones of inhibition 20 mm or greater in diameter. Unsatisfactory media will produce no zone of inhibition, growth within the zone, or a zone of less than 20 mm.

D. Effects of Variation in Divalent Cations

Variation in divalent cations, principally magnesium and calcium, will affect results of aminoglycoside and tetracycline tests with P. aeruginosa strains. Excessive cation content will reduce zone sizes, whereas low cation content may result in unacceptably large zones of inhibition. Excess zinc ions may reduce zone

sizes of carbapenems. Performance tests with each lot of Müeller-Hinton agar must conform to the control limits.

E. Testing strains that fail to grow satisfactorily

Only aerobic or facultative bacteria that grow well on unsupplemented Müeller-Hinton agar should be tested on that medium. Certain fastidious bacteria such as Haemophilus spp., N. gonorrhoeae, S. pneumoniae, and viridans and ß-haemolytic streptococci do not grow sufficiently on unsupplemented Müeller-Hinton agar. These organisms require supplements or different media to grow, and they should be tested on the media described in separate sections.

1.5.3.2 Methods of Antimicrobial Susceptibility Testing

Antimicrobial susceptibility testing methods are divided into types based on the principle applied in each system. They include:

Diffusion	Dilution	Diffusion & Dilution
Stokes method	Minimum Inhibitory Concentration	E-Test method
Kirby-Bauer method	I. Broth dilution II. Agar Dilution	

1.5.4 Disk Diffusion

1.5.4.1 Reagents for the Disk Diffusion Test

Müeller-Hinton Agar Medium

Of the many media available, Müeller-Hinton agar is considered to be the best for routine susceptibility testing of non fastidious bacteria for the following reasons:

a) It shows acceptable batch-to-batch reproducibility for susceptibility testing.

b) It is low in sulphonamide, trimethoprim, and tetracycline inhibitors.

c) It gives satisfactory growth of most nonfastidious pathogens.

d) A large body of data and experience has been collected concerning susceptibility tests performed with this medium.

Although Müeller-Hinton agar is reliable generally for susceptibility testing, results obtained with some batches may, on occasion, vary significantly. If a batch of medium does not support adequate growth of a test organism, zones obtained in a disk diffusion test will usually be larger than expected and may exceed the acceptable quality control limits. Only Müeller-Hinton medium formulations that have been tested according to, and that meet the acceptance limits described in, NCCLS document M62-A7- Protocols for Evaluating Dehydrated Müeller-Hinton Agar should be used.

Preparation of antibiotic stock solutions

Antibiotics may be received as powders or tablets. It is recommended to obtain pure antibiotics from commercial sources, and not use injectable solutions. Powders must be accurately weighed and dissolved in the appropriate diluents (Annexure III) to yield the required concentration, using sterile glassware. Standard strains of stock cultures should be used to evaluate the antibiotic stock solution. If satisfactory, the stock can be aliquoted in 5 ml volumes and frozen at -20ºC or -60ºC.

Storage of commercial antimicrobial discs

Cartridges containing commercially prepared paper disks specifically for susceptibility testing are generally packaged to ensure appropriate anhydrous conditions. Discs should be stored as follows:

[1] Refrigerate the containers at $8^{o}C$ or below, or freeze at $-14^{0}C$ or below, in a nonfrost-free freezer until needed. Sealed packages of disks that contain drugs from the ß-lactam class should be stored frozen, except for a small working supply, which may be refrigerated for at most one week. Some labile agents (e.g., imipenem, cofactor, and clavulanic acid combinations) may retain greater stability if stored frozen until the day of use.

[2] The unopened disc containers should be removed from the refrigerator or freezer one to two hours before use, so they may equilibrate to room temperature before opening. This procedure minimizes the amount of condensation that occurs when warm air contacts cold disks.

[3] Once a cartridge of discs has been removed from its sealed package, it should be placed in a tightly sealed, desiccated container. When using a disc-dispensing apparatus, it should be fitted with a tight cover and supplied with an adequate desiccant. The dispenser should be allowed to warm to room temperature before opening. Excessive moisture should be avoided by replacing the desiccant when the indicator changes color.

[4] When not in use, the dispensing apparatus containing the discs should always be refrigerated.

[5] Only those discs that have not reached the manufacturer's expiration date stated on the label may be used. Discs should be discarded on the expiration date.

Application of Discs to Inoculated Agar Plates

[1] The predetermined battery of antimicrobial discs is dispensed onto the surface of the inoculated agar plate. Each disc must be pressed down to ensure complete contact with the agar surface. Whether the discs are placed individually or with a dispensing apparatus, they must be distributed evenly so that they are no closer than 24 mm from center to center. Ordinarily, no more than 12 discs should be placed on one 150 mm plate or more than 5 discs on a 100 mm plate. Because some of the drug diffuses almost instantaneously, a disc should not be relocated once it has come into contact with the agar surface. Instead, place a new disc in another location on the agar.

[2] The plates are inverted and placed in an incubator set to 35^0C within 15 minutes after the discs are applied. With the exception of Haemophilus spp., streptococci and N. gonorrhoeae, the plates should not be incubated in an increased CO2 atmosphere, because the interpretive standards were developed by using ambient air incubation, and CO2 will significantly alter the size of the inhibitory zones of some agents.

Reading Plates and Interpreting Results

[1] After 16 to 18 hours of incubation, each plate is examined. If the plate was satisfactorily streaked, and the inoculum was correct, the resulting zones of inhibition will be uniformly circular and there will be a confluent lawn of growth. If individual colonies are apparent, the inoculum was too light and the test must be repeated. The diameters of the zones of complete

inhibition (as judged by the unaided eye) are measured, including the diameter of the disc. Zones are measured to the nearest whole millimeter, using sliding calipers or a ruler, which is held on the back of the inverted petri plate. The petri plate is held a few inches above a black, nonreflecting background and illuminated with reflected light. If blood was added to the agar base (as with streptococci), the zones are measured from the upper surface of the agar illuminated with reflected light, with the cover removed. If the test organism is a Staphylococcus or Enterococcus spp., 24 hours of incubation are required for vancomycin and oxacillin, but other agents can be read at 16 to 18 hours. Transmitted light (plate held up to light) is used to examine the oxacillin and vancomycin zones for light growth of methicillin- or vancomycin- resistant colonies, respectively, within apparent zones of inhibition. Any discernable growth within zone of inhibition is indicative of methicillin or vancomycin resistance.

[2] The zone margin should be taken as the area showing no obvious, visible growth that can be detected with the unaided eye. Faint growth of tiny colonies, which can be detected only with a magnifying lens at the edge of the zone of inhibited growth, is ignored. However, discrete colonies growing within a clear zone of inhibition should be sub-cultured, re-identified, and retested. Strains of Proteus spp. may swarm into areas of inhibited growth around certain antimicrobial agents. With Proteus spp., the thin veil of swarming growth in an otherwise obvious zone of inhibition should be ignored. When using blood-supplemented medium for testing streptococci, the zone of growth inhibition should be measured, not the zone of inhibition of hemolysis. With trimethoprim and the sulfonamides, antagonists in the medium may allow some slight growth; therefore, disregard slight growth (20% or less of the lawn of growth), and measure the more obvious margin to determine the zone diameter.

1.6 Literature Survey and Aim of the Present Work

Nano particle have been a source of great interest due to their nobel electrical, optical, physical chemical and magnetic properties. They have significant potential for a wide range of application such as catalysis, magnetic recording media, optoelectronic materials, magnetic fluids, composite materials, fuel cells, pigments and sensors. Their uniqueness arises from their high ratio of surface area to volume (aspect ratio), as these materials typically have diameters of 100 nm or less [64]. Nanophase metals and metal oxide with controlled particle size and shape, exhibit high surface and density populated unsaturated surface coordination sites that can result in significantly improved performance over conventional one [65-68]

There are several reports of physical/chemical processes for the production of nanoparticles in technical literature. Nanoparticles prepared by physical methods such as vapour deposition and spluttering are of high quality, i.e., they possess clean surface and uniform particle size distribution. However, industrial application for such particles is limited due low production rate and high cost. Alternative chemical production methods, such as thermal decomposition and precipitation are currently being studied for the preparation of a wide range of nanoparticles [65].

Cellulose on the other hand is abundant in nature, renewable, biodegradable and has good mechanical properties [69]. Therefore, it is an interesting material to consider as nano-reinforcement. There are two different types of nano-reinforcements that can be obtained from cellulose fibers micro-fibrils and nano-whiskers [70]. In plants or animals, the cellulose chains are synthesized to form micro-fibrils. These are bundles of molecules that are elongated and stabilized through hydrogen bonding [70]. One micro-fibril contains multiple elementary fibrils which are made up of multiple cellulose chains. These elementary fibrils have a diameter of around 2–20 nm depending on its origin [70]. The elementary fibril is made up of amorphous and crystalline parts [70]. The crystalline parts can be isolated by various treatments and these are the cellulose nano-whiskers [70]. As early as fifty years ago Ranby reported a process using acid hydrolysis that could separate cellulose whiskers from cellulose elementary fibrils [71]. It is thought that these whiskers have mechanical strength that corresponds to the

binding forces of neighboring atoms [70]. As a result cellulose whiskers have far better mechanical properties than a majority of the commonly used reinforcement materials. During the 1990s the research in this area accelerated. Today, it has been possible to isolate cellulose nano-whiskers from different sources like, tunicates[71-75], wheat straw [76] and bacteria [77]. These whiskers have been incorporated into a number of different matrixes like for example, cellulose acetate butyrate [76], poly(hydroxyalkanoates) [72], poly(lactic acid) [78], poly(oxyethylene) [75], poly(vinyl chloride) [71] and starch [73, 74]. Today, cellulose nanowhiskers are not commercially available, instead microcrystalline cellulose (MCC) which is a closely related item is commercially available. MCC is particles of hydrolyzed cellulose consisting of a very large amount of cellulose microcrystals together with amorphous areas, used as a thickening agent in pharmaceuticals.

As an adsorbent, cellulose is employed for the treatment of textile mill waste water to remove dyes or pigments [79]. This most abundant polymer is used as a raw material for many products in paper and textile industries and its derivatives find new applications in the pharmaceuticals industry in the drag delivery devices [80]. The dyeing of cellulose and cellulose materials is also of great interest in paper and textile industries. The investigation of dye adsorption on such materials is of fundamental importance for the understanding of the dyeing mechanism in the production of textile materials. The adsorption of dye in charged solids is an associated field of study [81]. Davidson has worked on the adsorption of methylene blue on ox-cellulose prepared by the action of alkaline hypobromite on cotton; the dye has the high affinity for the carboxyl group of the polymers [82].

Porous carbon materials have attracted significant attraction [81-84] for diversified applications including pollutant removal/ remediation, because of their high surface area, high porosity, adsorption capacity and excellent thermal /chemical stability. Among various fabrication procedure of carbon monoliths, of interest is the pyrolysis of a carbon rod produced from the polymerization of a resorcinol-formaldehyde copolymer on silica particle templates with iron serving as the catalyst for localized carbonization [86,87]. The resulting polymer can be doped with a metallic salt, in turn forming encapsulated metallic nanoparticles during the course of carbonization. Such nanoparticles play an an important role

in the conversation of a fraction of amorphous carbon monoliths by chemical/acid etching.

Nickel oxide and material based on this compound possesses valuable dialectic, semiconducting, magnetic and catalytic properties. They are used as electrode material [89-90], heterogeneous catalyst [91-92] and materials for active units of gas sensors [92-93]. Film of nickel oxides can find application in electrochromic devices [94-96]. High performance ultrahigh-frequency insulators are being development on this basis of complex oxides of cobalt and nickel [97]

Nano scale oxide particles of transition metals are gaining continues importance for various applications such as catalysis, passive electronic components and ceramic materials [98]. Due to their small size, nano particles exhibits novel material properties that are significantly different from those of their bulk counterparts. Nickel oxide nano particles with a uniform size and well dispersions are desirable for many applications in designing ceramic, magnetic, electrochromic and heterogeneous catalytic materials [99].

Nanostructure NiO has many applications in a wide range of area such as catalysis [100], electrochromic films [101], fuel cell electrodes [102], gas sensors [103], but there has been limited studies on heterogeneous catalysts and photocatalytic processes [104]. There are different methods reported for the synthesis of NiO nanoparticles such as hydrothermal or solvo-thermal synthesis [105-106], pulsed laser ablation [107] micro emulsion [108] precipitation-calcination [109], sonochemical [110-111] and sol-gel methods [112]. Particularly significant is hydrothermal synthesis as a well-known method for preparation of microporous crystals, complex oxides and inorganic hybrid materials [113].

Nickel oxide/graphene oxide (NiO/GO) nanocomposite was prepared by a hydrothermal method combining a subsequent calcination process, and investigated by X-ray diffraction (XRD), Raman spectrometer (Raman), high resolution transmission electron microscopy (HRTEM), selected area electron diffraction (SAED) and X-ray photo-electron spectroscopy (XPS) methods. The application of NiO/GO can be exploited by the removal of MD from aqueous solution through coupled adsorption and photocatalysis process A combined

system of photocatalysis and adsorption is established for simultaneous removal of MB from aqueous solution using nanocomposite. Effects of nanocomposite dose, pH and contact time on removal of MB were also investigated.

Wang et al. reported fabrication of hollow spheres and thin films of nickel hydroxide and nickel oxide with hierarchical structures using styrene-acrylic acid copolymer (PSA) latex particles as template [114]. Yang et al. prepared hierarchical β-$Ni(OH)_2$ and NiO carnations assembled from nano sheet building blocks via a hydrothermal method in mixed solvents of water and glycerol [115]. Zhu et al. synthesized three dimensional (3D) flower like hierarchical β-$Ni(OH)_2$ hollow architecture by facile hydrothermal route in mixed solvents of water and ethanol. Furthermore, the feasibility of $Ni(OH)_2$ and NiO nanoparticles for their for their application in water treatment is also reported and evaluated [115,116].

Farzaneh and Asgarpour [119] prepared nickel-chitosan hybrid, hydrothermally using $Ni(CH_3COO)_2, 4H_2O$, chitoran and waster as starting material, template and solvent respectively, followed by calcination at appropriate temperature in order to prepare nonoporous NiO. Congo red and methylene blue as cationic and anionic dyes served as model dyeing pollutant to evaluate the adsorption and photocatalytic degradation activity of the prepared catalysis.

Mn_3O_4 is a promising electrochromic material of anodic coloration since It has a reversible color change from brown (colored state) to yellow (bleached state) [120]. Mn_3O_4 is also known to be active catalyst in several oxidations or reductions, for example it can be used as catalyst for oxidation of methane and carbon monoxide [121] or the selective reduction of nitrobenzene [122]. Moreover, Mn_3O_4 with different polymorphs has been found to be active as stable catalyst for the combustion of organic compounds in the temperature range of 3773-773 K [123]. These combustions related catalytic technologies are of interest on relation to several air-pollution problems, allowing limitation of the emission of NOx and volatile organic compounds from waste gases of different origins [124].

Manganese oxides are also powerful oxidants due to their high reducing potential. It has already been reported that Mn^{3+} and Mn^{4+} oxides and hydroxides can oxidize many inorganic compounds including Co(II), Cr(III),

As(III), Sb(III) and Se(IV) [125-129] and also a variety –natural and xenobiotic organic compounds such as catechol, quinies, substituted phenols, aromatic amines, pesticides and explosives (e.g., TNT) [130-134]. Mn_3O_4 (hausmannite) is a complex oxide of Mn containing both di- and tri- valent manganese.

Bactericidal nanomaterials particularly metallic nanoparticles, exhibits great opportunity in medicinal science. The bactericidal effect of nano manganese oxide on the micro-organism is very well known. In this study , the aim is to explore the antibacterial activities of cellulose by modifying it with active nano manganese oxide.

ZnO nanorods coated paper matrices were used to study antibacterial activity against E. coli by the zone of inhibition method. The paper matrices showed an enhanced antibacterial activity in the presence of visible light compared to the dark. Khatri et al. reported the incorporation of saccha- ride $\text{capped} - \text{ZnO}$ nanoparticles in paper matrices and studied the antimicrobial activities as well as antibody immobilization [135]. The saccharide $\text{capped} - \text{ZnO}$ nanoparticles were synthesized by a microwave assisted method using carbohydrates.

Antimicrobial agents are applied on clothing and household textiles primarily to act against skin diseases, to prevent odor generation, and to hinder fabric discoloration [136]. The agent should ideally act against a broad spectrum of microbes and maintain adequate activity levels through multiple cleaning (i.e. laundering) cycles.

Eaning (i.e. laundering) cycles, prompted by the emergence of antibiotic-resistant microbes, there is a resurgence in the use of silver as antimicrobial agent [137]. Silver is effective against a broad spectrum of microorganisms (yeast, fungi, viruses, bacteria) [138], and is ‘oligodynamic’ [139] i.e. active in very small quantities.

So the aims of the present studies are –

[1] To prepare nano Nickel Oxide and nano Manganese oxide by precipitation and forced hydrolysis method.

[2] The dispersion of nps and MCC will be utilized in order to fabricate Mn_3O_4/MCC and NiO/MCC matrices.

[3] The structural and morphological analysis of nano NiO, nano Mn_3O_4, nano NiO/MCC, MCC and NiO/MCC, MCC and nano Mn_3O_4/MCC will be performed with FIIR,XRD,SEM and EDX techniques.

[4] The adsorption of MB on nano NiO, Nano NiO/MCC and MCC will be studied. The extent of dye removal by the nano NiO, nano NiO/MCC and MCC matrices will be monitored by UV-Vis spectroscopic means.

[5] Routine antibacterial responses of the nano Mn_3O_4 and nano Mn_3O_4 /MCC will be examined following the standard conventional method by treating yhr matrices suspensions to various pathogenic organisms at different pH.

Chapter 2
EXPERIMENTAL

2.1 Materials and Devices

2.1.1 Chemicals

The chemicals and reagent used in this work are listed below . These are analytical grade and used without further purification. Double distilled water was used as solvent to prepare most of the solution of this work.

I. Nickel Nitrate [Merck, India]
II. Nickel Chloride [Merck, India]
III. Urea [E.Merck, Germany]
IV. Ammonium bicarbonate [Merck, India]
V. Ammonium carbonate [Merck, India]
VI. Microcrystalline cellulose [E.Merck, Germany]
VII. Mn(II)acetate [Merck, India]
VIII. Sulphuric acid [E.Merck, Germany]
IX. Hydrochloric acid (37% Extra Pure) [E.Merck, Germany]
X. Acetone (Extra Pure) [E.Merck, Germany]
XI. Methylene blue [E.Merck, Germany]

2.1.2 Instruments

Analysis of the samples performed in this work employed the following devices:

I. Fourier Transform InfraRed spectrophotometer (Perkin Elmer, USA, and Model: Frontier FT-NIR/MIR)
II. UV-visible spectrophoto meter (UV-Vis) [UV-1601 PC, Shimadzu, Japan)
III. Scanning electron microscope (model JEOL JSM1600F, Japan)
IV. X-raydiffractometer [Philips, Expert Pro, Holland]
V. Centrifuge machine [Hermle,2200A , Germany]
VI. pH meter [Hanna , pH209, India]
VII. Shaker machine [Heidolph Unimax 1010]
VIII. Digital balance, [FR-200,Japan]
IX. Furnace [DK, England]

2.2 Preparation of Materials

2.2.1 Synthesis of *NiO nano* particles

The formation of metastable nickel precursor precipitates and the subsequent transformation to NiO by thermal treatment. The nickel precursor precipitates have been prepared by various methods, including the precipitation of $NiCl_2$ or $NiSO_4$ with $Na_2C_2O_4$, $(NH)_2CO$ or NaOH [140, 141], the decomposition of bis-cycloocta-1,5-diene nickel in the presence of water and dioxygen[142] etc. in these experiment nano NiO is prepared by air calcination of $Ni(OH)_2$. $NiCO_3$. x H2O [143]

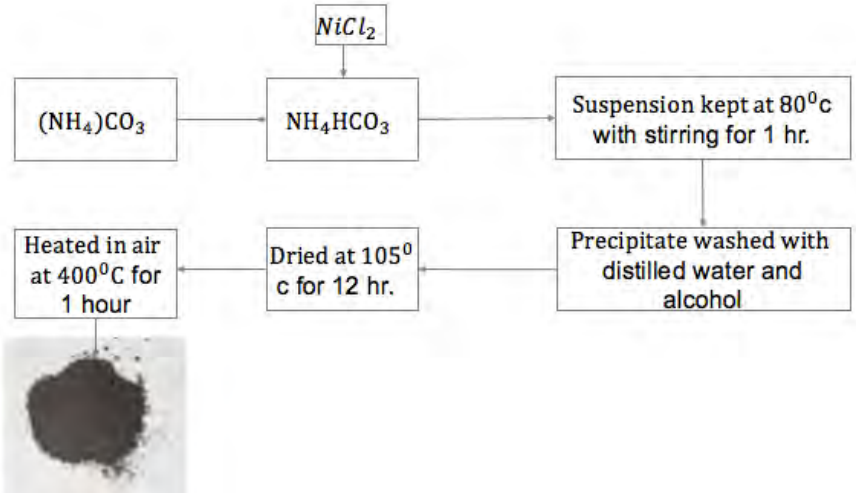

Figure 2.2.1 : Synthesis of *nano* NiO

Both stocked solution of nickel salts and precipitation agents (0.5 mol/L) are prepared by dissolving an appropriate amount of the corresponding chemicals in distilled water.100 ml of the precipitation solution dripped in 50ml of Ni2+ solution at the rate of 5.0 ml/min at constant temperature [800c for $CO(NH_2)_2$ system and 400c for both NH_4 HCO_3 and $(NH_4)_2CO_3$ system] with constant stirring (800 rpm)The suspension kept for 1 hour with stirring after the reagent addition.The precipitate was washed with distilled water and alcohol for three times and kept in the oven at 105^0 c for 12 hr.The precipitates is heated in air at 400^0 c for 1 hr.The sintering product was pulverized to get nano NiO. The nano NiO was confirmed by the confirmation experiment.

2.2.2 Synthesis of Mn_3O_4 *nano* particles:

Mn_3O_4 nanoparticles were prepared by forced hydrolysis of Mn(II) acetate following the procedure reported previously [144]. In brief, the procedure is as follows: freshly prepared 0.4M aqueous solution of $Mn(OOCCH_3)_2.4H_2O$ was heated in an oven at 80^0c for 2 h. The resulting brown dispersed product, Mn_3O_4, was then quenched in cool water and recovered by centrifugation. The product was then washed several times with double distilled water and dried in air in an oven at 40^0c. For experiments, this Mn_3O_4 either as powder or its suspension was used. To make the suspension, desired amount of nanoparticles ware just dispersed in the medium by gentle stirring.

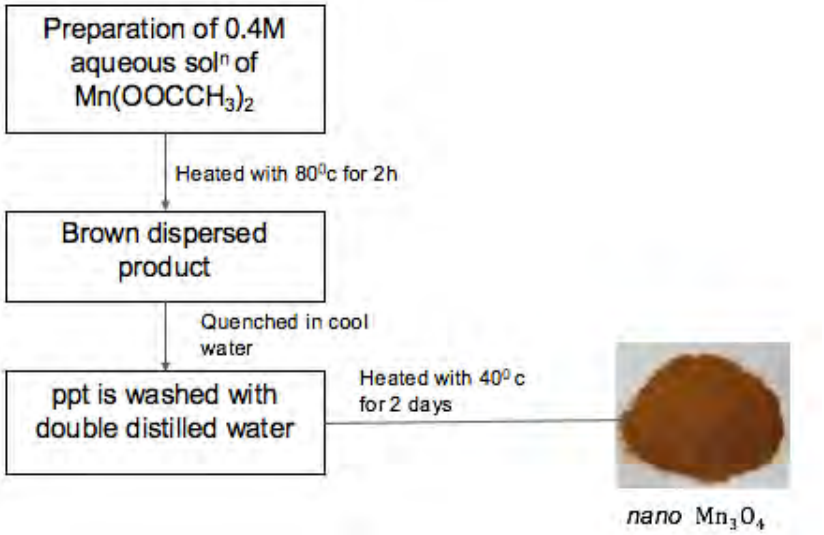

Figure 2.2.2 : Synthesis of *nano* Mn_3O_4

2.3 Dispersion of *nano* NiO in cellulose suspension

2.040 g microcrystalline cellulose (mcc) is taken in a beaker containing 200ml double distilled water. The beaker is placed on a hot plate magnetic stirrer. The temperature is maintaining at 35^0c and the rpm of the magnet is 400. After 15 min 0.202g *nano* NiO is added to the MCC suspension. Through keeping the same reaction condition and stirring for 30 more mins, the suspension was filtered with the help of the filter paper and fennel. The filtrate dried in oven at 40^0c to obtain the final product.

2.4 Dispersion of *nano*-Mn_3O_4 into cellulose suspension

2.040 g microcrystalline cellulose (mcc) is taken in a beaker containing 200ml double distilled water. The beaker is placed on a hot plate magnetic stirrer. The temperature is maintaining at 350c and the rpm of the magnet is 390. After 15 min 0.202g *nano*-Mn_3O_4 is added to the MCC suspension. Through keeping the same reaction condition and stirring for 30 more mins, the suspension was filtered with the help of the filter paper and fennel. The filtrate dried in oven at 400c to obtain the final product.

2.5 Characterization

2.5.1 Fourier Transform Infrared analysis (FTIR)

Fourier Transform Infra-Red (FTIR) is the preferred method of infrared spectroscopy. In infrared spectroscopy, IR radiation is passed through a sample. Some of the infrared radiation is absorbed by the sample and some of it is passed through (transmitted). The resulting spectrum represents the molecular absorption and transmission, creating a molecular finger prints of the sample. This makes infrared spectroscopy useful for several types of analysis like identifying unknown materials, determining the quality or consistency of a sample, and determining the amount of components in a mixture. Materials can be identified from their functional groups, chemical bonds etc. which can be detected through their characteristic infrared absorption frequencies or wave lengths. FTIR studies were conducted using (Perkin Elmer, USA, and Model: Frontier FT-NIR/MIR). Sample with KBr with a 1:100 “samples-to-KBr” ratio was maintained to prepare disk. The sample disks were then scanned in the wave number range of 4000 to 400 cm-1 with an average of 30 scans per measurement. The resolution of the spectrometer was 4cm-1.

2.5.2 X-ray Diffraction (XRD)

X-ray diffraction has played a pivotal role to identify and characterize solid samples. The nature of bonding and the working criteria for distinguishing

between short-range and long-range order of crystalline arrangements from the amorphous substances are largely derived from X-ray diffraction and thus it remains as a useful tool to obtain structural information. X-ray diffraction pattern of amorphous polymer will not show any sharp and high intensity peaks whereas the nano-composites of amorphous polymer show sharp and high intensity peaks. This is due to the development of crystallinity in the amorphous polymer.

XRD analysis was carried out by BRUKER, D 8 ADVANCE; Germany. All specimens for XRD were prepared by solution casting method. The sample film was cut into rectangular shape with dimensions 30mm × 10mm × 0.1mm (Length × Width× Thickness). The detail configuration of the instrument is as follows: Tube: Cu, Target: Cu K alpha (1.5406 A), Monochromator: Graphite, Voltage: 40kV, Current: 40 mA, Scan Step: 0.02 degree, Speed: 2.0 degree/min. XRD peaks were analyzed using Diffract Plus EVA 16.0 Software.

2.5.3 Scanning Electron Microscope (SEM) Analysis

The scanning electron microscope (SEM) uses a focused beam of high-energy electrons to generate a variety of signals at the surface of solid specimens. The signals that derive from electron-sample interactions reveal information about the sample including external morphology (texture), chemical composition, and crystalline structure and orientation of materials making up the sample. In most applications, data are collected over a selected area of the surface of the sample, and a 2-dimensional image is generated that displays spatial variations in these properties. Areas ranging from approximately 1 cm to 5 microns in width can be imaged in a scanning mode using conventional SEM techniques.

SEM were carried out by Field Emission scanning Electron Microscope, model JEOL JSM-1600F, Japan. The magnification range is from 20X to approximately 30,000X and spatial resolution of 50 to 100 nm. All sample were coated with platinum by auto fine coater, Model JEOL JFC-1600 before measurement.

2.5.4 Energy-dispersive X-ray spectroscopy (EDS)

Energy-dispersive X-ray spectroscopy (EDS, EDX, or XEDS), is an analytical technique used for the elemental analysis or chemical characterization

of a sample. It relies on an interaction of some source of X-ray excitation and a sample. Its characterization capabilities are due to the fundamental principle that each element has a unique atomic structure allowing unique set of peaks on its X-ray spectrum.

2.6 Adsorption phenomena

2.6.1 Determination of λ_{max} and molar absorption co-efficient of MB

The spectrum of aqueous solution of MB using water as a reference has a maximum absorbance at 664 nm at room temperature. To determine, the molar extinction co-efficient, a calibration curve was constructed by plotting the absorbance versus different concentration of MB solution. The absorbance of solution was measured at 664 nm. The experimental data and calibration curve has shown in table (2.6.1) figure (2.6.2) respectively. The molar extinction co-efficient, ε (in MB) was calculated from the slope of calibration curve.

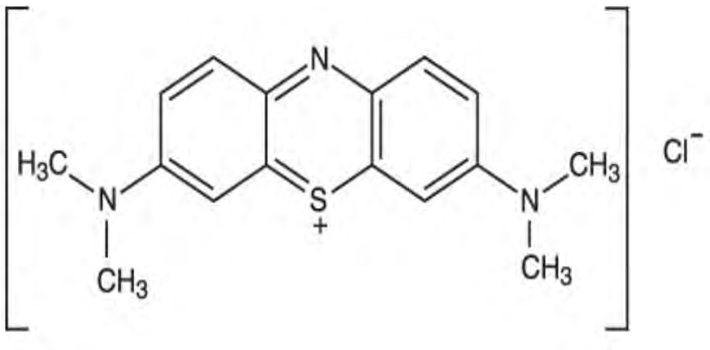

Figure2.6.1 : Chemical structure of MB

Determination of molar absorption co-efficient of MB

Reference : water
λ_{max} of MB solution : $664\ nm$
Temperature : 25^0 C
pH : 7.4

#Run no	Concentration (M)	Absorbance
1	0.2×10^{-5}	0.159
2	0.4×10^{-5}	0.206
3	0.6×10^{-5}	0.489
4	0.8×10^{-5}	0.678
5	1.0×10^{-5}	0.893
6	2.0×10^{-5}	1.727

Table 2.6.1 : Absorbance of MB solution at different concentration

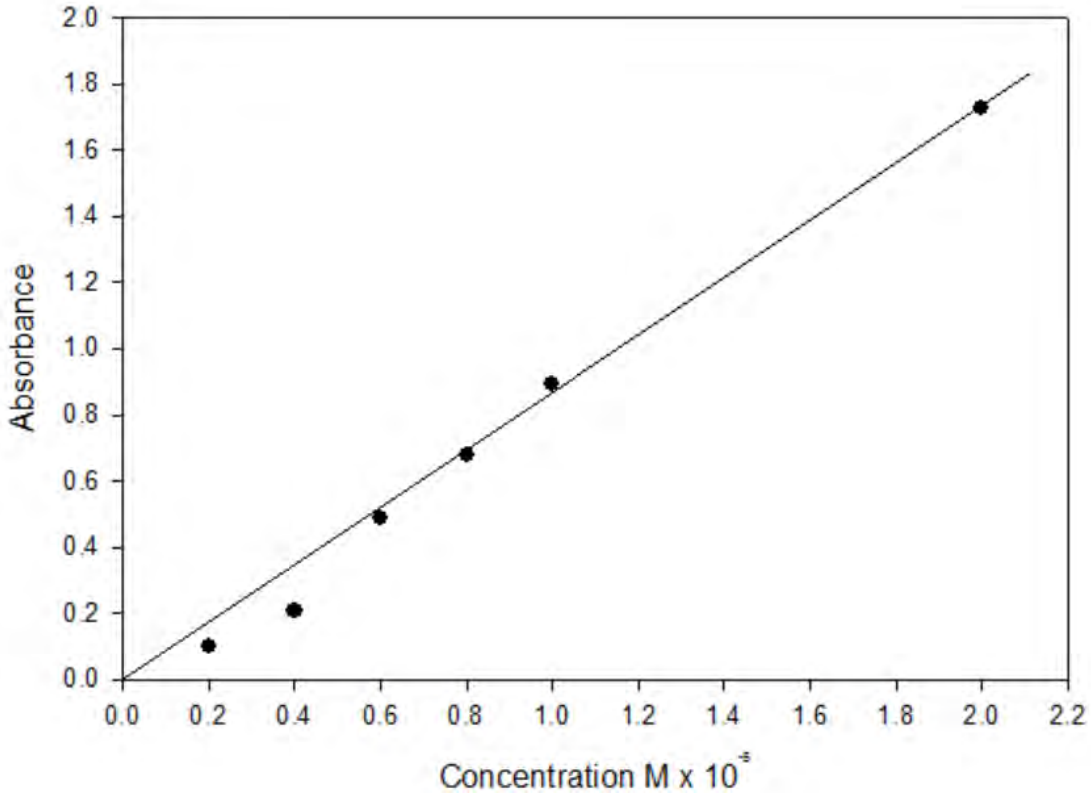

Figure2.6.2 : Calibration curve for MB

The molar adsorption co-efficient (ε) is 85000 $Lmol^{-1}$ cm^{-1}

2.6.2 Ultra Violet (UV) visible Spectroscopy analysis

The UV-Vis spectral analysis of the sample solutions employed a double beam spectrophotometer. UV-Vis spectroscopic analysis for the adsorption studies involved the different concentration of MB solution after the adsorbent added. The references in these cases were the corresponding aqueous solutions that used for preparing the adsorbed by substrate was done by spectroscopy on the visible region.

2.6.3 Preparation of Dye (MB) Solution

A. Stock dye solution

Molecular weight of Methylene Blue = 355.89 gm was required to prepare 2×10^{-3} M MB in a 250 mL volumetric flask,

$$= 355.89\ \text{g/mol} \times 250\times10^{-3}\ \text{mL} \times 2\times 10^{-3}$$

$$= 0.18\ \text{g}$$

Weight taken of MB = 0.18 g and concentration of MB = 2×10^{-3} M

B. Dilution of dye stock solution

With help of these stock solutions, dilute solutions of various concentrations were prepared by using the formula:

$$v_1 s_1 = v_2 s_2$$

2.6.4 Kinetic Study

In this work, adsorption of MB dye was carried out onto the MCC, MCC/nano NiO composite and NiO. The progress of adsorption was followed spectroscopically. The adsorption of MB was performed from the aqueous solution of pH (7.4).

A fixed amount of adsorbent sample was taken to the reaction vessels. Each vessel was charged with 5 mL MB solution to the concentration. Immediately after the addition of MB solution to the container, the shaking device was allowed to function the bottles were put down from the shaker by turn after 5 min, 10 min, 20 min, 30 min, 40 min, 60 min, 120 min, 240 min, 420 min, 960 min, and 1440 min respectively. After shaking, the solutions were centrifuged and the clear solutions were taken for spectroscopic analysis to determine the charge in concentration of MB. The same procedure was followed for the absorption study at different experimental conditions.

Run No	Time (min.)	Absorbance	Concentration (moles/L)	Number Of Moles (moles)	Number of moles Adsorbed (moles)	MB adsorbed in milligram (mg)	Adsorption at any time, q_t (mg/g)
1	0	1.726	2.03059E-05	1.01529E-07	0	0	0
2	5	0.357	0.0000042	0.000000021	8.05294E-08	0.028659612	0.286596124
3	10	0.322	3.78824E-06	1.89412E-08	8.25882E-08	0.029392327	0.293923271
4	20	0.4	4.70588E-06	2.35294E-08	0.000000078	0.02775942	0.2775942
5	30	0.36	4.23529E-06	2.11765E-08	8.03529E-08	0.028596808	0.285968082
6	40	0.421	4.95294E-06	2.47647E-08	7.67647E-08	0.027319791	0.273197912
7	60	0.295	3.47059E-06	1.73529E-08	8.41765E-08	0.029957564	0.299575641
8	120	0.42	4.94118E-06	2.47059E-08	7.68235E-08	0.027340726	0.273407259
9	240	0.1	1.17647E-06	5.88235E-09	9.56471E-08	0.034039832	0.340398318
10	420	0.145	1.70588E-06	8.52941E-09	0.000000093	0.03309777	0.3309777
11	960	0.347	4.08235E-06	2.04118E-08	8.11176E-08	0.028868959	0.288689594
12	1440	0.473	5.56471E-06	2.78235E-08	7.37059E-08	0.026231186	0.262311865

Table 2.6.4 : Data for the adsorption of MB on MCC at different time interval.

Run No	Time (min)	Absorbance	Concentration (moles/L)	Number Of Moles (moles)	Number of moles Adsorbed (moles)	MB adsorbed in milligram (mg)	Adsorption at any time, q_t (mg/g)
1	0	1.726	2.03059E-05	1.01529E-07	0	0	0
2	5	0.105	1.23529E-06	6.17647E-09	9.53529E-08	0.033935158	0.339351582
3	10	0.1	1.17647E-06	5.88235E-09	9.56471E-08	0.034039832	0.340398318
4	20	0.101	1.18824E-06	5.94118E-09	9.55882E-08	0.034018897	0.340188971
5	30	0.103	1.21176E-06	6.05882E-09	9.54706E-08	0.033977028	0.339770276
6	40	0.097	1.14118E-06	5.70588E-09	9.58235E-08	0.034102636	0.341026359
7	60	0.081	9.52941E-07	4.76471E-09	9.67647E-08	0.034437591	0.344375912
8	120	0.034	0.0000004	0.000000002	9.95294E-08	0.035421522	0.354215224
9	240	0.421	4.95294E-06	2.47647E-08	7.67647E-08	0.027319791	0.273197912
10	420	0.168	1.97647E-06	9.88235E-09	9.16471E-08	0.032616272	0.326162718
11	960	0.085	0.000001	0.000000005	9.65294E-08	0.034353852	0.343538524
12	1440	0.118	1.38824E-06	6.94118E-09	9.45882E-08	0.033663007	0.336630071

Table 2.6.5 : Data for the adsorption of MB on *nano* NiO/ MCC at different time interval.

2.6.5 Isothermal Study

To the series of MB solutions of 4.0×10^{-5} M, 3.5×10^{-5} M, 3.0×10^{-5} M, 2.5×10^{-5} M, 2.0×10^{-5} M, 1.5×10^{-5} M and 1.0×10^{-5} M, the same procedure of absorption was adopted for MCC, MCC/*nano* Mn_3O_4 and *nano* NiO for 2hrs.

Sample	:	MB solution
Volume of Solution	:	5 mL
Time	:	2 hours
Amount of Adsorption	:	0.1 g for cellulose and cellulose/*nano* NiO composite and 0.01g *nano* NiO
pH	:	7.4
Reference	:	Water
Temperature	:	25^0 C

	Concentration of MB initial (moles/L)	Absorbance	Concentration of MB final (moles/L)	Concentration difference (moles/L)	Number of moles adsorbed (moles)	milligram of MB adsorbed (mg)	MB adsorbed in equillibrium q_e (mg/g)
1	0.00004	0.698	8.21176E-06	3.17882E-05	1.58941E-07	0.056565575	0.565655753
2	0.000035	0.622	7.31765E-06	2.76824E-05	1.38412E-07	0.049259363	0.492593629
3	0.000025	0.378	4.44706E-06	2.05529E-05	1.02765E-07	0.036572931	0.365729312
4	0.00002	0.262	3.08235E-06	1.69176E-05	8.45882E-08	0.030104107	0.301041071
5	0.000015	0.175	2.05882E-06	1.29412E-05	6.47059E-08	0.023028176	0.230281765
6	0.00001	0.133	1.56471E-06	8.43529E-06	4.21765E-08	0.015010184	0.150101841

Table 2.6.6: Data for the adsorption of MB on MCC at different concentration of MB solution.

	Concentration of MB initial (moles/L)	Absorbance	Concentration of MB final (moles/L)	Concentration difference (moles/L)	Number of moles adsorbed (moles)	milligram of MB adsorbed (mg)	MB adsorbed in equilibrium q_e (mg/g)
1	0.00004	0.091	1.07059E-06	3.89294E-05	1.94647E-07	0.069272942	0.692729418
2	0.000035	0.074	8.70588E-07	3.41294E-05	1.70647E-07	0.060731582	0.607315818
3	0.00003	0.122	1.43529E-06	2.85647E-05	1.42824E-07	0.050829466	0.508294659
4	0.000025	0.097	1.14118E-06	2.38588E-05	1.19294E-07	0.042455584	0.424555835
5	0.00002	0.069	8.11765E-07	1.91882E-05	9.59412E-08	0.034144505	0.341445053
6	0.00001	0.06	7.05882E-07	9.29412E-06	4.64706E-08	0.016538418	0.165384176

Table2.6.7 : Data for the adsorption of MB on nano $NiO/\ MCC$ at different concentration of MB solution.

2.7 Antimicrobial Susceptibility Testing
(Agar disk diffusion method)

Mueller-Hinton agar medium is the only susceptibility test medium that has been validated by NCCLS (National Committee for Clinical Laboratory Standards). Mueller-Hinton tryptic soy agar media was used for disk diffusion susceptibility testing. A total seven bacterial stains including selected gram positive (Streptococcus pneumonia) and gram negative (Vibrio cholera, Escherichia coli, Salmonella typhi, Enterobacter cloacae, Acinelobacter baumanni, Pseudomonas aeruginosa) bacteria were selected to assess susceptibility pattern.

Each culture to be tested should be streaked onto a non-inhibitory agar medium (tryptic soy ager) to obtain isolated colonies. After autoclaving (121^0 c and certain pressure), cool Mueller-Hinton tryptic soy ager medium allowed it to cool to 50^0 c and measured (50 to 60 ml) media was poured into plastic petri dishes (150mm diameter) on a level pouring surface to a uniform depth of 4mm. Freshly prepared plates were used the same day. Each new lot was quality controlled before use by testing standard micro-organism strains.

Each culture of bacteria after incubation at 37^0 c overnight from the bacterial colonies, select 4 or 5 well-isolated colonies with an inoculating loop, and transfer the growth to a tube of sterile saline and vortex thoroughly. Incubate the saline broth at 35^0 c until the bacterial suspension properly turbid compared to the 0.5 McFarland standards.

Within 15 minutes after adjusting the turbidity of the inoculum suspension dip a sterile cotton swap into the suspensions. Pressing firmly against the inside wall of the tube just above the fluid level, rotate the swap to remove excess liquid. Streak the swab over the entire surface of the medium three times, rotating the plates approximately 60 degrees after each application to ensure an even distribution of the inoculums. Three tiny hole is created on the agar mediun by the forceps, using micro pipettes 50 µL, 100 µL and 150 µL drug-loaded suspension is apply to the petri plates as soon as possible, but no longer than 15 minutes after inoculation.

Invert the plate and incubate at 31 ± 10^{0}c for 18 hours. After incubation measure the diameter of the zones of complete inhibition and record it in millimeters (mm).

Chapter 3

Results and Discussion

3.1 Synthesis of NiO and Mn_3O_4 *nano* particles

NiO and Mn_3O_4 *nano* particles are synthesis by precipitation and forced hydrolysis method.

Aqueous solution containing $NiCl_2$ as the nickel source and NH_4HCO_3 as the precipitation agent. From these aqueous solution $Ni(OH)_2.NiCO_3.xH_2O$ precipitated obtained; after the air calcination of these precipitate NiO nano particles are obtained.

Mn_3O_4 *nano* particles were prepared by forced hydrolysis of Mn(II) acetate. Aqueous solution of $Mn(OOCCH_3)_2.4H_2O$ was heated over at 80^oC for $2h$. The resulting brown dispersed product is washed for several times and the dried in air to obtain Mn_3O_4 nanoparticles.

3.1.1 Characterization of *nano* NiO

Characterization of nano NiO is done by FTIR, XRD, SEM and EDS analysis.

3.1.1.1 FTIR Spectral analysis of *nano* NiO

IR spectral analysis studies provide some useful albeit qualitative information on the identification of compounds. Both organic and inorganic substances absorb IR light and thus IR active. In order to get some insight about the structure of the synthesized substrates, IR spectra of *nano* NiO are presented in figure (3.1.1.1).

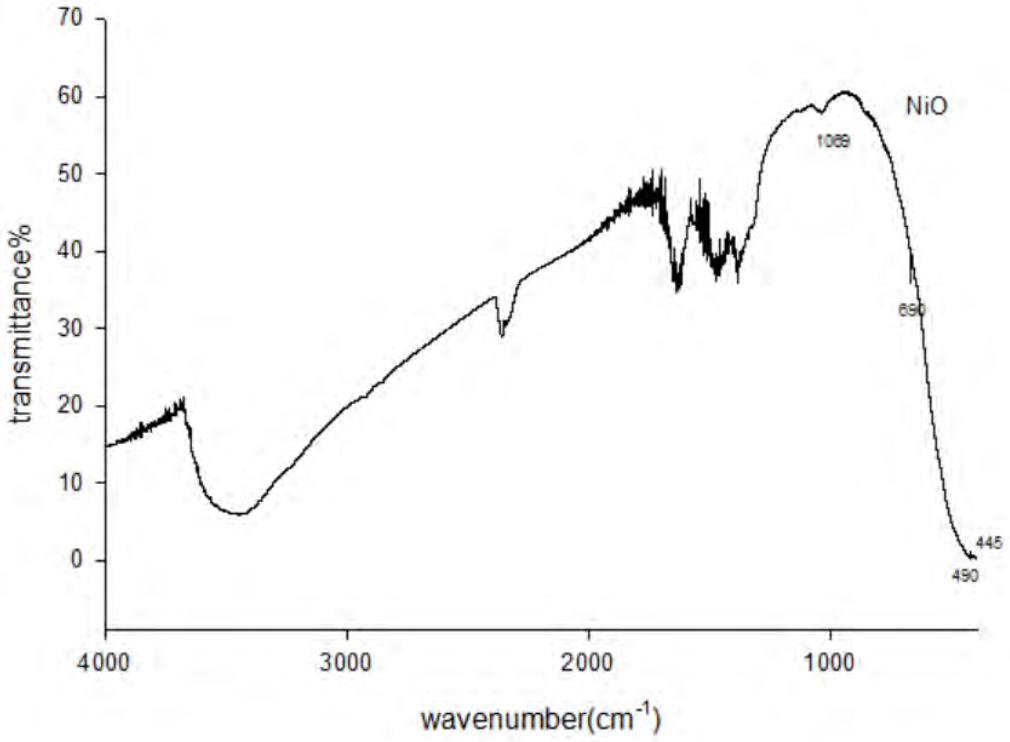

Figure 3.1.1.1 : FTIR spectrum of *nano* NiO

From FTIR spectrum of *nano* NiO , peaks located at about 445, 490, 690 and 1069 cm^{-1} are observed in spectrum of pure NiO. The peaks were found at 445 and 490 cm^{-1} for stretching vibration of Ni-O which is in agreement with previous work [145- 147]

NiO also exhibits some small bands at 1069 cm^{-1}. These peaks confirmed the formation of *nano* Nickel oxide materials.

3.1.1.2 XRD analysis for *nano* NiO

The x-ray technique is used for structural analysis of solids. This can provide . XRD pattern of the heat-treated sample prepared form $NiCl_2$-NH_4 HCO_3 system is given in figure (3.1.1.2) .The scatter pattern was found as a function of Bragg angle, 2θ at λ=1.54 Å for the studied sample powder. All the diffraction peaks of NiO samples exhibits standard peaks at 2θ values 37.3^0 , 43.2^0 and 62.9^0 [corresponding to (111), (200) and (220) reflection respectively] [148-150]. The

absence of any other peaks in the XRD pattern illustrates the purity of nano structures.

The average crystallite size was calculated from debye-scherrer formula

$$t = \frac{k\lambda}{\beta\cos\theta}$$

where t is crystallite size, β is the full width at half maximum of the peak λ is the x-ray wavelength, θ is the Braggs angle. The average crystallite size was found 22.5nm.

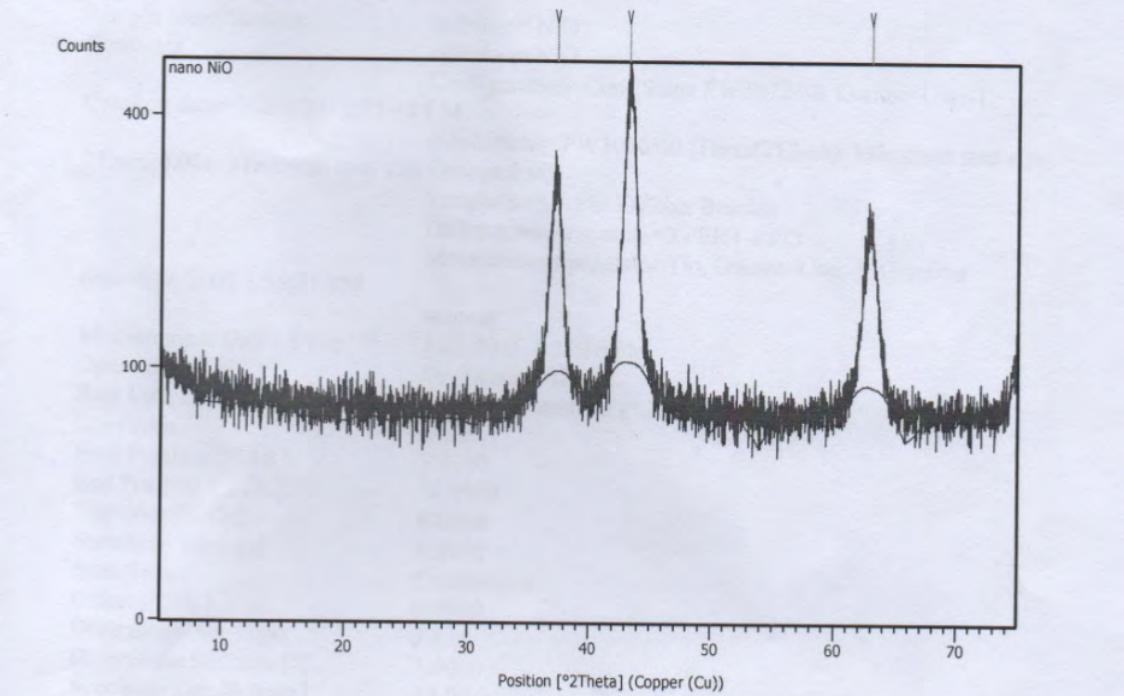

Peak List: (Bookmark 3)

Pos. [°2Th.]	Height [cts]	FWHM Left [°2Th.]	d-spacing [Å]	Rel. Int. [%]
37.2125	212.48	0.7872	2.41626	58.07
43.2058	365.93	0.3149	2.09396	100.00
62.8741	154.22	0.7872	1.47813	42.14

Figure 3.1.1.2 : XRD pattern for *nano* NiO

3.1.1.3 Scanning Electron Microscope (SEM) image for *nano* NiO

Typical SEM images of nickel oxide are shown in Figure (3.1.1.3). Figure (3.1.1.3) indicates that morphology of the nickel oxide *nano* particles are agglomerated and have spongy look with spherical shape with rough surface ranging from several hundred nanometers to few nanometers.

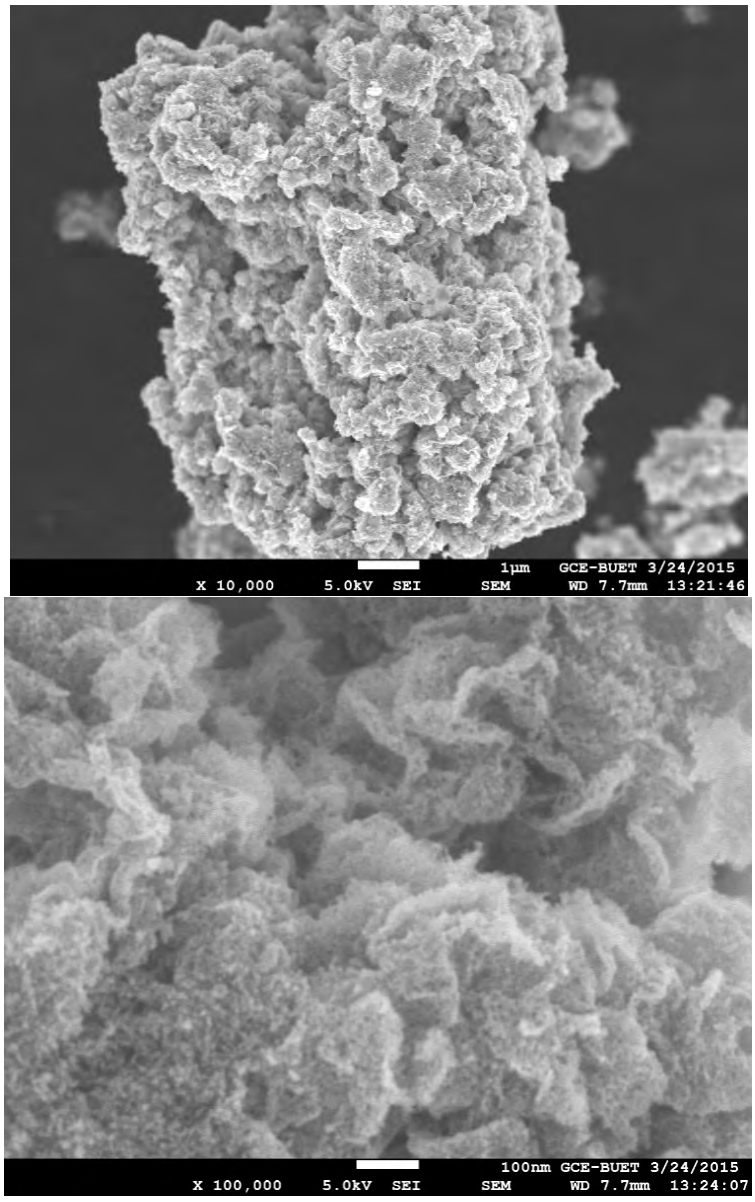

Figure 3.1.1.3: Scanning electron microscope (SEM) image of *nano* NiO

3.1.1.4 EDX Image for *nano* NiO :

EDS provides rapid qualitative and quantitative analysis of elemental composition. From the EDS spectrum which is shown in Fig (3.1.1.4). The lines observed at 7.48, 8.26 KeV and 0.85, 0.87 KeV are respectively for k(α, β) and L(α, β) lines of Ni element. The EDS line at 0.525 KeV represents the k line for O. The lines identified in this EDS result also concurs with the rapid findings reported elsewhere [151].

The qualitative result of the EDS data provided the percentage of each element presents in the prepared sample and thus allowed us to obtain directly the composition of the samples studied from EDS data. The percentage of Ni and O is 77.57% and 22.43% respectively which matches with the form of NiO.

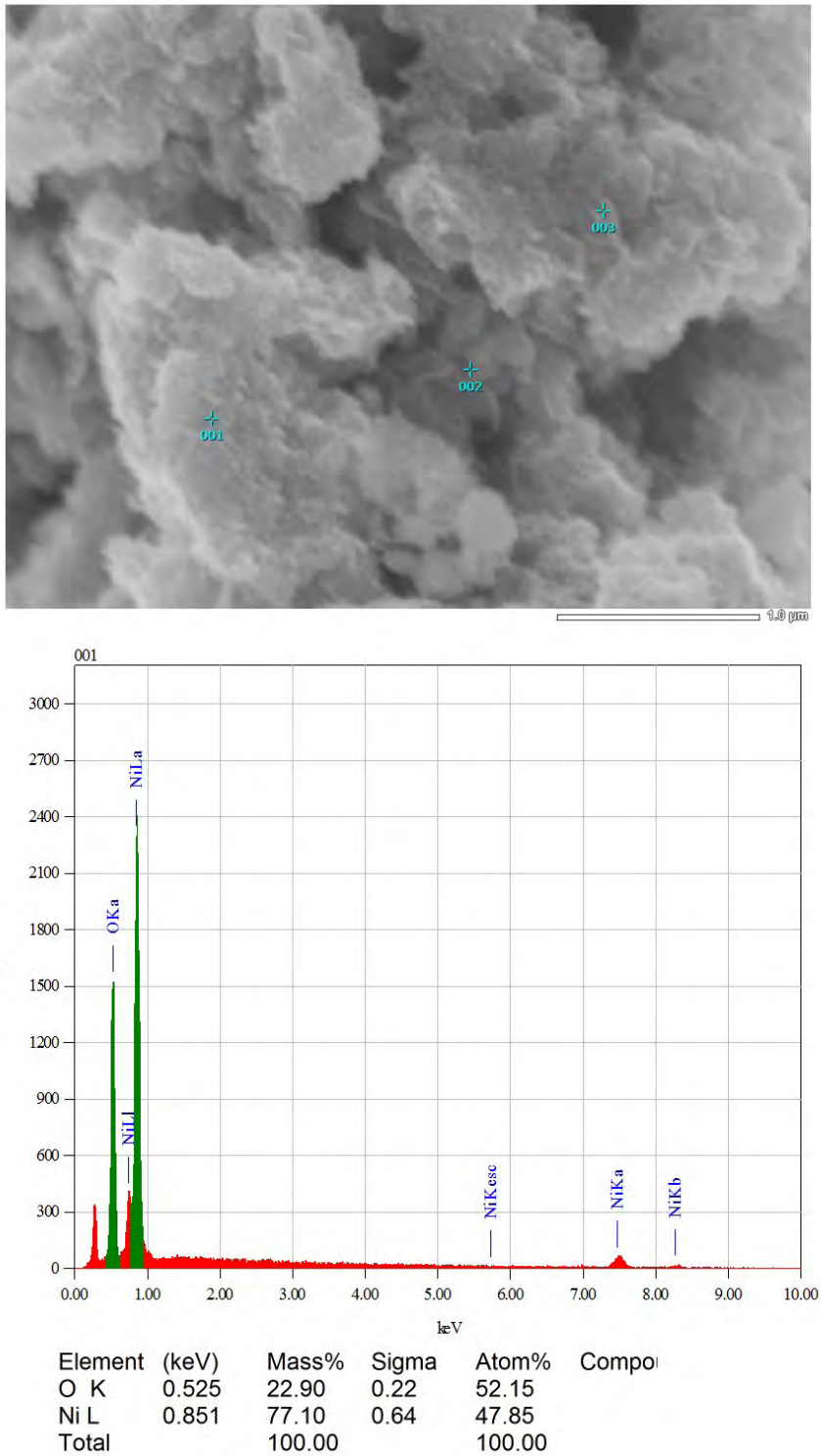

Figure 3.1.1.4: EDS image of *nano* NiO.

3.1.2 Characterization of *nano* Mn_3O_4

Characterization of *nano* Mn_3O_4 is done by FTIR, XRD, SEM and EDS analysis.

3.1.2.1 FTIR Spectral analysis of *nano* Mn_3O_4

IR spectral analysis studies provide some useful albeit qualitative information on the identification of compounds. Both organic and inorganic substances absorb IR light and thus IR active. In order to get some insight about the structure of the synthesized substrates, IR spectra of manganese oxides are presented in Figure (3.1.2.1).

IR spectrum of synthesized *nano* Mn_3O_4 particles at 631 and $525\ cm^{-1}$ due to the coupling modes between the Mn-O stretching modes of tetrahedral and octahedral sites [152,153].

The band at $405.0\ cm^{-1}$ is due to the band stretching mode of Mn-O at the octahedral sites.

Absorption peaks at around 3395 and 1580 cm^{-1} are by the absorbed water molecules and carbon dioxide because the *nano* materials exhibit a high surface to volume ratio The bending vibration of O-H bonds connected to Mn atoms observed at 1340 $cm^{-1}$and the band at 660 cm^{-1} is due to the Mn_3O_4 spinal. Thus the FTIR further confirm that the *nano* particle analyzed is Mn_3O_4.

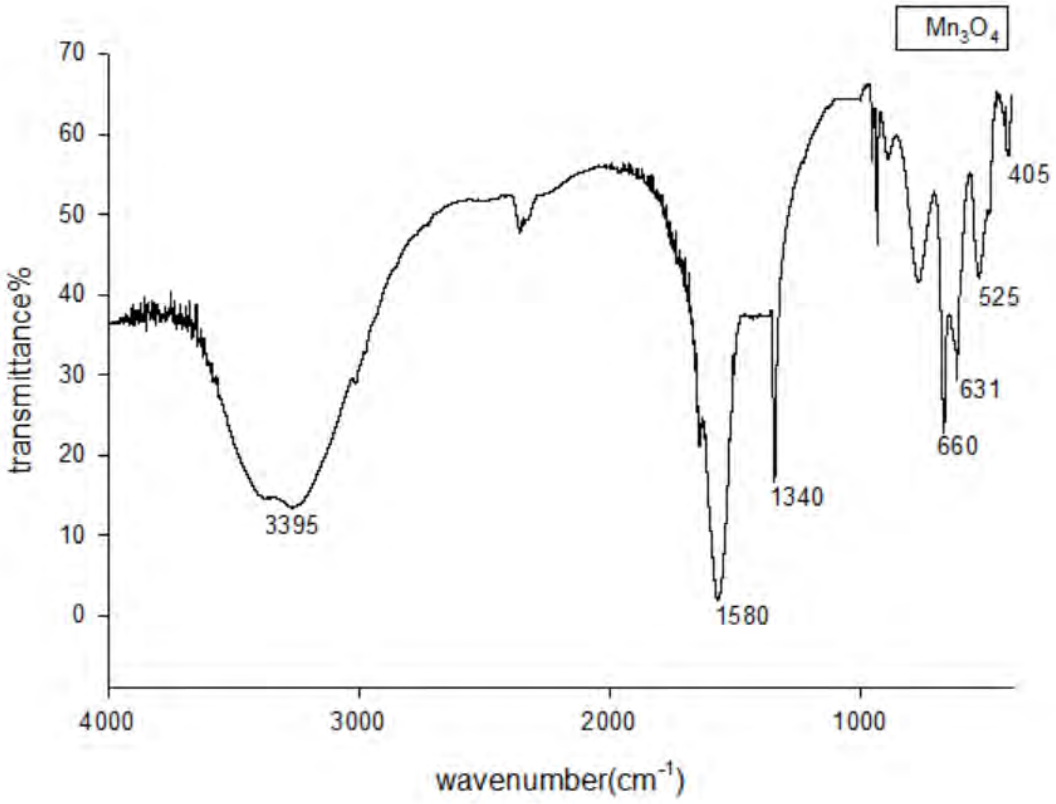

Figure 3.1.2.1 : FTIR spectrum of *nano* Mn_3O_4 MO_4

3.1.2.2 XRD analysis for *nano* Mn_3O_4

The XRD pattern of *nano* Mn_3O_4 showed in figure (3.1.2.2). the characteristic crystalline peak at about 10.8^0 and showed few amorphous peaks at 13.89^0 , 29.17^0 and 36.86^0. These peaks are sharp and featureless that indicate the of *nano* Mn_3O_4.

The average crystallite size of starch granules determined using Scherer's formula.

$$t = \frac{k\lambda}{\beta\cos\theta}$$

where t is crystallite size, β is the full width at half maximum of the peak and k is an instrumental constant. The average crystallite size was found 11.6 nm.

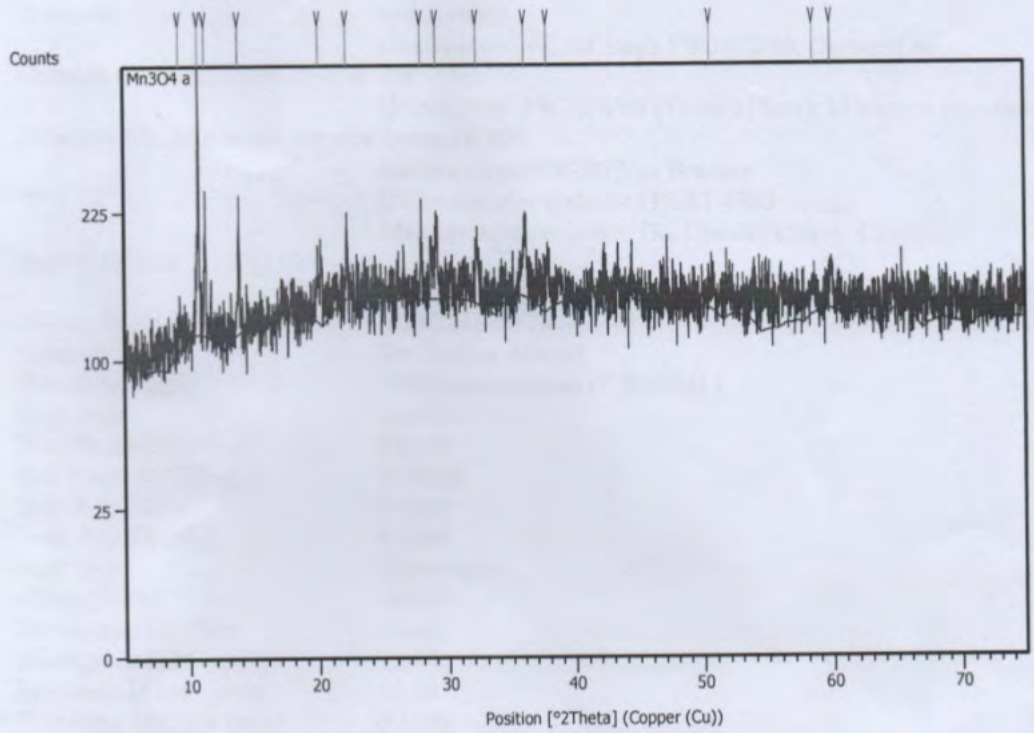

Peak List: (Bookmark 3)

Pos. [°2Th.]	Height [cts]	FWHM Left [°2Th.]	d-spacing [Å]	Rel. Int. [%]
9.3033	33.75	0.1181	9.50634	12.05
10.8140	280.06	0.0787	8.18145	100.00
11.3155	109.62	0.0787	7.81998	39.14
13.8972	104.26	0.0590	6.37248	37.23
20.1286	37.55	0.4723	4.41157	13.41
22.2390	74.40	0.0984	3.99748	26.56
28.0079	91.72	0.0787	3.18583	32.75
29.1780	65.58	0.1574	3.06069	23.42
32.3445	48.46	0.2362	2.76792	17.30
36.0862	57.76	0.2362	2.48904	20.62
37.9534	37.78	0.2362	2.37077	13.49
50.6084	18.10	0.7872	1.80368	6.46
58.5362	23.56	0.4723	1.57689	8.41
59.9033	35.75	0.3936	1.54413	12.77

Figure 3.1.2.2 : XRD pattern for nano Mn_3O_4

3.1.2.3 SEM image for *nano* Mn_3O_4:

The surface morphology of Mn_3O_4. Mn_3O_4 powder particles at the microscopic level was examined by SEM. SEM images of Mn_3O_4 powder particles are shown in Figure (3.1.2.3).

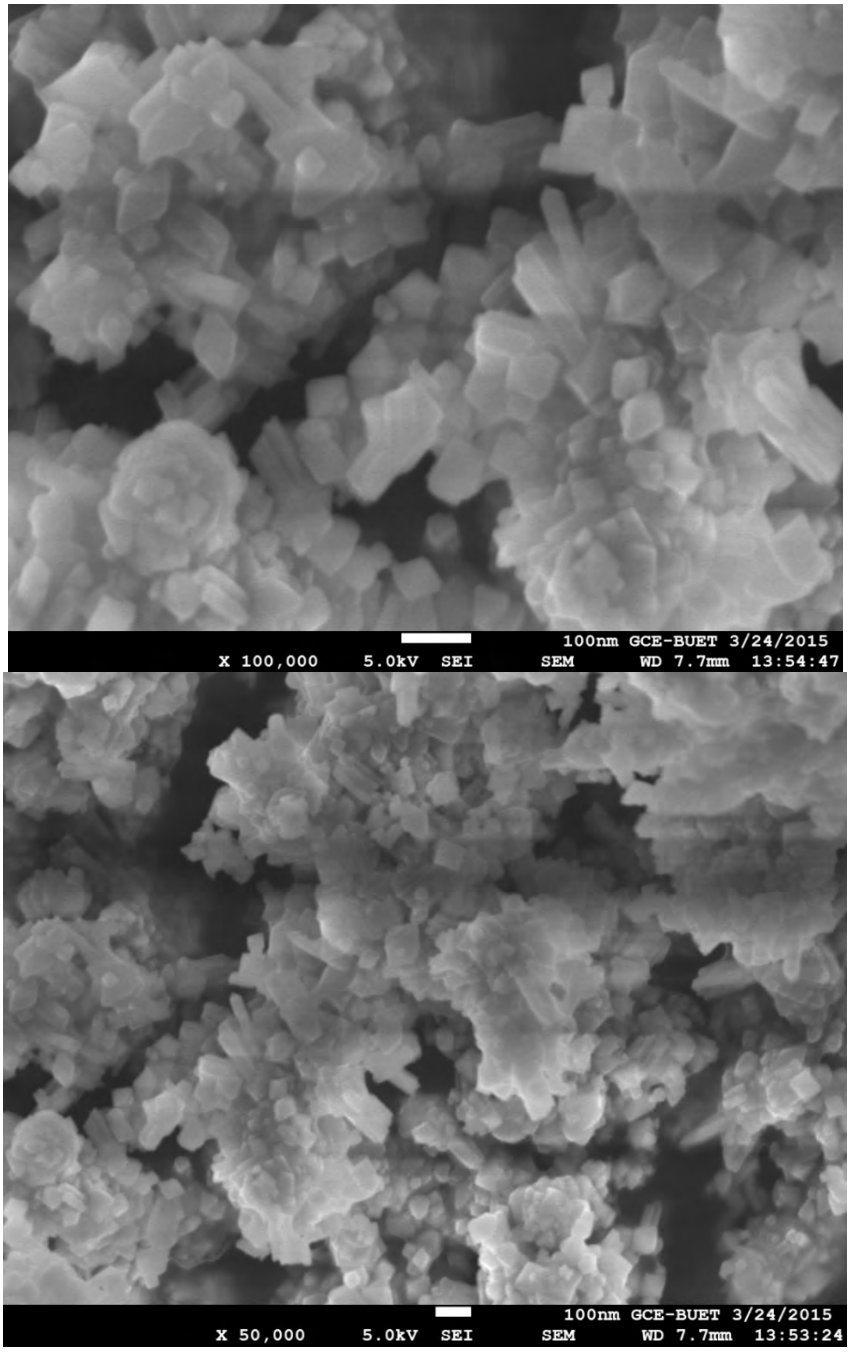

Figure 3.1.2.3 : SEM image for *nano* Mn_3O_4

It can be seen from the SEM images that Mn_3O_4 has grown with granular morphology and are cubic, rectangular or cuboid in shape with smooth surfaces and wide distribution of signs. Figure (3.1.2.3) shows different particle size distribution of Mn_3O_4 granules ranging from 20 nanometers to 80 nanometers.

3.1.2.4 EDX Image for *nano* Mn_3O_4

Energy dispersion X-ray spectroscopy is an analytical technique used for the elemental analysis and chemical characterization of a sample. Its characterization capabilities are due to in large part to the fundamental principle that each element has unique atomic structure allowing X-ray that are characteristic of an element's atomic structure to be identified uniquely from one another.

Elemental analysis of the powder nanoparticles was achieved from EDX spectra presented in Figure (3.1.2.4) The peaks are observed at 5.894 and 0.78 KeV are associated for K and L line of the Mn element, respectively.The line at 0.525 KeV is for K line of the oxygen element. The lines assigned to O and Mn Figure (3.1.2.4) agree with those found in previous report [153]. The average quantities of Mn and O in the prepared sample, according to the EDX spectrum are 75.55% and 24.45% respectively which matches the form Mn_3O_4 ando not match with other forms of Manganese Oxide.

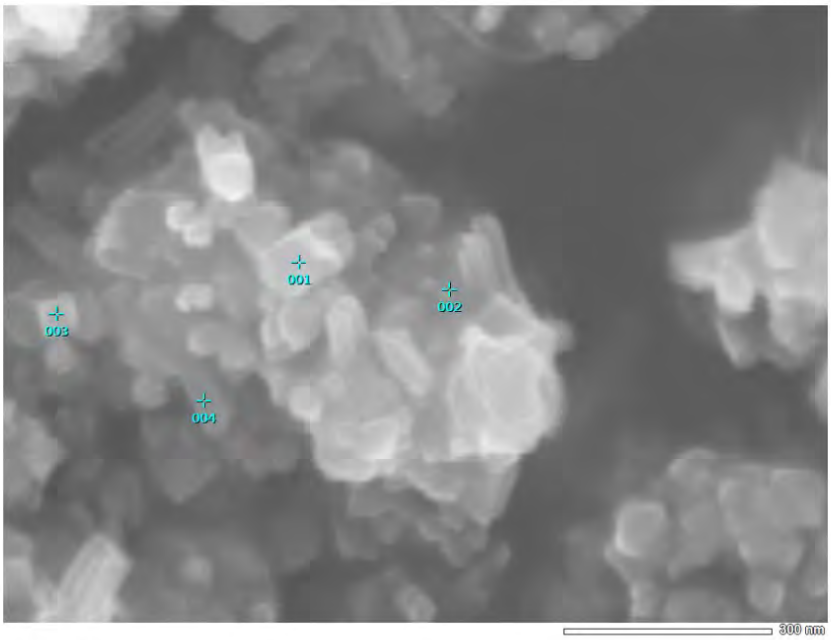

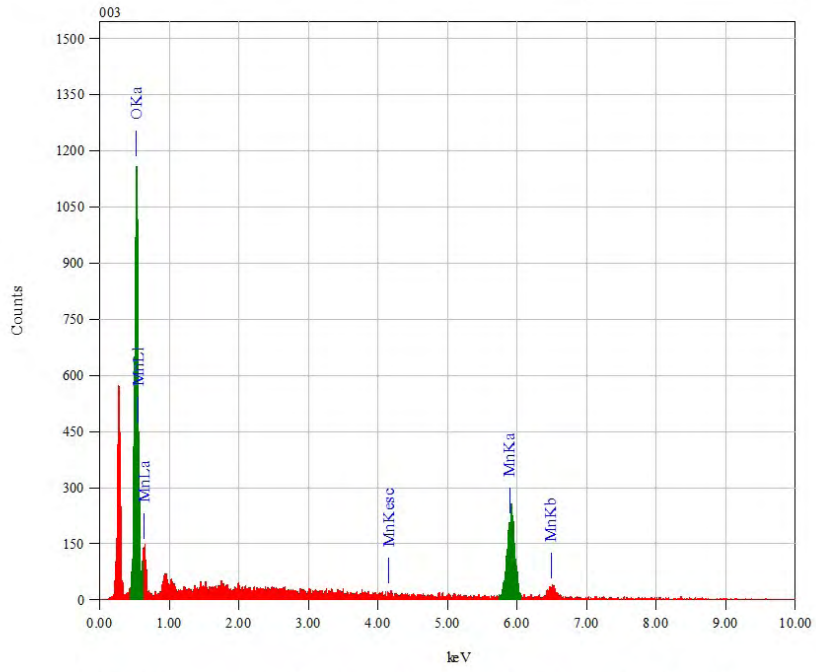

Element		(keV)	Mass%	Sigma	Atom%	C
O K		0.525	24.45	0.10	52.63	
Mn K	*	5.894	75.55	0.83	47.37	
Total			100.00		100.00	

Figure : EDS image for nano Mn_3O_4

3.2 Dispersion of NiO and Mn_3O_4 *nano* particles into MCC

Dispersion of *nano* NiO and *nano* Mn_3O_4 in cellulose suspension. Certain amount of MCC is taken in a beaker containing distilled water. At fixed condition small amount of *nano* NiO and nano Mn_3O_4 is added to the suspension. Through keeping the same reaction condition the suspension is filtered and dried to obtain final product.

3.2.1 Characterization of *nano* NiO/ MCC

Characterization of *nano* NiO/MCC is done by FTIR, XRD, SEM and EDS analysis.

3.2.1.1 FTIR Spectral analysis of nano NiO/MCC

The FTIR spectra of *nano* NiO, nano NiO/MCC, and MCC are shown in figure (3.2.1.1).The typical characteristic bands of *nano* NiO were observed in figure (3.1.1.1) respectively. For MCC, the bands at 3437 cm^{-1} (the stretching vibration of OH), 2900 cm^{-1} (asymmetrically stretching vibration of C-H groups), 1650 cm^{-1} (bending mode of absorbed water in the composites), 1430 cm^{-1} (CH_2 scissoring motion) and 1058 cm^{-1} (C-O-C pyranose ring skeletal vibration of cellulose) are observed [154]. The characteristic band of *nano* NiO is slightly shifted to the left found at 435 cm^{-1} [155-157] (actual 445 cm^{-1}) and 503 cm^{1} (actual 490 cm^{-1}). We also observed that when nano NiO is blended with MCC the peak intensities were weak at the band 3437 cm^{-1} and 2900 cm^{-1}.

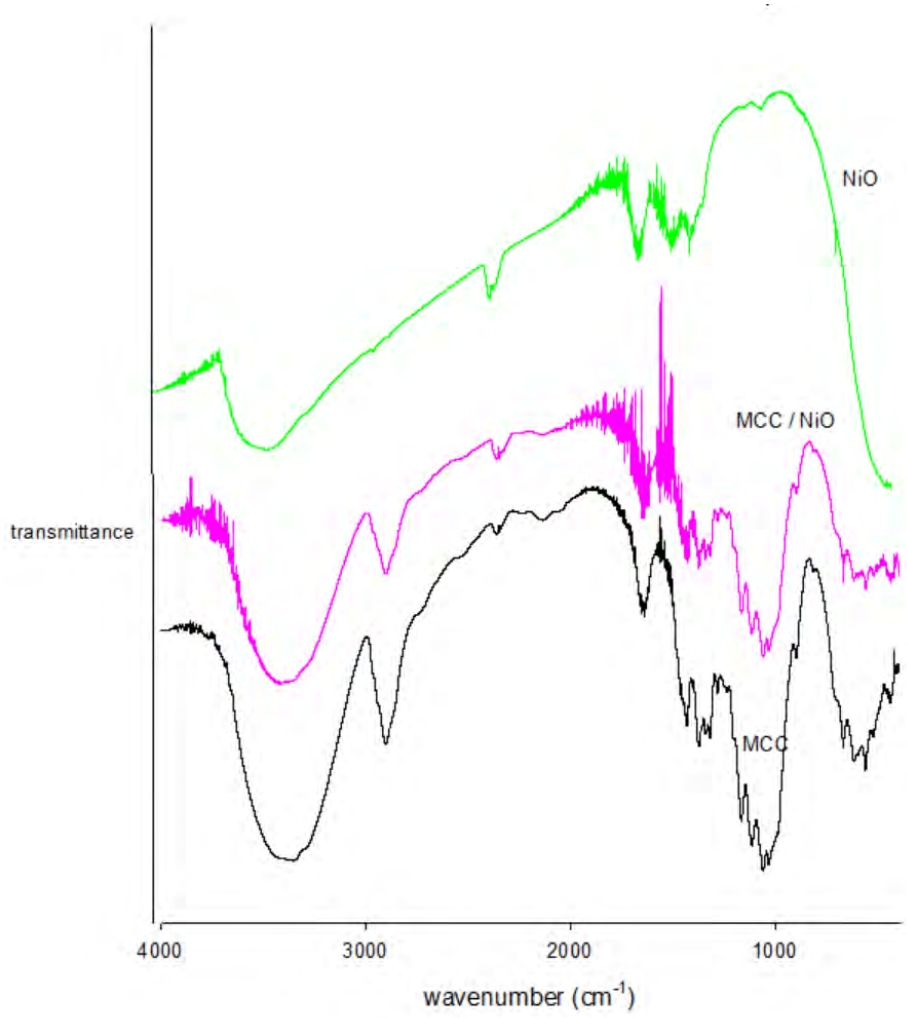

Figure 3.2.1.1: FTIR spectrum of *nano* NiO/MCC

3.2.1.2 XRD analysis for *nano* NiO/MCC

Structural analysis by x-ray can provide information on the intermolecular arrangement, i.e., the level if crystallinity of a material. The *nano* NiO/Cellulose samples prepared was examined for their structural analysis in the powdered state by using wide angle x-ray diffraction. The scattering patterns as a function of Bragg angle, 2θ at λ = 1.54 Å for the studied substrate powder in presented in figure (3.2.1.2)

All the diffraction peaks of the samples exhibits standard peaks at 2θ values of 15^0 , 22.5^0, 34.5^0, 37^0, 43.2^0 *and* 62.7^0. The diffraction peaks at 15^0

, 22.5^0 and 34.5^0 is responsible for MCC and for nano NiO the diffraction peaks at 2θ values of 37^0, 43.2^0 and 62.7^0.

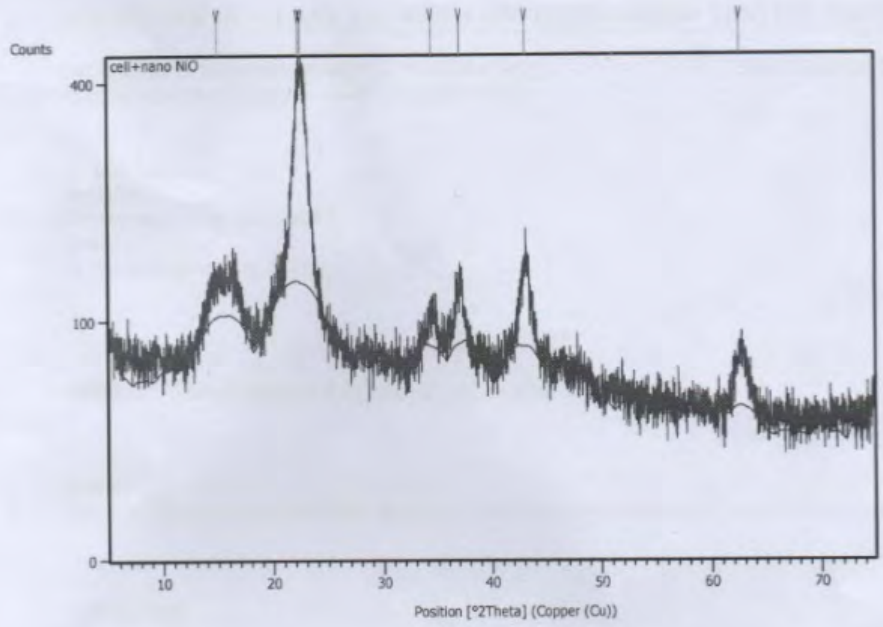

Peak List: (Bookmark 3)

Pos. [°2Th.]	Height [cts]	FWHM Left [°2Th.]	d-spacing [Å]	Rel. Int. [%]
15.0431	34.82	0.9446	5.88956	12.20
22.3905	277.35	0.2755	3.97078	97.18
22.5821	285.40	0.3936	3.93752	100.00
34.5400	30.95	0.4723	2.59684	10.85
37.1586	57.50	0.5510	2.41964	20.15
43.1954	86.46	0.3936	2.09444	30.29
62.6710	37.13	0.9446	1.48243	13.01

Figure 3.2.1.2: XRD pattern for *nano* NiO/MCC

3.2.1.3 SEM Analysis for *nano* NiO/MCC

Figure (3.2.1.3) represents the surface morphology of the *nano* NiO loaded MCC network. In this image, *nano* NiO particles were homogeneously dispersed in the network of MCC. The particles are distributed with granular shape and less packed to each other.

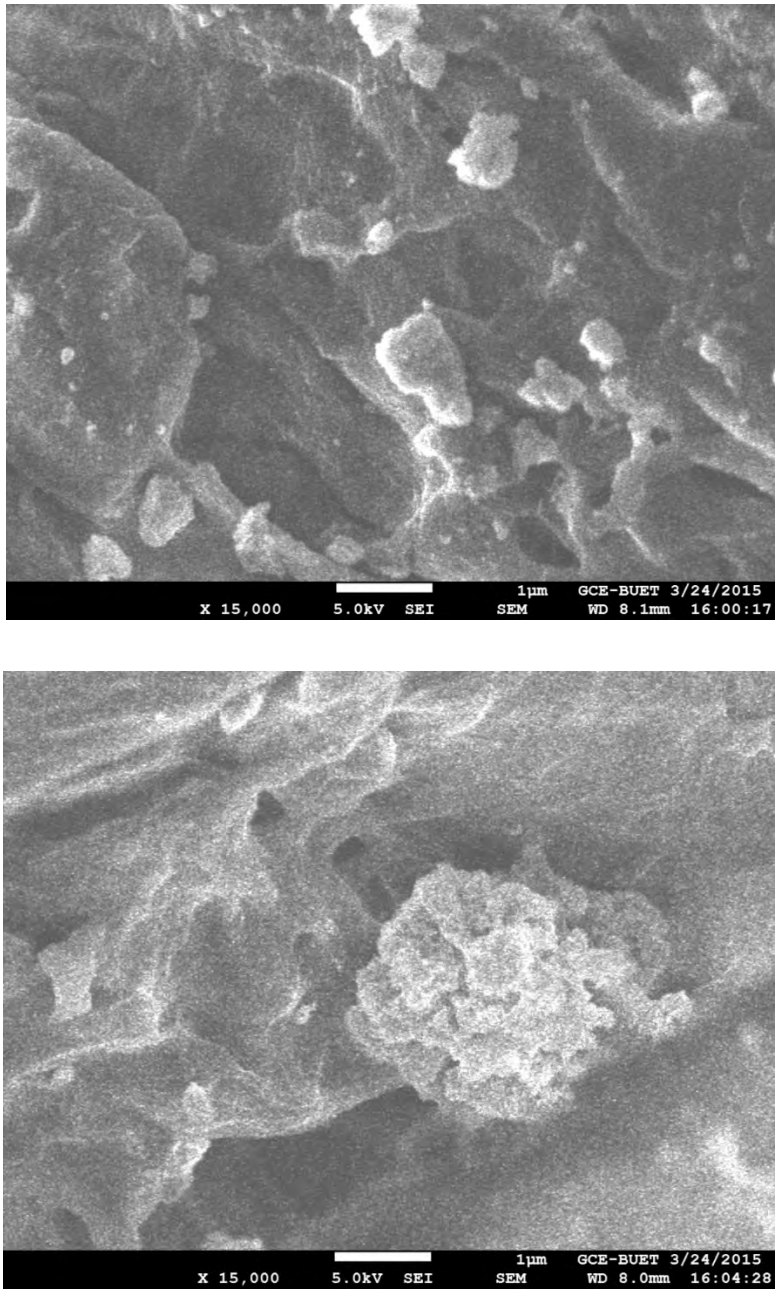

Figure 3.2.1.3: SEM image for nano NiO/MCC

3.2.1.4 EDX Analysis for *nano* NiO/MCC :

Figure (3.2.1.4) shows the buckscattered electron image of the prepared samples, along with the characteristic energy dispersive x-ray (EDX) spectra of the individual present phases. EDX analysis revealed that the light greyish part is NiO (Labelled `a`) and the dark looking part are MCC (Labelled `b`). This phase contained a very small amount of NiO, which is in agreement with low NiO solid solution in MCC. A quantitative analysis of the nano NiO gives 77.44% of Ni and 29.56% of O, which close to the percentage of Ni and O in *nano* NiO forms.

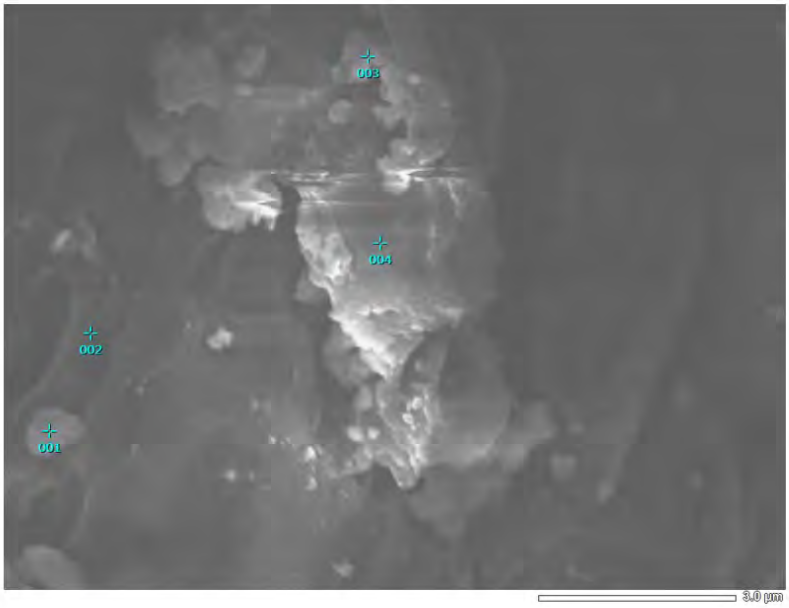

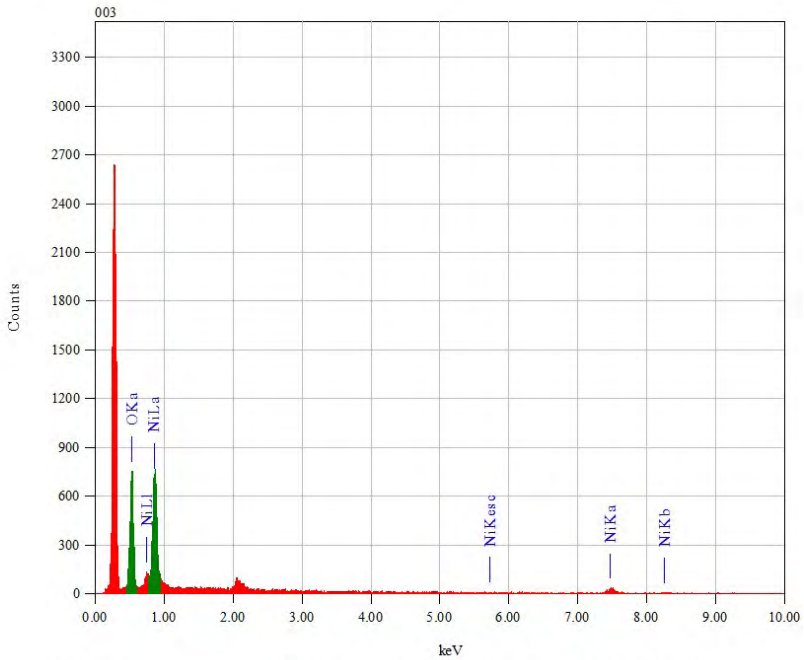

Element		(keV)	Mass%	Sigma	Atom%	(
O K		0.525	29.56	0.16	60.63	
Ni L	*	0.851	70.44	0.63	39.37	
Total			100.00		100.00	

Figure3.2.1.4 : EDX image for *nano* NiO/MCC

3.2.2 Characterization of *nano* Mn_3O_4 MCC

Characterization of *nano* $Mn_3O_4$is done by FTIR, XRD, SEM and EDS analysis.

3.2.2.1 FTIR Spectral Analysis of *nano* Mn_3O_4/MCC

The FTIR spectra of *nano* Mn_3O_4 ,*nano* Mn_3O_4/MCC, and MCC are shown in figure (3.2.2.1). The typical characteristic bands of *nano* Mn_3O_4 were observed in figure(3.1.2.1). For MCC, the bands at 3437 cm^{-1} (the stretching vibration of OH), 2900 cm^{-1} (asymmetrically stretching vibration of C-H groups), 1650 cm^{-1} (bending mode of absorbed water in the composites), 1430 cm^{-1} (CH_2 scissoring motion) and 1058 cm^{-1} (C-O-C pyranose ring skeletal vibration of cellulose) are observed. The characteristic band of *nano* Mn_3O_4 is slightly shifted to the right found at 615 cm^{-1} (actual 631 cm^{-1}) and 503 cm^{-1} (actual 525 cm^{-1}). We also observed that when *nano* Mn_3O_4 is blended with MCC the peak intensities were weak at the band 3437 $cm^{-1}$and 2900 cm^{-1}.

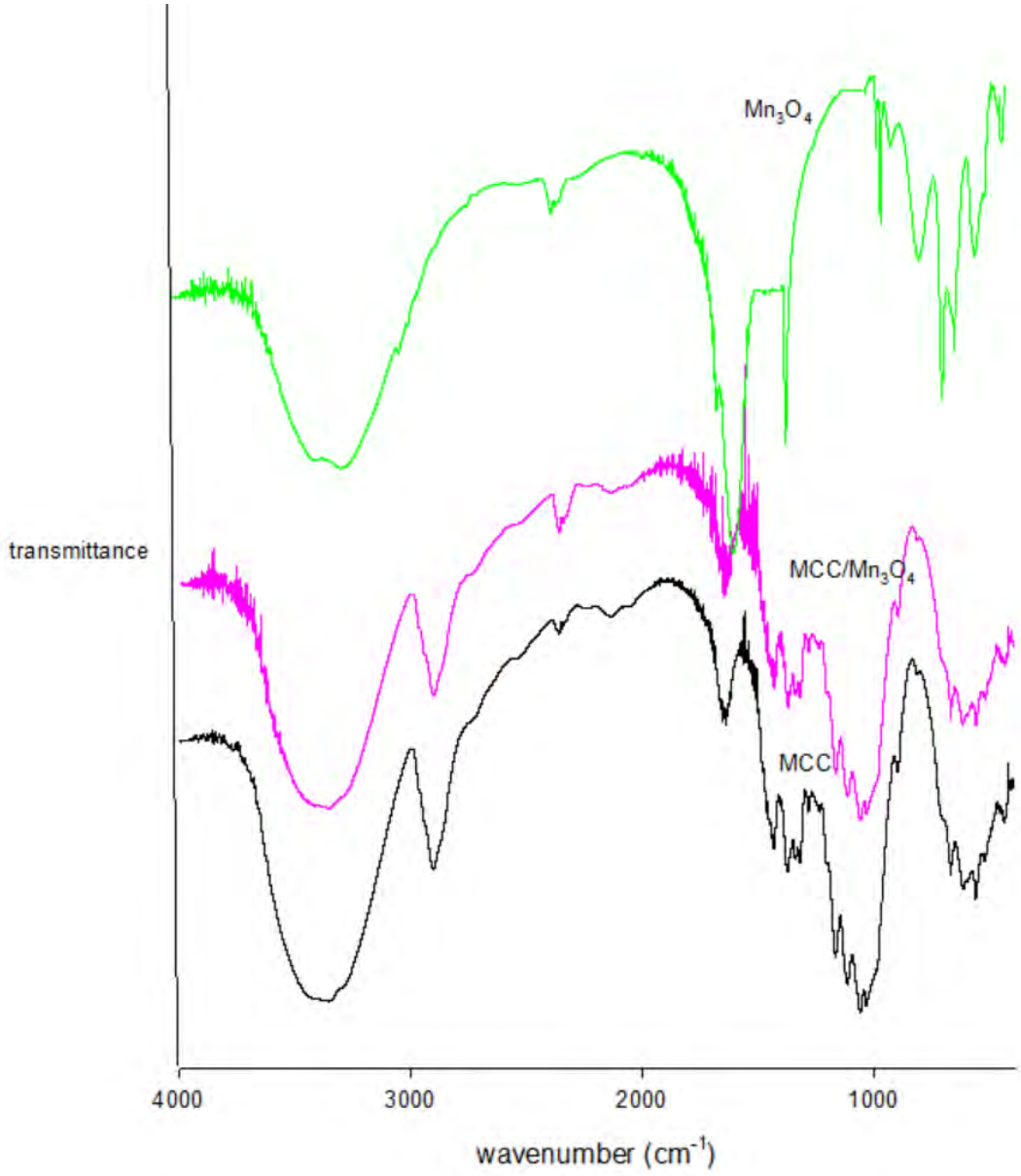

Figure 3.2.2.1 : FTIR analysis for *nano* Mn_3O_4/MCC

3.2.2.2 XRD Analysis for *nano* Mn_3O_4/MCC

Structural analysis by x-ray can provide information on the intermolecular arrangement, i.e., the level if crystallinity of a material. The *nano* Mn_3O_4/MCC samples prepared was examined for their structural analysis in the powdered state by using wide angle x-ray diffraction. The scattering patterns as a function of Bragg angle, 2θ at λ = 1.54 Å for the studied substrate powder in presented in figure (3.2.2.2)

All the diffraction peaks of the samples exhibits standard peaks at 2θ values of 15^0 , 22.5^0, 34.5^0, 13.89^0 , 29.17^0 and 36.86^0he diffraction peaks at 15^0 , 22.5^0 and 34.5^0 is responsible for MCC and for *nano* Mn_3O_4 the diffraction peaks at 2θ values of 13.89^0 , 29.17^0 and 36.86^0

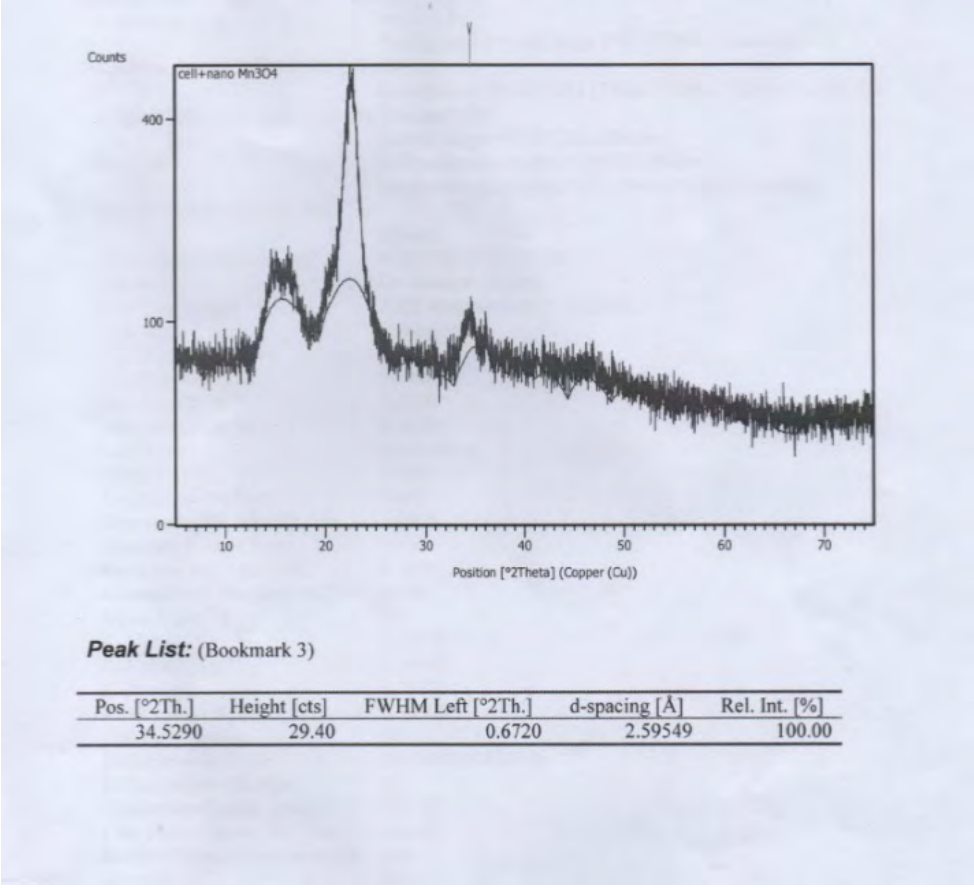

Peak List: (Bookmark 3)

Pos. [°2Th.]	Height [cts]	FWHM Left [°2Th.]	d-spacing [Å]	Rel. Int. [%]
34.5290	29.40	0.6720	2.59549	100.00

Figure3.2.2.2 : XRD pattern for *nano* Mn_3O_4/MCC

3.2.2.3 SEM Analysis for *nano* Mn_3O_4/MCC

Figure(3.2.2.3) shows the SEM images of dispersed *nano* Mn_3O_4 into MCC network. From this image it can be seen the particles are not well distributed and particles are distributed with granular shape and packed each other.

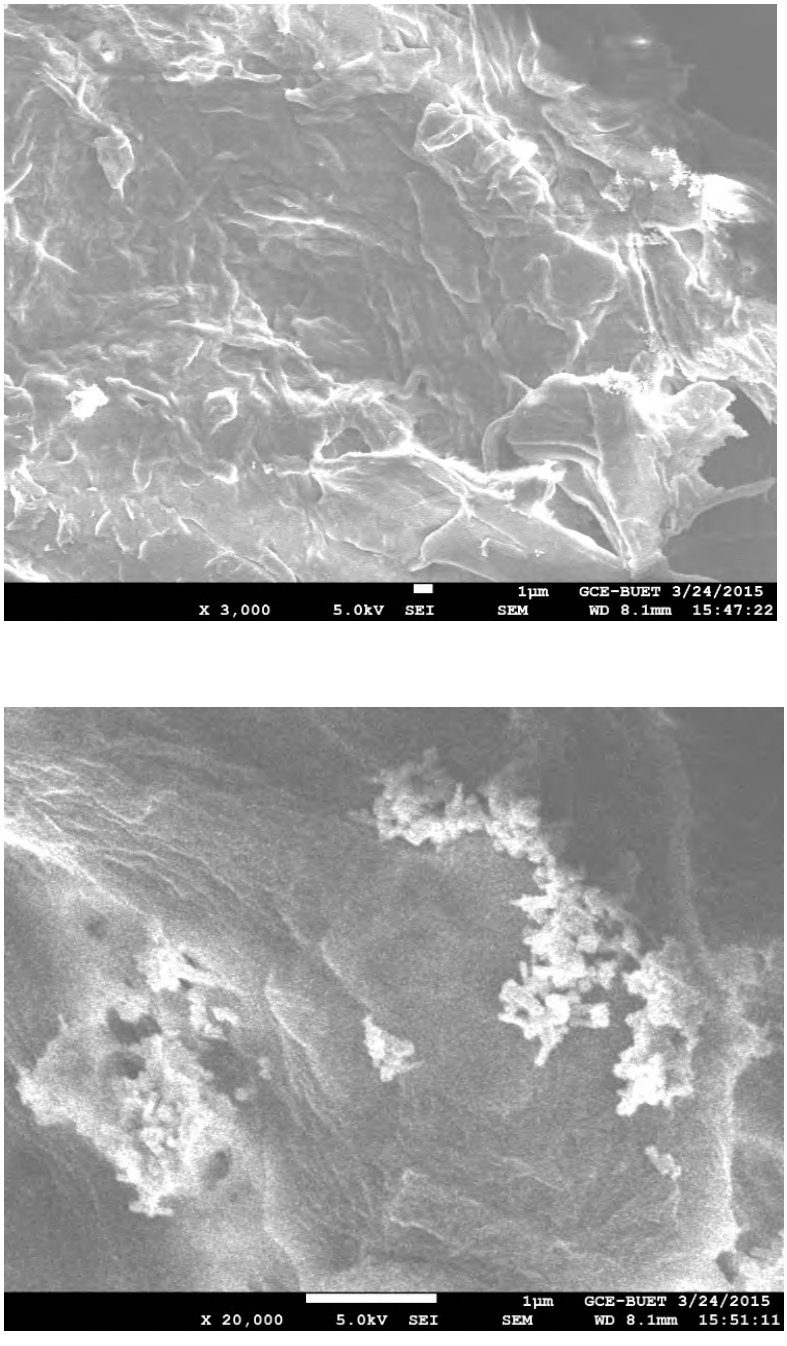

Figure 3.2.2.3: SEM images for *nano* Mn_3O_4/MCC

3.2.2.4 EDX Analysis for nano Mn_3O_4/MCC

The characteristic energy dispersive X-ray(EDX) of the individual present phases are shown in figure (3.2.2.4). Along with the backscattered electron image of prepared samples. The analysis revealed that the dark grayish phase is MCC (labelled “a”) and brighter looking part are *nano* Mn_3O_4.

Labelled “a” phase contained very small amount of Mn_3O_4. A quantitative analysis of the nano Mn_3O_4 gave an average percentage of Mn 80% and 0.20%, which is closed to the data reported for nano Mn_3O_4-MCC system.

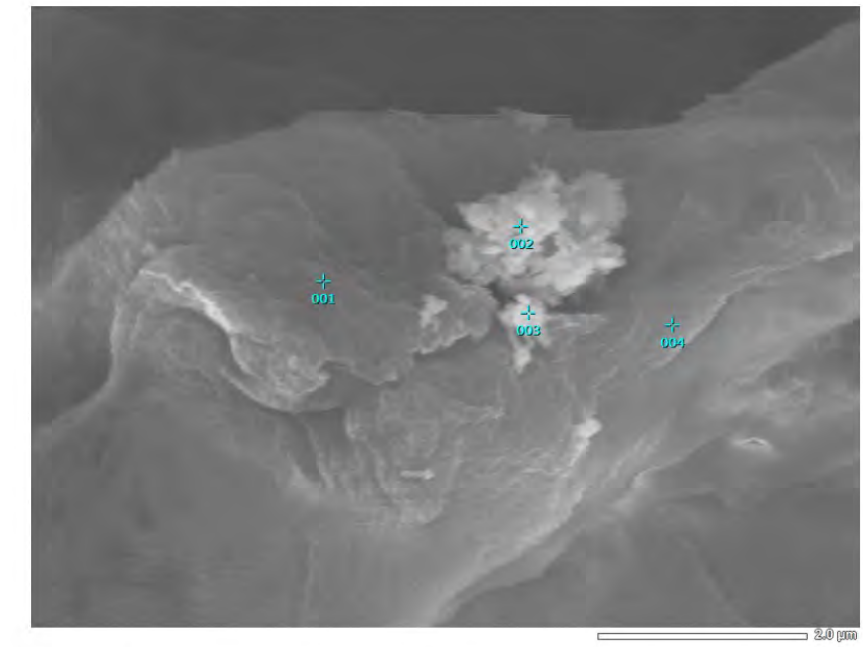

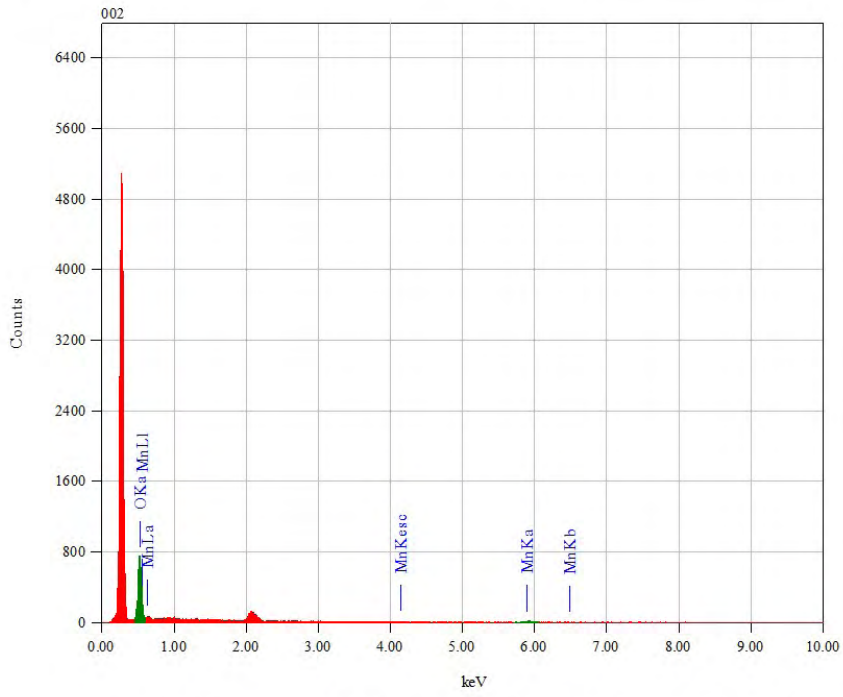

Element		(keV)	Mass%	Sigma	Atom%	C
O K	*	0.525	80.07	0.42	93.24	
Mn K	*	5.894	19.93	1.61	6.76	
Total			100.00		100.00	

Figure 3.2.2.4: EDX images for *nano* Mn_3O_4/MCC

3.3 Adsorption

3.3.1 Adsorption process

We have prepared *nano* NiO, MCC/*nano* NiO composite, *nano* Mn_3O_4, MCC/ *nano* Mn_3O_4 composite in our present work. Application of this materials have been discussed in chapter-1. The materials thus prepared may be used as adsorbents for adsorption process.

Metal oxides have been used as adsorbent nowadays and very important materials for the removal of the toxic chemicals from the environments. Our aim is to use the prepared materials as suitable adsorbents for the removal of dyes from solutions.

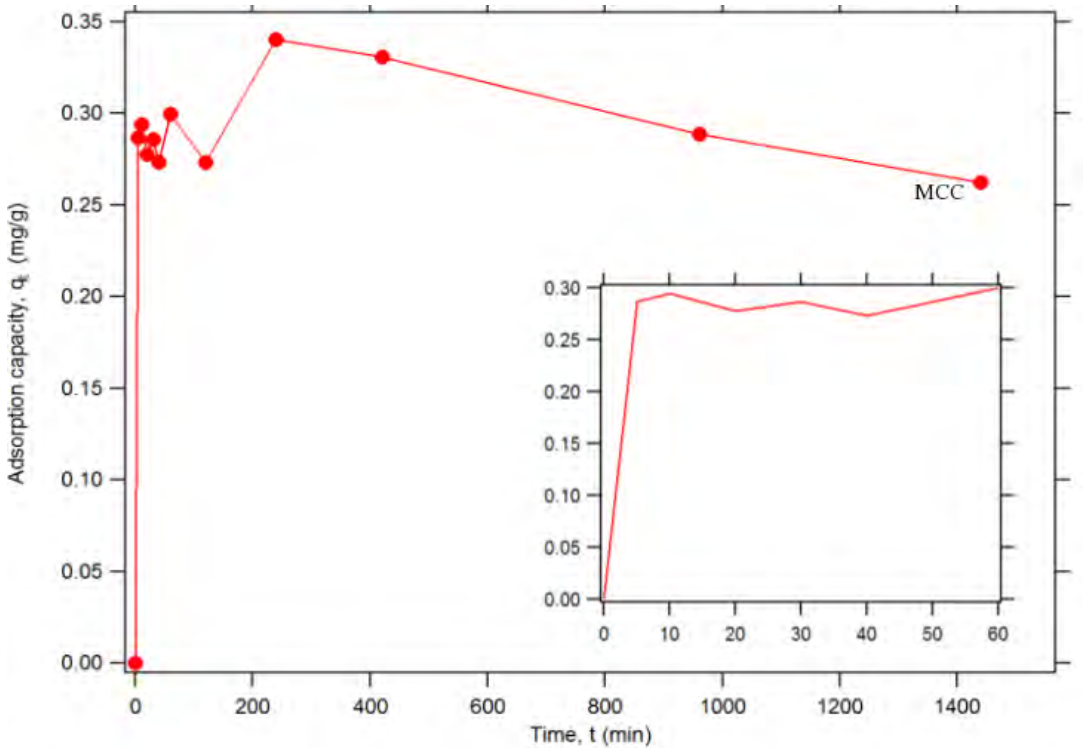

Figure 3.3.1 : Adsorption capacity qt of MB on MCC as a function of adsorption time t (inset shows the adsorption profile of MB on MCC in the initial adsorption stage)

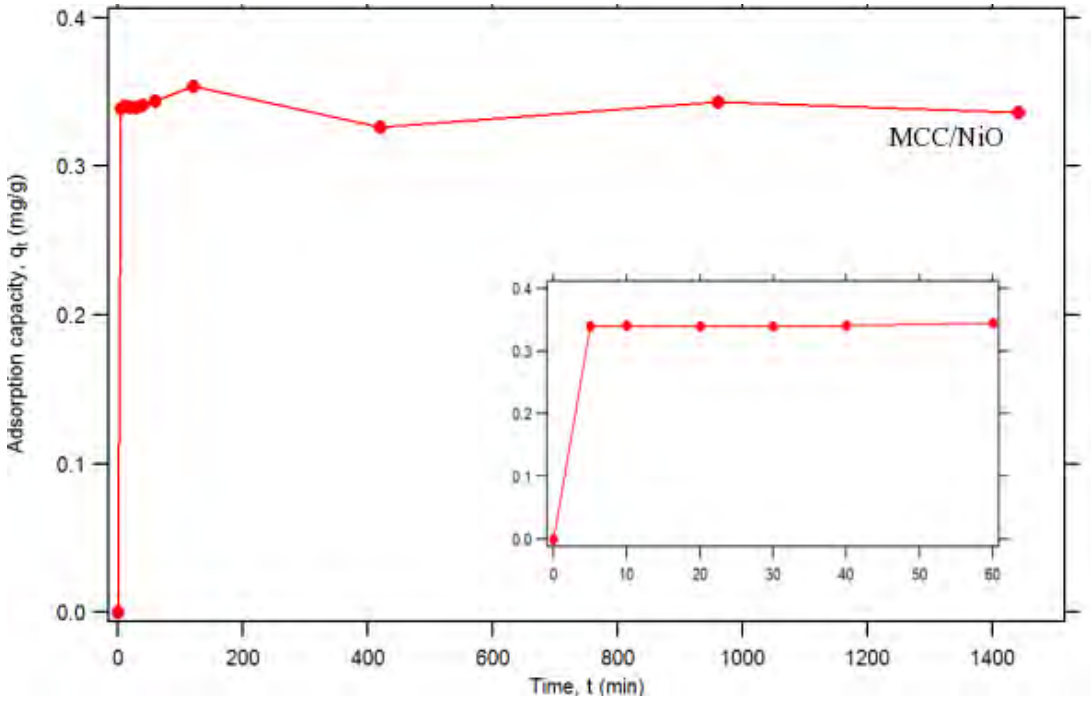

Figure3.3.2 : Adsorption capacity q_t of MB on nano NiO/ MCC as a function of adsorption time t (inset shows the adsorption profile of MB on nano NiO/MCC in the initial adsorption stage)

The adsorption capacity of MB on cellulose and cellulose /*nano* NiO composites was investigated while the condition was fixed at amount of adsorbent 0.1g MB solution is about 5ml and Ph 7.4.

The suspension was centrifuged and the final dye concentration was measured using UV-Vis spectrophotometer at ʎ max = 664nm. MB uptake at equilibrium adsorbed was calculated by means of $q_e=V\ (C_0-C_e)/W$ equation in which C_0 and C_e (mg/L) stands for MB concentration at initial and equilibrium times respectively, V(L) as the solution of volume and W(g) as the used adsorbent mass.

The adsorption capacity q_t of MB on cellulose and cellulose / *nano* NiO composites is displayed on Figure 3.3.1 and Figure 3.3.2 respectively and as a function of adsorption time, t. Figure 3.3.1 and Figure 3.3.2 exhibits that adsorption of MB drastically increases with time in the first 1 hour and then gradually reaches equilibrium. The adsorption capacity q_t at time of MB on cellulose/*nano* NiO is slightly higher than that on cellulose. For example q_t = 0.3443 mgg^{-1} and 0.2995 mgg^{-1} at t = 60 min for cellulose/*nano* NiO and

cellulose respectively, showing that the functionalization of *nano* NiO on cellulose slightly improved the adsorption capacity of MB of the composite materials.

3.3.2 Adsorption kinetic study:

In order to investigate the adsorption process of Methylene Blue on cellulose and cellulose/ *nano* NiO composites, pseudo first order and pseudo second order kinetics were experimented [155,156]. The pseudo first order kinetic model assumes that the adsorption is proportional to the available number of adsorption sites; while the pseudo second order kinetic model assumes that the adsorption rate is proportional to the squire of the available number of adsorption sites [157]

Pseudo first order kinetic model:

$$\log(q_e - q_t) = \log q_e - \frac{k.t}{2.303}$$

Pseudo second order kinetic model:

$$\frac{t}{q_t} = \frac{1}{q_e k_2} + \frac{t}{q_e}$$

$q_e$and q_t (mgg^{-1}) represent the amount of MB adsorbed at equilibrium and any adsorption time t. k_1 (min^{-1}) and k_2 (min^{-1}) are pseudo first-order and pseudo second-order rate constants, respectively.

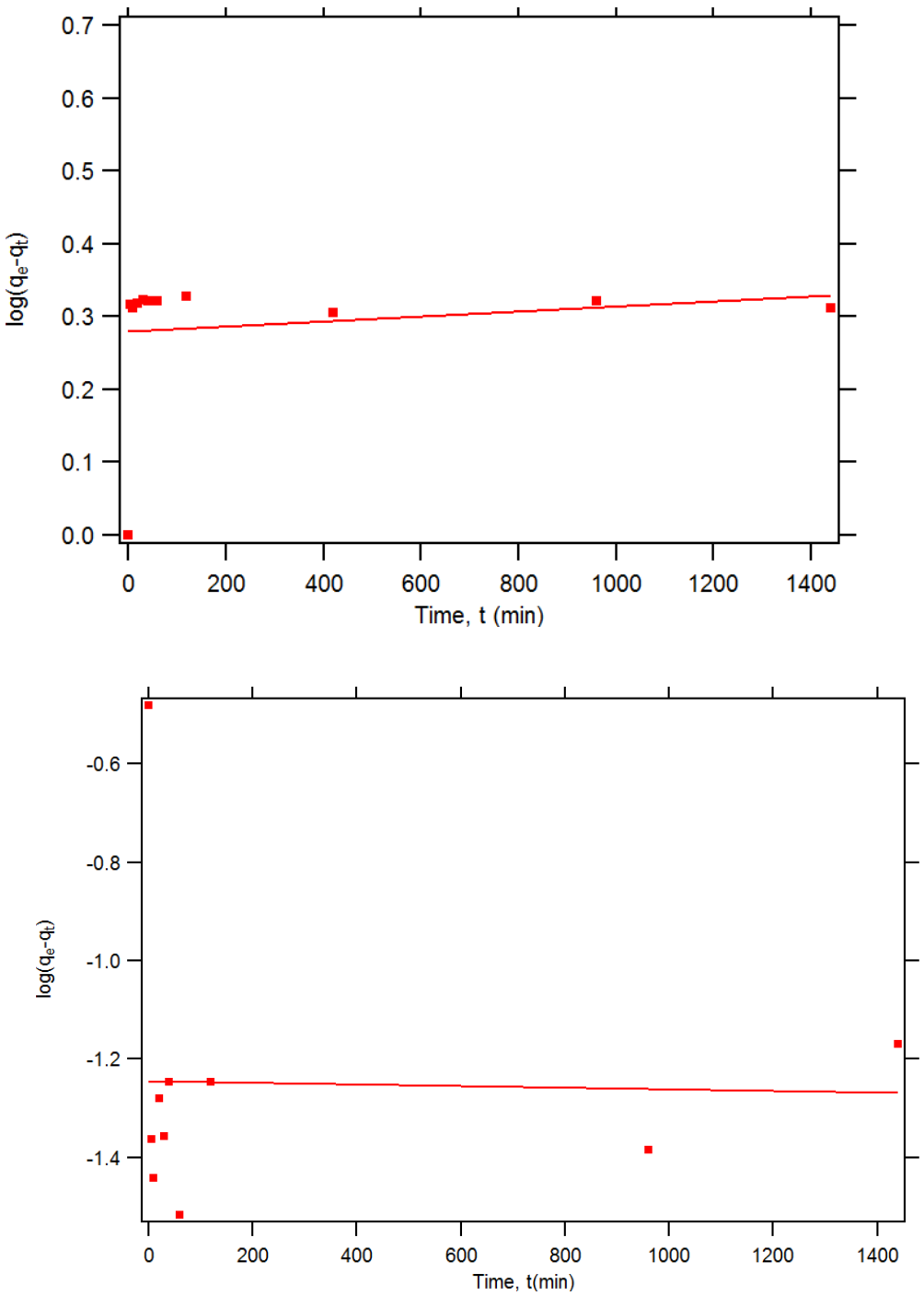

Figure 3.3.2: Fitting of the adsorption kinetics of MB on MCC / *nano* NiO (a)composites and MCC (b) using pseudo first order kinetic models

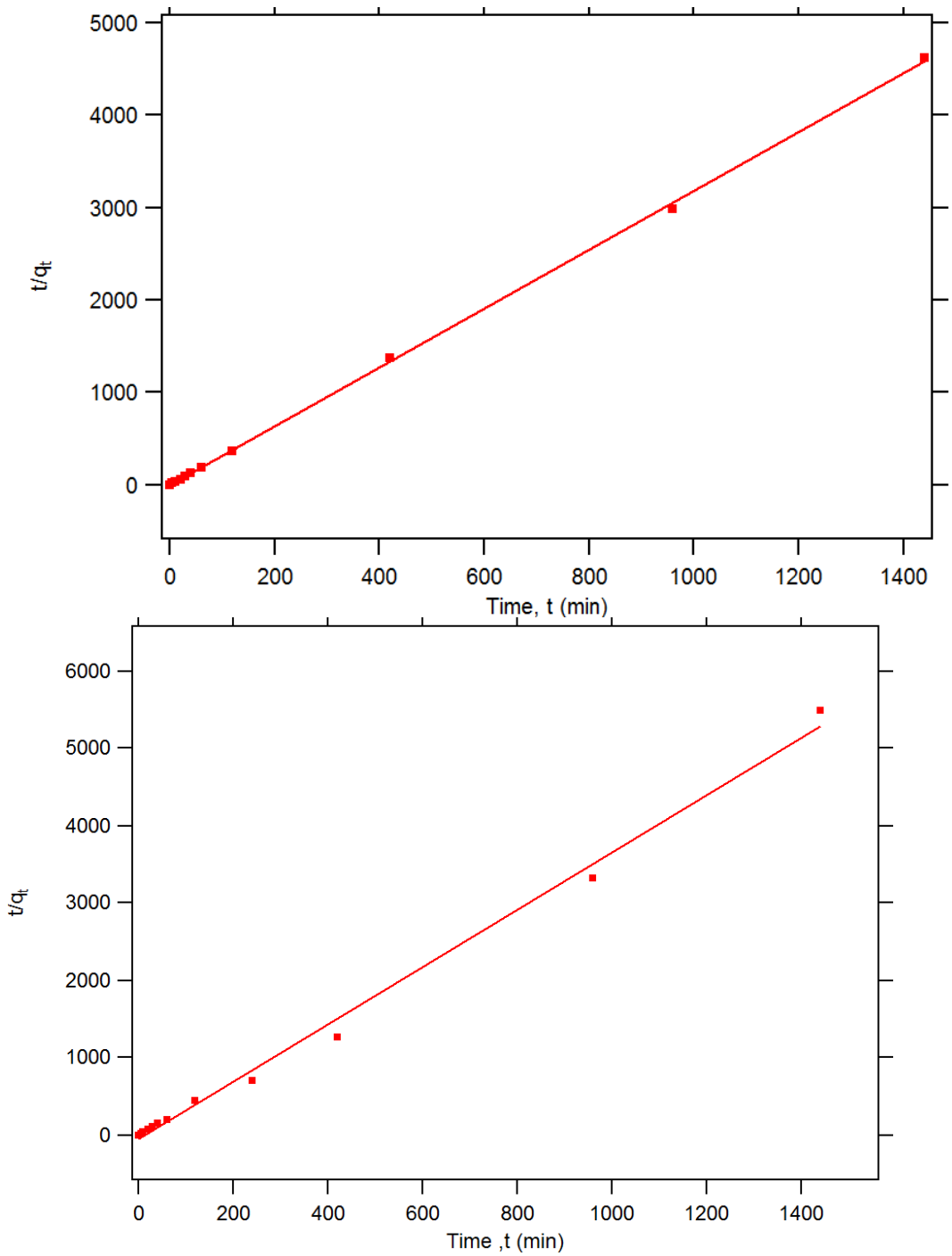

Figure 3.3.3: Fitting of the adsorption kinetics of MB on MCC / *nano* NiO (a)composites and MCC (b) using pseudo first order kinetic models

Pseudo first order kinetics			
adsorbents	q_e (mg/g)	K_1 (g $mg^{-1}min^{-1}$)	r^2
MCC / *nano* NiO composites	17.55	0.0534	0.00297299
MCC	1.90	0.0257	0.000841468

Table 3.3.2 : Parameters for the fitting of the adsorption of MB on MCC and MCC / *nano* NiO composites using pseudo first order kinetic models

Pseudo second order kinetics			
adsorbents	q_e (mg/g)	K_1 (g $mg^{-1}min^{-1}$)	r^2
MCC/ *nano* NiO composites	0.317	0.167	0.99968
MCC	0.269	0.282	0.994828

Table 3.3.3: Parameters for the fitting of the adsorption of MB on MCC and MCC / *nano* NiO composites using pseudo second order kinetic models

Figure (3.3.2) and Figure (3.3.3) show the fitting for adsorption of MB on cellulose and cellulose/*nano* NiO composites using the pseudo first-order kinetics and pseudo second-order kinetics respectively. All kinetics parameters are obtained by linear regression of two kinetic models are summarized in Table 3.3.2 and Table 3.3.3. The adsorption of MB on cellulose and cellulose/*nano* NiO composites exhibits better fit to pseudo second order kinetic model than the pseudo first order kinetic model by giving greater r^2 value (Table 3.3.2 and 3.3.3)

3.3.3 Equilibrium isotherm modeling:

To better understand the interactions between MB and the adsorbents, the equilibrium experimental data were analyzed using Freundlich and Langmuir isotherm models [158, 159].

Langmuir isotherm

The Langmuir theory describes the monolayer coverage of adsorbent on a homogeneous adsorbent surface. The adsorption isotherm is based on the assumption that sorption takes place at specific homogeneous sites with constant adsorption energy.

$$\frac{C_e}{q_e} = \frac{1}{b g_m} + \frac{C_e}{q_m}$$

Rearranging equation given equations

$$\frac{1}{q_e} = \frac{1}{b\, q_n} \cdot \frac{1}{C_e} + \frac{1}{q_m} \qquad \text{---- (1)}$$

Freundlich isotherm

The adsorption equilibrium of the dye in solution and on the adsorbent surface using a multisite adsorption isotherm for heterogeneous surfaces especially these involving organic compounds is described by equation

$$q_e = k_f C_e^{\frac{1}{n}}$$

it rearranges to linear equation by taking the logarithms

$$\log q_e = \log k_f + \frac{1}{n} \log C_e \qquad \text{---- (2)}$$

Ce(mgL^{-1}) is the equilibrium concentration of the MB. q_2(mgg^{-1}) is the maximum Langmuir monolayer adsorption capacity. b is related to the energy of the adsorption [160]. q_m and b can be obtained from the fitting of experimental data by equation (1) .

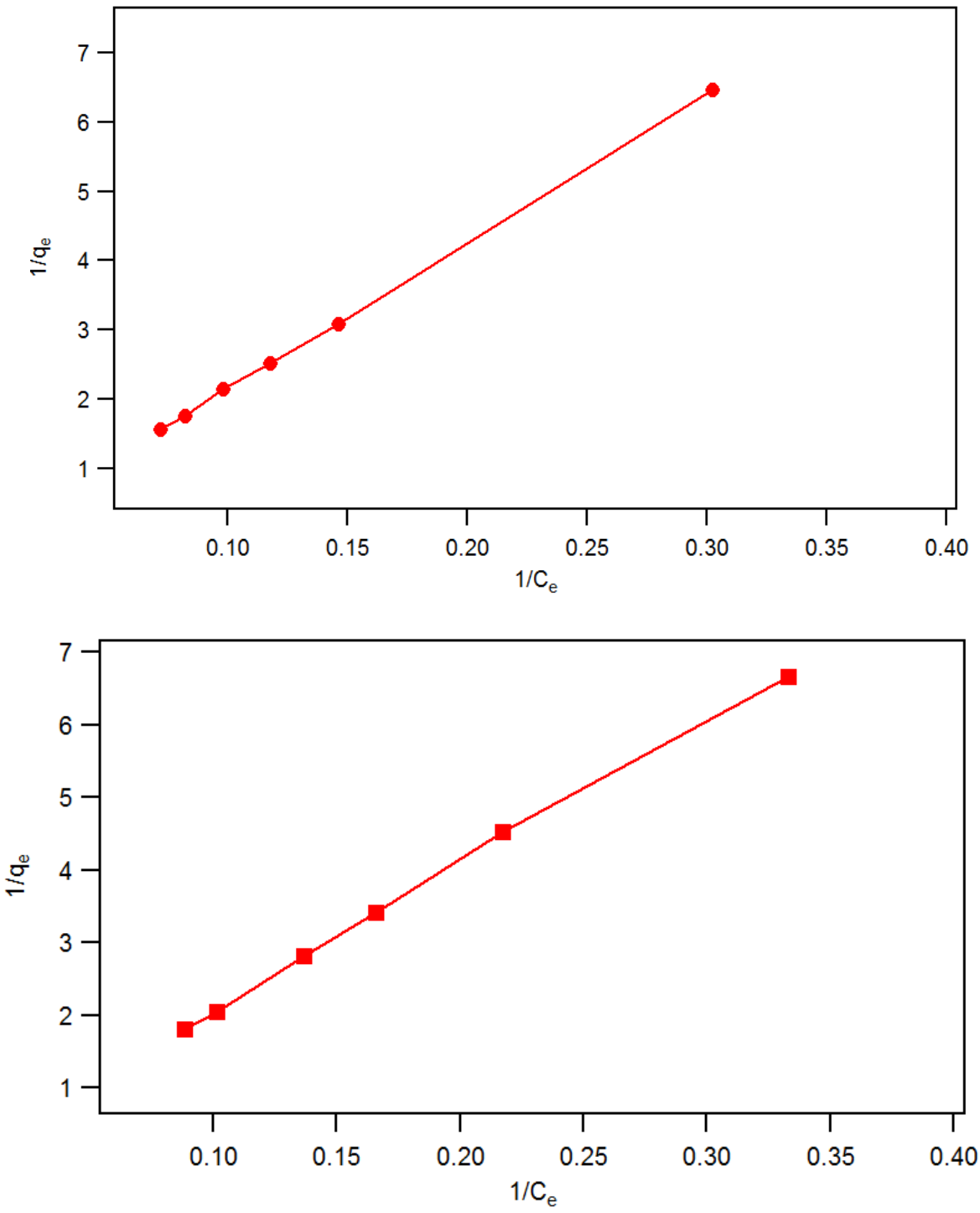

Figure3.3.4: Lanfmuir isotherms of the adsorption of MB on MCC / *nano* NiO composites (a) and MCC (b)

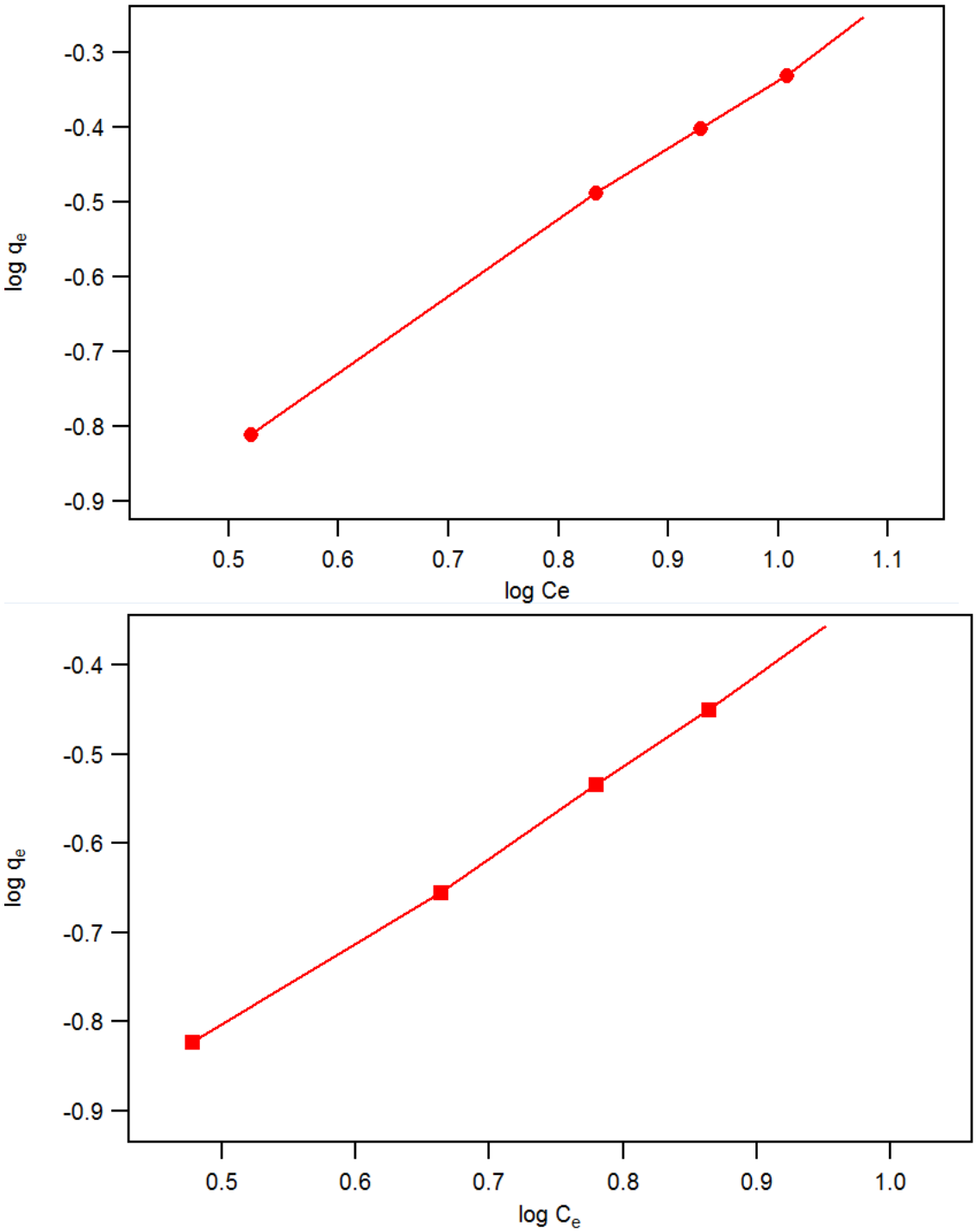

Figure3.3.5: Freundlich isotherms of the adsorption of MB on MCC / *nano* NiO composites (a) and MCC (b)

The Freundlich isotherm model is an empirical model assuming a heterogeneous surface of adsorbent. K_f and n are the indicators of the adsorption capacity and adsorption intensity respectively., which can be determined from the fitting of experimental data by equation (2)

Langmuir Model			
adsorbent	$b(mg\ L^{-1})$	$q_m(mg\ g^{-1})$	R^2
Cellulose	21.317	13.927	0.999702
Cellulose / *nano* NiO composites	19.981	95.475	0.998767

Table 3.3.4: Fitting parameters of the adsorption of MB on cellulose and Cellulose/*nano* NiO composites using Langmuir Model.

Freundlich Model			
adsorbent	k_f	n	R^2
Cellulose	21.023	1.009	0.599496
Cellulose / *nano* NiO composites	20.27	1.004	0.6799152

Table 3.3.5: Fitting parameters of the adsorption of MB on cellulose and Cellulose/*nano* NiO composites using Freundlich Model

Table (3.3.4) and Table (3.3.5) show the fitting of adsorption data using the Langmuir and Freundlich models for the adsorption of MB on MCC and *nano* NiO/MCC, respectively. The fitting parameters are summarized in Table (3.3.4). and (3.3.5). The regression coefficients (R^2) suggest that the Langmuir model fits the adsorption better, which implies that both MCC and *nano* NiO/MCC likely possess homogeneous adsorption surface and the adsorption of MB on these two

adsorbents is likely monolayer. However, it should be noted previous studies have shown that certain heterogeneous materials/surfaces and heterogeneous adsorption could also obey the Langmuir model [158,161]. The qm of MB on nano NiO/MCC (95.475) is much higher than The q_m of MB on MCC (13.927) due to the inter-corporation of *nano* NiO.

3.4 Antibacterial susceptibility testing (Agar disk diffusion method)

The measurement of the antibacterial activity of individual drug pure Mn_3O_4 nanoparticles and MCC /*nano* Mn_3O_4 composite was done by Mueller-Hinton agar disk diffusion susceptibility testing method according to NCCLS (National Committee for Clinical Laboratory Standard) and international guidelines. A total seven bacterial stains including selected gram positive (streptococcus pneumoriac) and gram negative (Acinetobacter Baumanni, Pseuclomonos aeruginosa, salmonela typhi, vibrio cholerac, enterobacter cloacae, Aninetobacter baumanni) bacteria were selected to assess susceptibility pattern.

The measurements of the zones of inhibition (including the diameter of the disk) were made with a ruler on the undersurface of the plate without the bid. The zones of growth inhibition were compared with standard drug loaded disks. The results are expensed as mean±sd (standard deviation).

Name of Bacteria	Diameter of zone of inhibition of different volumes (mm)					
	Pure Mn_3O_4 (mm)			Standard disk(mm)		
	50 µL	**100** µL	**150** µL	**50** µL	**100** µL	**150** µL
Escherichia coli	33.5	41	46	33	41	48
Pseudomonas aeruginosa	31	35	40	30.5	36	38
Streptococcus pneumonia	33	42.5	47	32	39	43.5
Vibrio cholerae	32	39	-	33	41	49
Salmonella typhi	28	35	-	25	33.5	42
Enterobacter cloacae	33	41	-	35	42	47.5
Acinetobacter baumannii	34	43	46	31	40	47.5

Table 3.4.1: Antibacterial activity of the Mn_3O_4 *nano*particles suspension($0.25gL^{-1}$) against following pathogenic organisms

Name of Bacteria	Diameter of zone of inhibition of different volumes (mm)					
	Cellulose+ Mn_3O_4 (mm)			Pure Mn_3O_4 (mm)		
	50 µL	**100** µL	**150** µL	**50** µL	**100** µL	**150** µL
Vibrio cholerae	31	37.5	45	32	39	-
Salmonella typhi	24.5	32	40	28	35	-
Enterobacter cloacae	20	31.5	38	33	41	-
Acinetobacter baumannii	19	32	40	34	43	46

Table 3.4.2: Antibacterial activity of the suspension of Mn_3O_4 nps dispersed in cellulose ($0.25gL^{-1}$)) against following pathogenic organisms.

It can be seen from the result given in Table 3.4.1 that the activity of *nano* Mn_3O_4 against the bacterial growth is almost same as control ciprofloxacin antibiotic suggesting a high antibacterial activity against the bacteria samples tested. This results implies that Mn_3O_4 nanoparticles can kill some bacteria and interact with them strongly.

It can be seen from the result given in Table 3.4.2 that the activity of *nano* Mn_3O_4/MCC against the growth of pathogenic organism is slightly less than pure Mn_3O_4 suspension.

Three small holes are created in the stilled ager medium in Petridis using forceps. Further, we poured 50, 100 and 150 μL *nano* Mn_3O_4 and nano Mn_3O_4/MCC suspension using micropipettes.

Following are some images of zones of inhibitions by *nano* $Mn_3O_4$and *nano* Mn_3O_4/MCC suspension against certain types of bacteria.

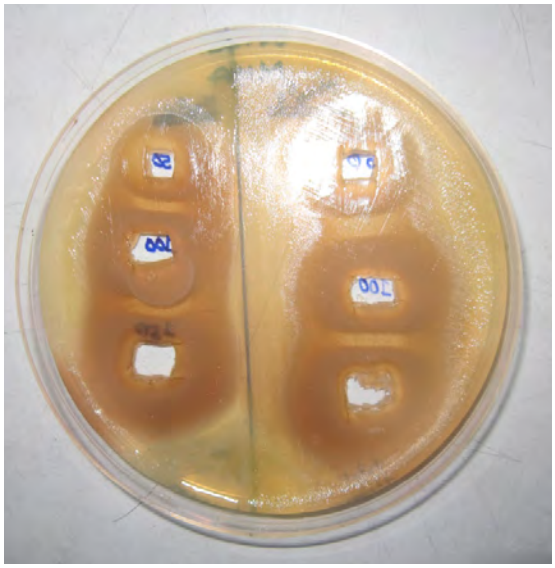

a

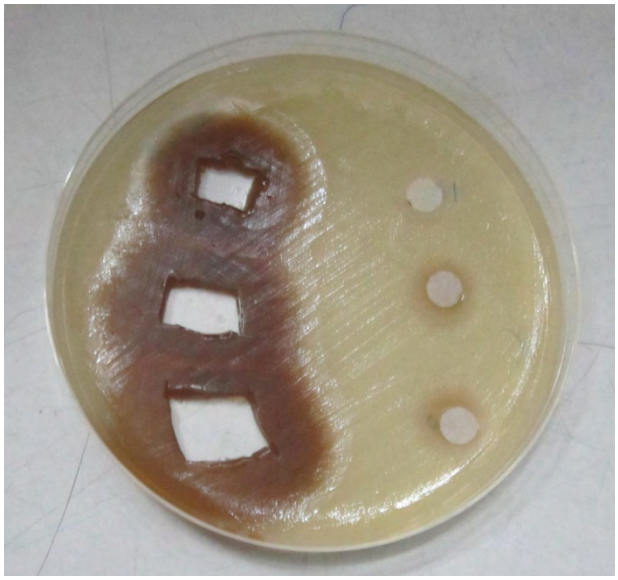

b

a

Figure 3.4.1: Images of zone of inhibition by *nano* Mn_3O_4 (a) *Escherichia coli (L) and Acinetobacter baumannii (R)* (b) *Pseudomonas aeruginosa* (c) *Salmonella typhi*

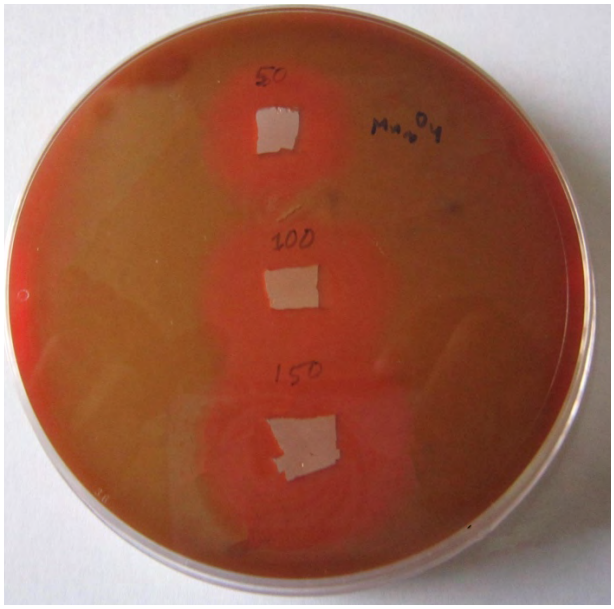

b

c

Figure3.4.2 : Figure: Images of zone of inhibition by *nano* Mn_3O_4 (c) *Streptococcus pneumonia* (d) *Vibrio cholerae* (L) and *Enterobacter cloacae(R)*

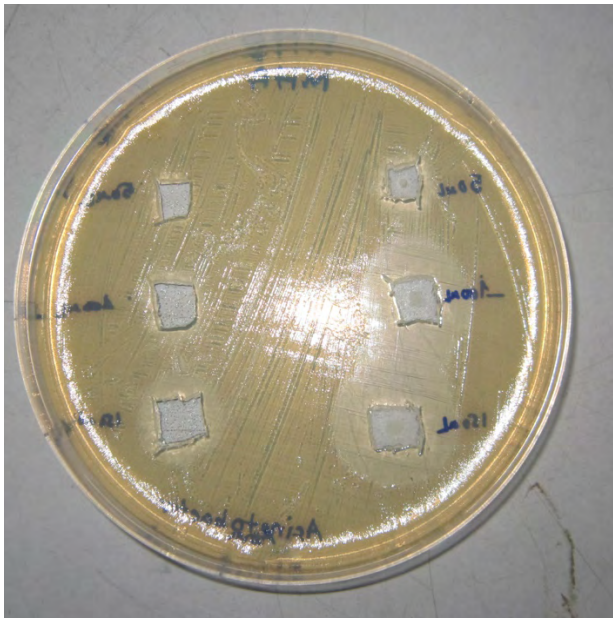

(a)

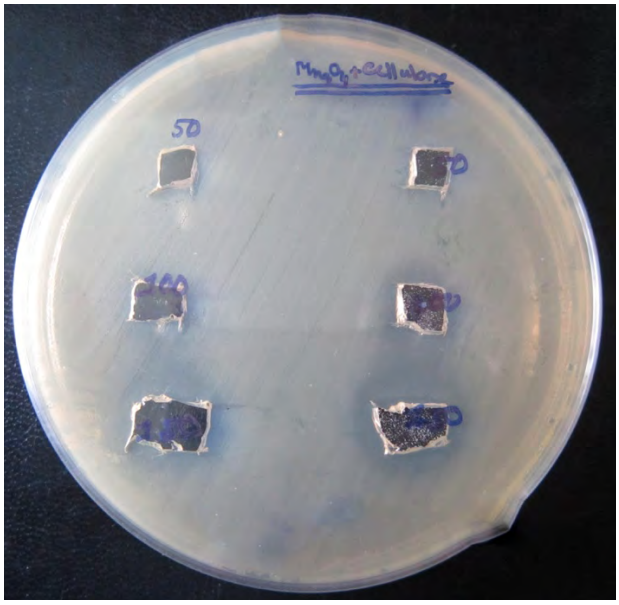

(b)

Figure 3.4.3 : Images of zone of inhibition by nano Mn_3O_4/MCC (a) *Acinetobacter baumannii* (b) *Enterobacter cloacae*

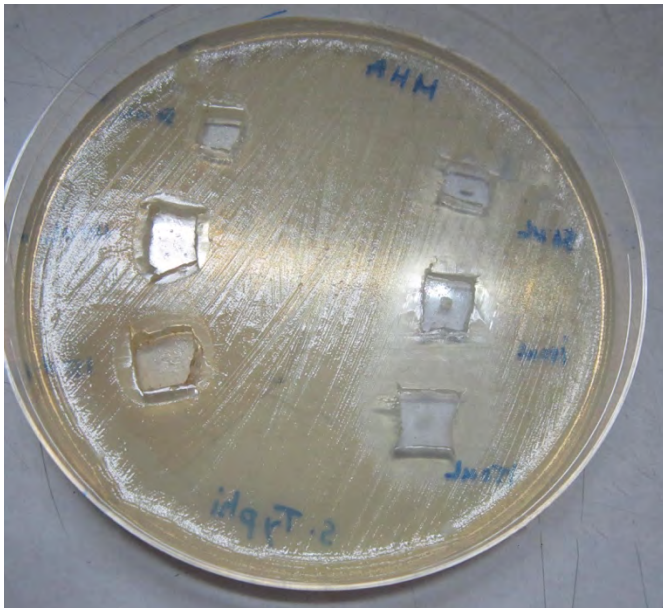

(c)

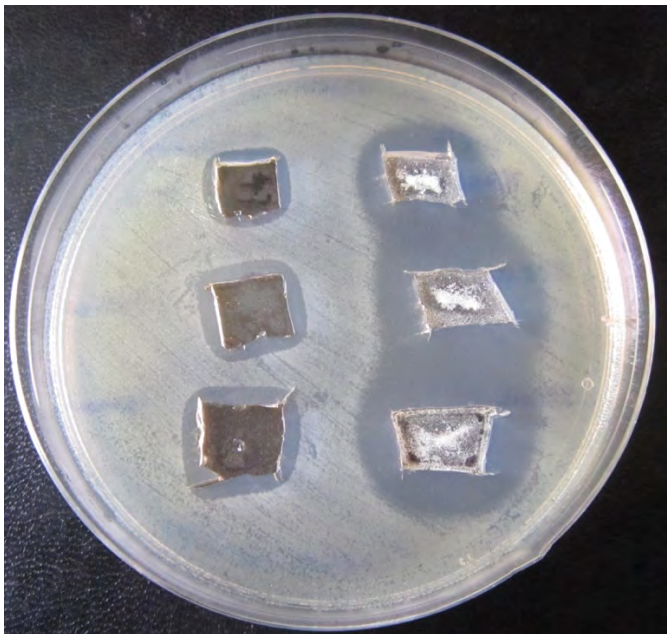

(d)

Figure3.4.4 :Images of zone of inhibition by nano Mn_3O_4/ MCC (c) *Salmonella typhi* (d) *Vibrio cholerae*

CONCLUSION

The aim of this research work was to investigate and explore the versatility of cellulose as a functional material towards its oxidative and antibacterial activities by modifying the cellulose matrix with active *nano* components such as *nano* NiO and *nano* Mn_3O_4. Nickle oxides and Manganese oxide *nano* particles were prepared by following two distinct simple chemical methods. NiO nano particles resulted from the precipitation reaction of Nickel salts ($NiCl_2$ and $NiNO_3$) and precipitation agents ($CO(NH_2)_2$, NH_4HCO_3). NiO particles were obtained using air calcination of $Ni(OH)_2.NiCO_3$ x H_2O . Mn_3O_4 nano particles were prepared by forced hydrolysis of $Mn(II)$ acetate. Aqueous solution of $Mn(OOCCH_3).4H_2O)$ was heated at 80^0C for 2 hours. The resulting brown dispersed product was washed for several times, then dried in air to obtain Mn_3O_4 nano particles. After that these *nano* particles were fabricated into MCC matrix by filtering suspension containing both MCC and nano particles at a fixed condition.

All chemically synthesized compounds i.e., *nano* NiO , *nano* Mn_3O_4, *nano* NiO/MCC and *nano* Mn_3O_4/MCC were characterized by FTIR, XRD, SEM and EDX methods.

IR spectral analysis provides the information on the identification of the compounds. The actual band characteristics of NiO is at $445cm^{-1}$ and $490cm^{-1}$ but when dispersed in MCC matrices , the characteristic band of *nano* NiO is slightly shifted to the right and found at $435cm^{-1}$ and $503cm^{-1}$. The characteristic band of *nano* Mn_3O_4 is also shifted to the right at $615cm^{-1}$(actual $631cm^{-1}$) and $503cm^{-1}$(actual $525cm^{-1}$)

We also observed that when nano particles were blended with MC, the peak intensities were weak at the band $3437cm^{-1}$ and $2900cm^{-1}$. From x-ray analysis, it was observed that *nano* NiO/MCC and *nano* Mn_3O_4/MCC are crystalline in nature. The average crystallite size was found for *nano* NiO , *nano* Mn_3O_4 is $22.5\ nm$ and $11.6\ nm$ respectively.. The surface morphologies of the samples were predicted by SEM, the surface of the individual oxides seem to be granular while it was fibril with MCC and the nano metal oxide distribution over the substrate is not homogeneous.

For the removal of dyes for solution *nano* NiO/MCC and MCC is used as adsorbents. The adsorption capacity $q_t$at any time of MB on *nano* NiO/MCC is slightly higher than cellulose like as, q_t = 0.3443 mgg^{-1} and 0.2995 mgg^{-1} at t = 60 min for cellulose/nano NiO and cellulose respectively, showing that the functionalization of *nano* NiO on cellulose slightly improved the adsorption capacity of MB of the composite materials.

The Adsorption kinetic study exhibits that the adsorption of MB on MCC and MCC/ *nano* NiO composites are better fit to pseudo second order kinetic model than the pseudo first order kinetic model by giving greater r^2 value. To better understand the interactions between MB and the adsorbents,The equilibrium experimental data were analyzed using Freundlich and Langmuir isotherm models. From the fitting parameters, regression coefficients (R2) suggest that the Langmuir model fits the adsorption better and The qm of MB on nano NiO/MCC (95.475) is much higher than The qm of MB on MCC (13.927) due to the intercorporation of nano NiO. which implies that both MCC and *nano* NiO/MCC likely possess homogeneous adsorption surface and the adsorption of MB on these two adsorbents is likely monolayer.

The measurement of the antibacterial activity of individual drug pure Mn_3O_4 nanoparticles and MCC /*nano* Mn_3O_4 composite was done by Mueller-Hinton agar disk diffusion method. A total seven bacterial stains including selected gram positive (streptococcus pneumoriac) and gram negative (Acinetobacter Baumanni , Pseuclomonos aeruginosa, salmonela typhi, vibrio cholerac, enterobacter cloacae, Aninetobacter baumanni) bacteria were selected to assess susceptibility pattern. It can be seen that both *nano* $Mn_3O_4$and *nano* Mn_3O_4/MCC suggesting a antibacterial activity against the bacteria samples tested. This results implies that Mn_3O_4 *nano*particles and *nano* Mn_3O_4/MCC composite kill some bacteria and interact with them strongly.

References

[1] S. Berlioz, S. Molina, Y. Nishiyama, and L. Heux. "Gas-phase surface esterification of cellulose microfibrils and whiskers." Biomacromolecules, 2009, 10, 2144-2151.

[2] P. T. Vasudevan, M. D. Gagnon, and M. S. Briggs, "Environmentally sustainable biofuels– The case for biodiesel, biobutanol and cellulosic ethanol." Sustainable Biotechnology, 2010, 43-62.

[3] M. Nogi, S. Iwamoto, A. N. Nakagaito, and H. Yano. "Optically transparent nanofiber paper." Advanced Materials, 2009, 21, 1595-1598. H. Koga, T. Kitaoka, and A. Isogai. "In situ modification of cellulose paper with amino groups for catalytic applications." Journal of Materials Chemistry, 2011, 21, 9356-9361.

[4] M. M. Ruiz, J. Y. Cavaille, A. Dufresne, C. Graillat, and J. F. Gérard. "New waterborne epoxy coatings based on cellulose nanofillers." Macromolecular Symposia, 2001, 169, 211-222.

[5] N. Ljungberg, C. Bonini, F. Bortolussi, C. Boisson, L. Heux, and J. Y. Cavaillé. "New nanocomposite materials reinforced with cellulose whiskers in atactic polypropylene: effect of surface and dispersion characteristics." Biomacromolecules, 2005, 6, 2732-2739.

[6] J. Svagan, M. S. Hedenqvist, and L. Berglund. "Reduced water vapour sorption in cellulose nanocomposites with starch matrix." Composites Science and Technology, 2009, 69, 500-506.

[7] V. Tserki, N. E. Zafeiropoulos, F. Simon, and C. Panayiotou. "A study of the effect of acetylation and propionylation surface treatments on natural fibres." Composites part A: Applied Science and Manufacturing, 2005, 36, 1110-1118.

[8] M. C. Azeredo. "Nanocomposites for food packaging applications." Food Research International, 2009, 42, 1240-1253.

[9] S. V. Vlierberghe, P. Dubruel, and E. Schacht. "Biopolymer-based hydrogels as scaffolds for tissue engineering applications: a review." Biomacromolecules, 2011, 12 ,1387-1408.

[10] V. de ven and L. Godbout (Eds). “Cellulose - Medical, Pharmaceutical and Electronic Applications”, 2013, ISBN 978-953-51-1191-7, DOI: 10.5772/3470, Publisher: InTech.

[11] Fahlman. B.D., Materials chemistry; (2007),1, 282-283.

[12] Nishiyama,y., Langen,p. and Changy,H., “ Crystal Structure and Hdrogen-Bonding System in Cellulose I β from Synchrotron X-ray Neutron fiber Diffraction” Am. Chem.Soc. 124, 9074-82,2002

[13] Klemm, D., Shmauder, H.P., Heinze,T., Cellulose In Biopolymers, Polysaccharides II; Vandamme,E.J., De Bates, S., Steinbchuel, A., Eds., 6,275-319, 2002.

[14] Sanchez, C., Rozes, L., Ribot, F., Laberty-Robert, C., Grosso, D., Sassoye, C., Boissiere, C., & Nicole, L. (2010). Chimie douce: A land of opportunities for the designed construction of functional inorganic and hybrid organic-inorganic nanomaterials. C. R. Chim., 1, 3 -39 .

[15] Manorama, S. V., Basak, P., & Singh, S. (2011). Anti-Microbial Polymer Nanocomposites. In Trindade T. & Daniel-da-Silva A. L. (Eds.) Nanocomposite Particles for BioApplications. Singapura Pan Stanford Publishing , 249-264.

[16] Belgacem, M. N., & Gandini, A. (2008). Monomers Polymers and Composites from Renewable Resources. Amesterdam:Elsevier.

[17] Goncalves, G., Marques, P. A. A. P., Pinto, R. J. B., Trindade, T., & Pascoal, Neto. C. (2009). Surface modification of cellulosic fibres for multi-purpose TiO(2) based nanocomposites. Compos. Sci. Technol., 69(7-8), 1051 -1056 .

[18] Martins, N. C. T., Freire, C. S. R., Pinto, R. J. B., Fernandes, S. C. M., Neto, C. P., Silvestre, A. J. D., Causio, J., Baldi, G., Sadocco, P., &

Trindade, T. (2012). Electrostatic assembly of Ag nanoparticles onto nanofibrillated cellulose for antibacterial paper products. Submitted.

[19] Thomas, V., Namdeo, M., Mohan, Y. M., Bajpai, S. K., & Bajpai, M. (2008). Review on polymer, hydrogel and microgel metal nanocomposites: A facile nanotechnological approach. J. Macromol. Sci. Part A-Pure Appl. Chem., 45(1), 107-119.

[20] Martins, N. C. T., Freire, C., Pinto, R. J. B., Fernandes, S., Pascoal, Neto. C., Silvestre, A., Causio, J., Baldi, G., Sadocco, P., & Trindade, T. (2012). Electrostatic assembly of silver nanoparticles onto nanofibrillated cellulose for the development of antibacterial paper products. Cellulose, DOI: 10.1007/s10570-10012-19713-10575.

[21] Dankovich, T. A., & Gray, D. G. (2011). Bactericidal Paper Impregnated with Silver Nanoparticles for Point-of-Use Water Treatment. Environ. Sci. Technol., 45(5), 1992-1998.

[22] Wu, D., & Fang, Y. (2003). The adsorption behavior of p-hydroxybenzoic acid on a silver-coated filter paper by surface enhanced Raman scattering. J. Colloid Interface Sci., 265(2), 234-238.

[23] Ngo, Y. H., Li, D., Simon, G. P., & Gamier, G. (2011). Paper surfaces functionalized by nanoparticles. Adv. Colloid Interface Sci., 163(1), 23-38.

[24] Jiang, T., Liu, L., & Yao, J. (2011). In situ Deposition of Silver Nanoparticles on the Cotton Fabrics. Fiber. Polym., 12(5), 620-625.

[25] Tankhiwale, R., & Bajpai, S. K. (2009). Graft copolymerization onto cellulose-based filter paper and its further development as silver nanoparticles loaded antibacterial food-packaging material. Colloid Surf. B-Biointerfaces, 69(2), 164-168.

[26] Marques, P. A. A. P., Nogueira, H. I. S., Pinto, R. J. B., Neto, C. P., & Trindade, T. (2008). Silver-bacterial cellulosic sponges as active SERS substrates. J. Raman Spectrosc., 39(4), 439-443.

[27] Carlson, C., Hussain, S. M., Schrand, A. M., Braydich-Stolle, L. K., Hess, K. L., Jones, R. L., & Schlager, J. J. (2008). Unique Cellular Interaction of Silver Nanoparticles: Size-Dependent Generation of Reactive Oxygen Species. J. Phys. Chem. B, 112(43), 13608-13619.

[28] Fernandez, A., Picouet, P., & Lloret, E. (2010). Cellulose-silver nanoparticle hybrid materials to control spoilage-related microflora in absorbent pads located in trays of fresh-cut melon. Int. J. Food Microbiol., 142(1-2), 222 -228 .

[29] Kim, S. S., Park, J. E., & Lee, J. (2011). Properties and Antimicrobial Efficacy of Cellulose Fiber Coated with Silver Nanoparticles and 3-Mercaptopropyltrimethoxysilane (3-MPTMS). J. Appl. Polym. Sci., 119(4), 2261-2267.

[30] Niu, Z., & Fang, Y. (2006). Surface-enhanced Raman scattering of single-walled carbon nanotubes on silver-coated and gold-coated filter paper. J. Colloid Interface Sci., 303(1), 224-228.

[31] Cabalin, L. M., & Laserna, J. J. (1995). Fast spatially resolved surface-enhanced Raman spectrometry on a silver coated filter paper using charge-coupled device detection. Anal. Chim. Acta, 310(2), 337-345.

[32] Johnston, J. H., & Nilsson, T. (2012). Nanogold and nanosilver composites with lignin-containing cellulose fibres. J. Mater. Sci., 47(3), 1103-1112.

[33] Ishida, T., Watanabe, H., Bebeko, T., Akita, T., & Haruta, M. (2010). Aerobic oxidation of glucose over gold nanoparticles deposited on cellulose. Appl. Catal. A-Gen., 377(1-2), 42 -46 .

[34] Zhang, T., Wang, W., Zhang, D., Zhang, X., Ma, Y., Zhou, Y., & Qi, L. (2010). Biotemplated Synthesis of Gold Nanoparticle-Bacteria Cellulose Nanofiber Nanocomposites and Their Application in Biosensing. Adv. Funct. Mater., 20(7), 1152-1160.

[35] Wang, W., Zhang, T. J., Zhang, D. W., Li, H. Y., Ma, Y. R., Qi, L. M., Zhou, Y. L., & Zhang, X. X. (2011). Amperometric hydrogen peroxide biosensor based on the immobilization of heme proteins on gold nanoparticles-bacteria cellulose nanofibers nanocomposite. Talanta, 84(1), 71-77.

[36] Wang, W., Li, H. Y., Zhang, D. W., Jiang, J., Cui, Y. R., Qiu, S., Zhou, Y. L., & Zhang, X. X. (2010). Fabrication of Bienzymatic Glucose Biosensor Based on Novel Gold Nanoparticles-Bacteria Cellulose Nanofibers Nanocomposite. Electroanalysis, 22(21), 2543-2550.

[37] Liu, Z., Li, M., Turyanska, L., Makarovsky, O., Patane, A., Wu, W., & Mann, S. (2010). Self-Assembly of Electrically Conducting Biopolymer Thin Films by Cellulose Regeneration in Gold Nanoparticle Aqueous Dispersions. Chem. Mater., 22(8), 2675-2680.

[38] Koga, H., Tokunaga, E., Hidaka, M., Umemura, Y., Saito, T., Isogai, A., & Kitaoka, T. (2010). Topochemical synthesis and catalysis of metal nanoparticles exposed on crystalline cellulose nanofibers. Chem. Commun., 46(45), 8567-8569.

[39] An, D., Ye, A., Deng, W., Zhang, Q., & Wang, Y. (2012). Selective Conversion of Cellobiose and Cellulose into Gluconic Acid in Water in the Presence of Oxygen, Catalyzed by Polyoxometalate-Supported Gold Nanoparticles. Chemistry-A European Journal, 18(10), 2938-2947.

[40] Tan, X., Deng, W., Liu, M., Zhang, Q., & Wang, Y. (2009). Carbon nanotube-supported gold nanoparticles as efficient catalysts for selective oxidation of cellobiose into gluconic acid in aqueous medium. Chem. Commun. [46], 7179 -81 .

[41] Luckham, R. E., & Brennan, J. D. (2010). Bioactive paper dipstick sensors for acetylcholinesterase inhibitors based on sol-gel/enzyme/gold nanoparticle composites. Analyst, 135(8), 2028-2035.

[42] Turyanska, L., Makarovsky, O., Patane, A., Kozlova, N. V., Liu, Z., Li, M., & Mann, S. (2012). High magnetic field quantum transport in Au nanoparticle-cellulose films. Nanotechnology, 23(4), 045702

[43] Vainio, U., Pirkkalainen, K., Kisko, K., Goerigk, G., Kotelnikova, N. E., & Serimaa, R. (2007). Copper and copper oxide nanoparticles in a cellulose support studied using anomalous small-angle X-ray scattering. Eur. Phys. J. D, 42(1), 93-101.

[44] Li, Q., Yao, G., Zeng, X., Jing, Z., Huo, Z., & Jin, F. (2012). Facile and Green Production of Cu from CuO Using Cellulose under Hydrothermal Conditions. Ind. Eng. Chem. Res., 51(7), 3129-3136.

[45] Mary, G., Bajpai, S. K., & Chand, N. (2009). Copper (II) Ions and Copper Nanoparticles-Loaded Chemically Modified Cotton Cellulose Fibers with Fair Antibacterial Properties. J. Appl. Polym. Sci., 113(2), 757-766.

[46] Kotelnikova, N., Vainio, U., Pirkkatainen, K., & Serimaa, R. (2007). Novel approaches to metallization of cellulose by reduction of cellulose-incorporated copper and nickel ions. Macromol. Symp., 25474-79.

[47] Cady, N. C., Behnke, J. L., & Strickland, A. D. (2011). Copper-Based Nanostructured Coatings on Natural Cellulose: Nanocomposites Exhibiting Rapid and Efficient Inhibition of a Multi-Drug Resistant Wound Pathogen, A. baumannii, and Mammalian Cell Biocompatibility In Vitro. Adv. Funct. Mater., 21(13), 2506-2514.

[48] Pinto, R. J. B., Neves, M. C., Pascoal, Neto. C., & Trindade, T. (2012). Growth and chemical stability of copper nanostructures on cellulosic fibers ACS.

[49] Gamarra, D., Munuera, G., Hungría, A. B., Fernández-García, M., Conesa, J. C., Midgley, P. A., Wang, X. Q., Hanson, J. C., Rodríguez, J. A., & Martínez-Arias, A. (2007). Structure−Activity Relationship in

Nanostructured Copper−Ceria-Based Preferential CO Oxidation Catalysts. J. Phys. Chem. C, 111(29), 11026-11038.

[50] Guillot, S., Chemelli, A., Bhattacharyya, S., Warmont, F., & Glatter, O. (2009). Ordered Structures in Carboxymethylcellulose-Cationic Surfactants-Copper Ions Precipitated Phases: in Situ Formation of Copper Nanoparticles. J. Phys. Chem. B, 113(1), 15-23.

[51] Benaissi, K., Johnson, L., Walsh, D. A., & Thielemans, W. (2010). Synthesis of platinum nanoparticles using cellulosic reducing agents. Green Chem., 12(2), 220-222.

[52] Johnson, L., Thielemans, W., & Walsh, D. A. (2011). Synthesis of carbon-supported Pt nanoparticle electrocatalysts using nanocrystalline cellulose as reducing agent. Green Chem., 13(7), 1686-1693.

[53] Dong, H., & Hinestroza, J. P. (2009). Metal Nanoparticles on Natural Cellulose Fibers: Electrostatic Assembly and In Situ Synthesis. ACS Appl. Mater. Interfaces, 1(4), 797-803.

[54] Cai, J., Kimura, S., Wada, M., & Kuga, S. (2009). Nanoporous Cellulose as Metal Nanoparticles Support. Biomacromolecules, 10(1), 87-94.

[55] He, J. H., Kunitake, T., & Nakao, A. (2004). Facile fabrication of composites of platinum nanoparticles and amorphous carbon films by catalyzed carbonization of cellulose fibers. Chem. Commun [4], 410 -411 .

[56] Wang, W., Li, H. Y., Zhang, D. W., Jiang, J., Cui, Y. R., Qiu, S., Zhou, Y. L., & Zhang, X. X. (2010). Fabrication of Bienzymatic Glucose Biosensor Based on Novel Gold Nanoparticles-Bacteria Cellulose Nanofibers Nanocomposite. Electroanalysis, 22(21), 2543-2550.

[57] Yang, J., Sun, D., Li, J., Yang, X., Yu, J., Hao, Q., Liu, W., Liu, J., Zou, Z., & Gu, J. (2009). In situ deposition of platinum nanoparticles on

bacterial cellulose membranes and evaluation of PEM fuel cell performance. Electrochim. Acta, 54(26), 6300-6305

[58] Gelesky, M. A., Scheeren, C. W., Foppa, L., Pavan, F. A., Dias, S. L. P., & Dupont, J. (2009). Metal Nanoparticle/Ionic Liquid/Cellulose: New Catalytically Active Membrane Materials for Hydrogenation Reactions. Biomacromolecules, 10(7), 1888-1893.

[59] Himeshima, N., & Amao, Y. (2003). Photoinduced hydrogen production from cellulose derivative with chlorophyll-a and platinum nanoparticles system. Energy Fuels, 17(6), 1641-1644.

[60] Pirkkalainen, K., Leppanen, K., Vainio, U., Webb, M. A., Elbra, T., Kohout, T., Nykanen, A., Ruokolainen, J., Kotelnikova, N., & Serimaa, R. (2008). Nanocomposites of magnetic cobalt nanoparticles and cellulose. Eur. Phys. J. D, 49(3), 333-342.

[61] Olsson, R. T., Samir, M. A. S. A., Salazar-Alvarez, G., Belova, L., Strom, V., Berglund, L. A., Ikkala, O., Nogues, J., & Gedde, U. W. (2010). Making flexible magnetic aerogels and stiff magnetic nanopaper using cellulose nanofibrils as templates. Nat. Nanotechnol., 5(8), 584-588.

[62] Ferrando, R., Jellinek, J., & Johnston, R. L. (2008). Nanoalloys: From theory to applications of alloy clusters and nanoparticles. Chem. Rev., 108(3), 845-910.

[63] Yamada, M., Tsuji, T., Miyake, M., & Miyazawa, T. (2009). Fabrication of a tubular FeCo bimetallic nanostructure using a cellulose-cobalt hexacyanoferrate composite as a precursor. Chem. Commun. [12], 1538 -1540 .

[64] Ghos. P., Kumale A., and Vandana “Preparation of Cu, Ag, Fe and Al nanoparticles by the exploding wire technique” Indian Academy of Sciences, (2003) 115, 499-508.

[65] Moser. W. R., E. “Advanced catalyst and Nanostructured Materials;” Academic Press,” New York, (1996).

[66] Valden, M., Lai. X., Goodman. D. W. Science, (1998), 281, 1647-1650.

[67] McGea. K. R., Parker. J. S., Somorjai. G.; J. Phys. Chem. B, 106, 10854-10863.

[68] Ahmadi. I. S., Wang. Z. L., Green. T. C., Henglein. A., El-Syad. M. A., Science, (1996), 2721924.

[69] Hamad W. Cellulosic materials: fibers, networks and composites. TheNetherlands: Kluwer Academic Publishers; 2002. p 47.

[70] Azizi Samir MAS, Alloin F, Dufresne A. Review of recent research into cellulosic whiskers, their properties and their application in nanocomposite Field. Biomacromolecules 2005;6:612–26.

[71] Chazeau L, Cavaille´ JY, Ganova G, Dendievel R, Boutherin B.Viscoelastic properties of plasticized PVC reinforced with cellulosewhiskers. J Appl Polym Sci 1999;71:1797–808.

[72] Dufresne A, Kellerhals MB, Witholt B. Transcrystallization in Mcl-PHAs/cellulose whiskers composites. Macromolecules 1999;32:7396–401.

[73] Angle` s MN, Dufresne A. Plasticized starch/tunicin whiskers nano-composite materials. 2. Mechanical behavior. Macromolecules 2001;34:2921–31.

[74] Mathew AP, Dufresne A. Morphological investigation of nanocomp-osites from sorbitol plasticized starch and tunicin whiskers. Bio-macromolecules 2002;3:609–17.

[75] Azizi Samir MAS, Alloin F, Sanchez J-Y, Dufresne A. Cellulose nanocrystals reinforced poly(oxyethylene). Polymer 2004;45:4149–57.

[76] Helbert W, Cavaille´ JY, Dufresne A. Thermoplastic nanocomposite filled with wheat straw cellulose whiskers. Part 1: Processing and mechanical behavior. Polym Compos 1996;17:604–11.

[77] Grunert M, Winter WT. Nanocomposites of cellulose acetate butyrate reinforced with cellulose nanocrystals. J Polym Environ2002;10:27–30.

[78] Oksman K, Mathew AP, Bondeson D, Kvien I. Manufacturing process of cellulose whisker/polylactic acid nanocomposites. Compos Sci Technol, under review.

[79] Yang Y, Ladisch C M & Ladisch M R, Enzyme Microb Technol, 10(10) (1988) 632.

[80] Holmberg M, Berg J, Stemme S, Odberg L, Rasmusson J & Claesson P, J coll interfacesci. 186 (1977) 369.

[81] Wu G, Koliadima A, Sheintter Y & Matijevic E, J coll interfaceSci, 1956 (1997) 222.

[82] Davidson G F, J text Inst, 39 (1948) 87

[83] J. Lee, J. Kim; Hyeon, T Adv. Mater. 2006, 18, 2073-2094

[84] Liang, C.; Li, Z.; Dai, S. Angew. Chem., Int. Ed. 2008, 47, 3696-3717

[85] Lu, A. H.; Hao, G. P.; Sun, Q.; Zhang, X. Q.; Li, W, C. Macromal. Chem. Phys. 2012, 213, 1107-1131.

[86] Ryoo, R.; Joo, S.H.; Kruk, M.; Jaroniec, M. Adv. Mater. 2001, 13, 677-681.

[87] Meng, Y.; Gu, D.; Zhang, F. Q.; Shi, Y.F.; Yang, H. F.; Li, Z.; Yu, C. Z.; Tu, B.; Zhao, D. Y. Angew, G. React. Kinet. Mech. Catal. 2011, 102, 127-142.

[88] P. Paizot, S. Laruelle, S. Grugeon,; Nature (London), 407, 496 (2000).

[89] Y. Nuli, S. Zhao and Q. Qin, j. Power Sources, 14, 113-120 (2003)

[90] A.s. Ahmed, G. A. El-Shobaky, A.N. Al Niaimi, et. al., Mater Lett. 26, 107-112 (1996)

[91] M. L. Curr, A. Agotiano, F, Mavelli, et al. Mater . Eng, C. Biomim Mater. Sens. Syst., 22, 423 (2002)

[92] J. A. Dirksen, K. Duval and T.A. Ring, Sens, Actuators B Chem, 80, 106-115 (2001)

[93] I. Hotovey, J. Huran, Li. Spiess, et. al., Vacuum, 58, 300-307 (2000)

[94] F. Svegl, B. Opel, M.G. Hutchins, et. al. J. Electrochem. Soc., 143 1532 (1996)

[95] Handbook of Inorganic Electrochemical Materials, Grangist, C. G., Ed., Amsterdam, Elseviar, 325-334 (1995)

[96] E. L. Miller and R. E. Rochellau, J. Electrochem.Soc; 144, 3072 (1997)

[97] T. Takanashi, Jpn. J. Appl. Phys., 39, 3072 (2000)

[98] Fedman C, Jungk H. O., Angew. Chem. Int. Ed. 40, 359 (2001).

[99] Tao, F. Wei, Mater. Let. 58, 3226 (2004)

[100] Berchmans S., Gomathi H., and Rao G.P., Electro-oxidation of alcohols and sugars catalyzed on a nickel oxide modified glassy carbon electrode. J, Electroanal. Chem. 394: 267-270 (1995)

[101] Kitao M., Izawa K., Urabe K., Komastu T., Kuwano S., and Yamada S., Preparation and electrochromic properties of RF-sputtered NiOx films prepared in Ar/O2/H2 atmosphere, Kinetics of the oxygen electrode reactions in molten Li+ Na carbonate cutectic. Jpn. J. Appl. Phys. Part 1, 33;6656-6656 (1994)

[102] Tomezyk P., and Morderski G., Kinetics of the oxygen electrode reaction in molten Li+ Na carbonate cutectic. J Electroanal Chem. 353; 177-193(1993)

[103] Dirksen J.A., Duval K., and Ring T.A. NiO thin-film formaldechyde gas sensor. Sensor. Actuat. B: Chem. 80: 106-115(2001)

[104] Gondal M. A.; Sayeed M.N., and Seddigi Z., Laser enhanced photo-catalytic removal of phenol from water using p-type NiO semiconductor catalyst. J Hazard. Mater, 155:83-89 (2008)

[105] Wang X., Li L., Zhang Y., Wang S., Zhang Z., Fei L., and Qian Y., High yield synthesis of NiO nanoparticles and their excellent electrochemical performance. Cryst. Growth Des., 6:2163-2165 (2006)

[106] Anadan K., Rejendran V., Morphological and size effects of NiO nanoparticles via solvothermal process. 14:43-47(2011)

[107] Wang Y., and Qin Q.Z. A nanocrystalline NiO thin-film electrode prepared by pulsed laser ablation for Li-ion batteries. J Electrochem. Soc., 149:A873 (2002).

[108] Han D., Yang H., Shen C., Zhou X., and Wang F., Synthesis and size control of NiO nanoparticles by water-in-oil microemulsion. Powder Technol., 147:113-116(2004).

[109] Xing W., Li F., Yan Z., and Lu G., Synthesis and electrochemical properties of mesoporous nickel oxide. J. Power Sources, 134: 324-330 (2004).

[110] Aslania A., Oriijpoura V., and Fallahi M., Sonochemical synthesis, size controlling and gas sensing properties of NiO nanoparticles. Appl. Surf. Sci. 257:4056-4061(2011).

[111] Zhu W., Shui A., Xu L., Cheng X., Liu P., and Wang H., Template-free sonochemical systheis of hierarchically porous NiO microsphere. Ultrsound. Sonochem. 21:1707:1713(2014).

[112] Yang Q., Sha J., Ma X., Synthesis NiO nanowires by a sol-gel process. D. Yang, Mater. Lett., 59 1967-1970(2005)

[113] Feng S., Xu R., New material in Hydrothermal synthesis. Account. Chem. Res., 34: 239-247 (2001)

[114] D.B. Wang, C.X. Song, Z.S. Hu, X. Fu, Fabrication of hollow spheres and thin films of nickel hydroxide and nickel oxide with hierarchical structures. J. Phys. Chem. B 109 (2005) 1125-1129

[115] L.X. Yang, Y.J. Zhu, H. Tong, Z.H. Liang, W.W. Wang, Hierarchical β-Ni(OH)2 and NiO carnations assembled from nanosheet building blocks. Cryst. Growth Des. 7 (2007) 2716-2719.

[116] L.P. Zhu, G.H. Liao, Y. Yang, H. M. Xiao, J.F. Wang, S.Y. Fu, self-assembled 3D flower like hierarchical β-Ni(OH)2 hollow architecture and their in-situ thermal conversion to NiO, Nanoscale Res. Lett. 4 (2009) 550-557.

[117] X.F. Song, L.Gao, Facile route to nonporous NiO structures from the alpha Ni(OH)2/EG precursor and application in water treatment. J. Am. Ceram. Soc. 91 (2008) 4105-4108.

[118] Z. Song, L.F. Chen, J.C. Hu, R. Richards, NiO(111) nanosheet as efficient and recyclable adsorbents for dye pollutant removal from waste water. Nanotechnology 20 (2009) 275707.

[119] F. Farzahneh. , Z. Asgharpour. “Nickel-chitosan hybrid as a precursor for Nickel Oxide Nanoporous particles fir organic dyes photodegredation”. Journal of sciences. 25(2), 2014.

[120] S.I.C de Toressi , A. Gorenstein, Electrochromic behaviour of manganese dioxide electrodes in slightly alkaline solutions, Electrochim. Acta 37 (1992) 2015-2019.

[121] E.R. Stobhe, B.A.D. Boer, J.W. Geus. The reduction of oxidation behaviour of manganese oxides, Catal. Today 47 (1999) 161-167.

[122] E.J. Groottendost, y. Verbeek, V. Ponce, The role of the Mars andVan Krevelen mechanism in the selective oxidation of nitrosobenzene and the deoxygenation of nitrobenzene on oxidic catalysts. J. Catal. 157 (1995) 706-712.

[123] M. Baldi, E. Finocchio, F. Milella, G. Busca, Catalytic combustion of $C3$ hydro-carbons and oxygenates over Mn_3O_4. Appl. Catal. B: Environ. 16 (1998) 43-51.

[124] M.M. Zwinkels, S.G. Jaras, P.G. Menon, T.A. Griffin, Catalytic materials for high temperature combustion. Catal. Rev. Sci. Eng. 35 (1993), 319-358.

[125] A. Manceau, V.A. Drits, E. Silvester, C. Bartoli, B. Lanson, Structural mechanism of Co^{2+} oxidation by the phyllomanganate buserite, Am. Miner. 82 (1997), 1150-1175.

[126] J.G. Kim, J.B. Dixon, C.C. Chusuri, Y. Deng, Oxidation of chromium (III) to (VI) by manganese oxides, Soil Sci. Technol. 34 (2000) 2029-2034.

[127] V.Q.Chiu, J.G. Hering. Arsenic adsorption and oxidization at manganese surfaces.1. Method for simultaneous determination of adsorbed and dissolved arsenic species. Environ. Sci. Technol. 34 (2000) 2029-2034.

[128] N.Belzile, Y. W. Chen , Z. Wang, Oxidation of antimony(III) by amorphous iron and manganese oxyhydroxides. Chem. Geol. 174 (2001) 379-387.

[129] M.J. Scott, J.J. Morgan. Reactions at oxide surfaces. 2. Oxidation of Se(IV) by synthetic birnessite, Environ. Sci. Technol. 30 (1996) 1990-1996.

[130] C.J. Matocha, D.L. Sparks, J.E. Amonette, R.K. Kukkadapu, Kinetics and mechanism of birnessite reduction by catechol. Soil Sci. Soc. Am. J. 65 (2001) 58-66

[131] R.A. Petrie, P.R. Grossl, R.C. Sims, Oxidation of pentachlorophenol in manganese oxide suspensions under controlled Eh and pH environments. Environ. Sci. Technol. 36 (2002) 3744-3748.

[132] H. Li, L.S. Lee, D.G. Schulze, C. Guest, Role of soil manganese in the oxidation of aromatic amines. Environ. Sci. Technol. 37 (2003) 2686-2693.

[133] H. Zhang, C.H. Huang, Oxidative transformation of fluoroquinolone antibacterial agents and structurally related amines by manganese oxide. Environ. Sci. Technol. 39 (2005) 4474-4483.

[134] K.H. Kang, D.M. Lim, H. Shin. Oxidative-coupling reaction in TNT reduction products by manganese oxide. Water Res. 40 (2006) 903-910.

[135] V. Khatri, K. Halasz, L. V. Tranda lovic, S. Dimitrijevic-Brankovic, P. Mohanty, V. Djokovic and L. Csoka, Carbohydr. Polym., 2014, 109, 139–147.

[136] G. Yuan, R. Cranston, 2008. Recent advances in antimicrobial treatments of textiles. Textile Research Journal 78 (1), 60e72.

[137] K.K.Y. Wong, X. Liu, 2010. Silver nanoparticles-the real “silver bullet” in clinical medicine? Medicinal Chemistry Communications 1 (2), 125e131.

[138] J. Kim, S. Kwon, E. Ostler, 2009. Antimicrobial effect of silver-impregnated cellulose: potential for antimicrobial therapy. Journal of Biological Engineering 3 (20)

[139] J.L. Clement, P.S. Jarrett, 1994. Antibacterial silver. Metal-Based Drugs 1 (5e6), 467e482.

[140] N Cordente, B Toustou, V colliere, C Amiens, M Verelst, et al., Chemistry 2001, 4:143.

[141] G Zhou, S Liu, Y. J Zheng, Inorg Chem 1997; 13(1):43 (in chinese)

[142] G. Wang, L. Zhang, J. Mou, Acta Phys Chem Sinica 1997; 13(5):445.

[143] [143] L. Xiang, X. Y. Deng, & Y. Jin, Experimental study on synthesis of NiO nano-particles. Scripta Materialia, (2002), 47(4), 219-224.

[144] A. N. Chowdhury, M. S. Azam, M. Aktaruzzaman, & A .Rahim, (2009). Oxidative and antibacterial activity of Mn_3O_4. Journal of hazardous materials, 172(2), 1229-1235.

[145] N. Dharmaraj, P. prabu, S. Nagarajan, C. H. Kim.; Mat. Sc. Eng. , **B 128,** 111-114 (2006)

[146] H. Guan, C. Shoa, S.Wen, J.Gong, X. Yang, Inorg. Chem. Commun., **6** ,1302 (2003)

[147] P. S. Patil, L. D. Kadam, Appl. Sur. Sci. 199, 211 (2002)

[148] B. J. Enrique, Spectroscopic investigation of the /chitosan interaction, Carbohydr. Polym. 74: 704-706 (2008).

[149] T. P. Braga, E. C. C. Gomes, A. F. D. Sousa, N. L. V. Carreno, E. Longhinotti, A. Valentini A., Synthesis of hybrid mesoporous spheres using the shitosan as template. J. Non-Cryst. Solids, 355: 860-866 (2009).

[150] Q. Li, V. Kumar, Y. Li, H Zhang, T. J. marks and R. P.F. Chang, Fabrication of nanorods and nanotubes in aqueous solutions, Chem. Mater., 17: 2341-2359 (2000).

[151] Z. Li, Y. Deng, B. Shen, W. Hu, J. Phys. Appl. Phys. 42 , 145002 (2009)

[152] V.Chiu, J. Hering, Arsenic adsorption and oxidation at magnetic surfaces, Environ. Sci. Technol.34 (2000) ,2029-2034

[153] A. K. H. Nohman, M. I. Zaki, S. A. A. Monsur, R. B. Fahim, C. Kappenstein, Characterization of thermal genesis course of manganese oxides from inorganic Precursors, Thermochim. Acta 210 , 103-121, (1992)

[154] N. Y. Uesu, E. A. Gomez Pineda and A. A. W. Hechenleitner, Internat. J. Pharmaceutics, 206, 86-96 (2000)

[155] J. Araki, M. Wada, S. Kagu and T. Okano, Colloids and Surfaces A: Physicochemical and Engineering Aspects, 142, 75-82 (1998)

[156] N. Wang, E. Ding and R. Cheng, Polymer, 48, 3486-3493 (2007)

[157] V.R. Gowarikar, N.V. Viswanathan and Dreedhar Jaydev; Polymer Science, New Age International (P) Limited, New Delhi, 1986

[158] I. Langmuir, J. Am. Chem. Soc. 1916, 38, 2221-2295

[159] H. Freundlich, Zeitschrift fur Physikalische, 1906, 57, 384-470.

[160] R. I. Masel, Principles of adsorption and reaction on solid surfaces. John Wiley & Sons 1996.

[161] A. Dabrowski, Adv Colloid Interface Sci. 2001, 93, 135-224.